UCLouvain

École polytechnique de Louvain

Evaluating the Environmental Viability and Performance of Hydrogen-Fueled Wankel Rotary Engines

Authors: **Juan Facundo Funes Albanese, Pierre Meiers**
Supervisor: **Francesco Contino**
Readers: **Mauro Daese, Hervé Jeanmart**
Academic year 2022–2023
Master [120] in Electro-mechanical Engineering
Master [120] in Mechanical Engineering

Abstract

In the context of the climate crisis, it is crucial to cut down on greenhouse gas emissions. For automobile solutions, hydrogen emerges as a promising alternative fuel for ICEs, with the Wankel rotary engine presenting potential when paired with it. This research evaluates first the viability of the hydrogen-fueled Wankel rotary engine against other green automotive technologies by undertaking a Life Cycle Assessment aiming to determine its position in the industry. Hydrogen's use in ICEs presents challenges such as increased heat flux. The Wankel rotary engine's unique design accentuates heat losses and reduces the efficiency due to its higher surface-to-volume ratio and longer stroke. While varying air-fuel ratio significantly impacts combustion, efficiency, heat loss and power in ICEs, this study also seeks to understand the balance between them in the Wankel rotary engine when fueled with hydrogen. Key insights emphasize the complex nature of assessing environmental impacts, underlining the necessity to consider beyond just carbon dioxide emissions. The internal combustion engine vehicles as well as a certain kind of hybrid vehicles, both containing a hydrogen-fueled Wankel engine in its powertrain, present remarkable results, surpassing certain battery electric vehicles, even when excluding battery replacement considerations. Remarkably, some vehicles using grey or blue hydrogen were identified as more environmentally viable than some other vehicles using green hydrogen. Performance analysis of the hydrogen-fueled Wankel rotary engine reveals that adjusting the air-fuel ratio from $\lambda = 1.4$ to $\lambda = 2.0$ could reduce the heat loss ratio by 15%, increase the efficiency by 4.95%, but also decrease the power by 20.8%.

Acknowledgment

First and foremost, profound thanks are directed to Mauro for his consistent support throughout the development of this master thesis. His guidance and availability across the year were invaluable in keeping the project on track.

Recognition must also be given to Pr. Francesco Contino, the thesis supervisor. His feedback during our periodic meetings was instrumental, challenging our perspectives and promoting rigorous analysis. Appreciation is also extended to Pr. Hervé Jeanmart, both for his willingness to serve as a reader and for his valued participation on the jury.

Additionally, it's essential to express gratitude to the dedicated CREDEM technical staff. Pr. Herman, Simon, Frank, Julien, Arnaud, and Hervé have each made significant contributions, and their efforts were pivotal in the completion of this work.

Lastly, gratitude is extended to our friends and families for their unwavering support, not only during the formulation of this thesis but throughout our entire academic journey at the university.

Contents

Introduction **1**

1 Literature review **3**
1.1 Hydrogen . . . 3
1.1.1 Hydrogen fuel characteristics . . . 3
1.1.2 Hydrogen production . . . 6
1.1.3 Hydrogen in internal combustion engines . . . 13
1.2 Wankel rotary engine . . . 14
1.3 Hydrogen Wankle rotary engine . . . 19
1.4 Heat loss in internal combustion engines . . . 20
1.5 Hydrogen fueled vehicles . . . 20
1.5.1 Hydrogen Wankel rotary engine vehicles . . . 21
1.5.2 Hydrogen Wankel engine in hybrid vehicles . . . 21
1.5.3 Fuel cell vehicles . . . 23
1.5.4 Hydrogen storage . . . 26
1.5.5 Assessing the vehicle's viability . . . 26
1.6 From literature to inquiry . . . 28

2 Methodology **29**
2.1 Viability of vehicles . . . 29
2.1.1 Life cycle assessment . . . 29
2.1.2 Software and tools . . . 30
2.1.3 Goal and scope . . . 32
2.1.4 Life cycle inventory . . . 34
2.1.5 Life cycle impact assessment . . . 50
2.1.6 Normalization . . . 52
2.1.7 Sensitivity analysis . . . 54
2.2 Performance of the hydrogen Wankel rotary engine . . . 54
2.2.1 Data pre-processing . . . 54
2.2.2 Data post-processing . . . 56

3 Results **73**
3.1 Viability of vehicles . . . 73
3.1.1 Life Cycle Impact Assessment results . . . 73
3.1.2 Normalization . . . 84
3.1.3 Sensitivity analysis . . . 88
3.2 Performance of the hydrogen Wankel rotary engine . . . 92
3.2.1 Combustion analysis . . . 92
3.2.2 Heat loss . . . 93
3.2.3 Efficiencies . . . 98
3.2.4 Power and IMEP . . . 100
3.3 Discussion . . . 101

Conclusion **104**

A Experimental Part **115**
A.1 Engine Identification . . . 115
A.1.1 Modified Parts . . . 117
A.1.2 Missing Parts . . . 117
A.1.3 Oil Nozzles . . . 117
A.1.4 Injectors . . . 118
A.1.5 Turbocharger . . . 118
A.1.6 Metering Oil Pump . . . 118
A.2 Engine Block condition assessment . . . 121
A.2.1 Visual Inspection . . . 121
A.2.2 Compression and Starter Test . . . 122
A.2.3 Engine Block Condition Conclusion . . . 128
A.3 Sensors . . . 129
A.3.1 MAP Sensor . . . 129
A.3.2 Temperature Sensors . . . 130
A.3.3 Oil Pressure Sensor . . . 134
A.3.4 Crank Angle Sensor . . . 134
A.4 Ignition circuit . . . 135
A.5 Bench . . . 141
A.5.1 P&ID . . . 141
A.5.2 Engine mounts . . . 142
A.5.3 Pressure sensor adaptor . . . 144

List of Figures

1.1 Steam Methane Reforming process [1] 7
1.2 Gasification [2] 9
1.3 Basic electrolyzer [3] 11
1.4 Unipolar (left) and bipolar (right) alkaline electrolyzers [3] 11
1.5 Cross-section of SPE water electrolyzer [4] 12
1.6 Schematic diagram of on-site electrolysis [1] 13
1.7 Basic construction of WRE [5] 15
1.8 Rotor motion and peritrochoid generation [5] 16
1.9 WRE and RPE strokes. Adapted from [6] 17
1.10 Individual PEM cell 25

2.1 Life Cycle Models in LCA [7] 33
2.2 Simplified view of this LCA [8] 34
2.3 Method for calculating size-specific non-exhaust emissions from vehicles [9] 43
2.4 Disposal of vehicles [10] 49
2.5 Disposal of battery [10] 49
2.6 ReCiPe midpoints and endpoints 51
2.7 Representation of the Wankel Rotary Engine. Adapted from [6] . . 55
2.8 In-cylinder pressure trace 56
2.9 In-cylinder mass trace 56
2.10 Side Area of the working chamber [5] 58
2.11 Iteration process overview for the MFB determination. 64
2.12 Post-processing method overview 72

3.1 Global warming potential 74
3.2 Freshwater ecotoxicity potential 76
3.3 Marine ecotoxicity potential 77
3.4 Terrestrial ecotoxicity potential 78
3.5 Human toxicity potential (carcinogenic) 79
3.6 Human toxicity potential (non-carcinogenic) 81
3.7 Terrestrial acidification potential potential 82

3.8 Particulate matter formation potential . . . 83
3.9 ReCiPe normalization results . . . 84
3.10 ReCiPe normalization and weighting results: single score . . . 85
3.11 Belgian MMG method normalization and weighting results: single score . . . 87
3.12 Variation of lifetime of vehicles . . . 88
3.13 Battery replacement considered . . . 89
3.14 Variation of hydrogen consumption . . . 90
3.15 SMR+CCS: Comparison of two models of this production method . . . 91
3.16 Mass fraction burned profile at varying air-fuel ratios . . . 93
3.17 (a) The flame development angle and (b) the combustion duration, at varying air-fuel ratios. . . . 94
3.18 (a) In-cylinder peak pressures with (b) their corresponding ESAD moment, at varying air-fuel ratios. . . . 94
3.19 Combustion velocity term, at varying excess ratios. . . . 95
3.20 Heat transfer coefficient, at varying excess ratios. . . . 96
3.21 In-cylinder temperature trace, at varying excess ratios. . . . 96
3.22 Heat flux using Woshcni model, at varying excess ratios. . . . 97
3.23 (a) In-cylinder heat flux with (b) their corresponding ESAD moment, at varying air-fuel ratios. . . . 97
3.24 Efficiencies, at varying air-fuel ratios. . . . 99
3.25 Engine IMEP, at varying excess ratios. . . . 100
3.26 Engine power vs efficiency, at varying excess ratios. . . . 101

A.1 Wankel 13B-DEI detailed specifications [11] . . . 116
A.2 Engine pre and post-disassembly . . . 116
A.3 Intercooler comparison [11, 12] . . . 117
A.4 Oil Nozzle test [13] . . . 118
A.5 Turbocharger test [13] . . . 119
A.6 In-cylinder Inspection . . . 121
A.7 Front Setup . . . 124
A.8 Back Setup (1/2) . . . 124
A.9 Back Setup (2/2) . . . 125
A.10 First rotor . . . 127
A.11 Second rotor . . . 127
A.12 MAP sensor calibration setup . . . 129
A.13 Map sensor calibration (relative pressure) . . . 130
A.14 Temperature sensors calibration setup . . . 131
A.15 Intake air temperature sensor calibration . . . 132
A.16 Water temperature sensor calibration . . . 132

A.17 Water (after exchange) temperature sensor calibration 133
A.18 Ignition circuit setup 136
A.19 Visible sparks on spark plugs 136
A.20 Trailing coil 1 - ignition timing 137
A.21 Trailing coil 2 - ignition timing 137
A.22 Double leading coil - ignition timing 138
A.23 Signals from the three coils - ignition timing 138
A.24 Leading coil signal subtracted from trailing coil signal 138
A.25 Ignition circuit 140
A.26 P&ID 141
A.27 Main engine mount 142
A.28 Secondary engine mount 143
A.29 Pressure sensor adaptor 144

List of Tables

1.1 Properties of Gasoline, Methane, and Hydrogen at 1 atm and 300K ([a] at stoichiometric conditions, [b] at 360 K). Adapted from [14] and [15]. 5
1.2 Advantages and drawbacks of the Wankel rotary engine 18

2.1 Vehicles assessed 33
2.2 Weight distribution of components in a Battery Electric Vehicle (BEV) based on [16] 36
2.3 Predicted mass of a Type IV 700-bar compressed hydrogen system [17] 37
2.4 Breakdown of Balance of Plant (BoP) categories and their respective weights (%) 38
2.5 Battery capacity and weight for different types of vehicles 40
2.6 Weight distribution of an electric vehicle's powertrain 42
2.7 Non-exhaust emission types and their respective parameters 44
2.8 Input values and direct emissions for SMR+CCS process. [18] . . . 45
2.9 Vehicle Maintenance Amounts 47
2.10 Impact Categories and Normalization Factors 52
2.11 MMC method 53
2.12 Specification of the Wankel Rotary engine. Adapted form [19] . . . 56

3.1 Summary table 101

A.1 Metering oil pump inputs and outputs table: Vertical axis: pressure (kPa) ; Horizontal axis: Speed (RPM) ; Table values: Position of stepper (%) 120

Nomenclature

Abbreviations

$ATDC$ After Top Dead Center

BEV Battery electric vehicle

$BTDC$ Before Top Dead Center

CCS Carbon capture and storage

FCV Fuel cell vehicle

$ICEV$ Internal combustion engine vehicle

$IMEP$ Indicated Mean Effective Pressure

SMR Steam methane reforming

ESAD Eccentric Shaft Angle Degree

EVO Exhaust Valve Opening

HRPE Hydrogen Fueled Reciprocating Engine

HWRE Hydrogen Fueled Wankel Rotary Engine

ICE Internal Combustion Engine

IVC Intake Valve Closing

LCA Life Cycle Assessment

RPE Reciprocating Engine

TDC Top Dead Center

WRE Wankel Rotary Engine

Symbols

A	In-Cylinder Surface Area
b	Rotor Width
c_p	Specific Heat Capacity at constant pressure
e	Eccentricity
h_c	Heat Transfer Coefficient
L	Rotor Length
m_f	Mass of Fuel
M_m^i	Molar mass of species i
m_{IVC}	Mass of mixture at intake valce closing
m_{RG}	Mass of Residual Gas In-Cylinder
N	Eccentric Shaft RPM
n_c	Number of Power Stroke Per Shaft Rotation
p	In-Cylinder Pressure
Q_{ch}	Chemical Heat Released
Q_{net}	Net Heat Released
Q_w	Wall Heat transfer loss
R	Generating Radius
R	Universal gas constant
T	In-Cylinder temperature
U	Internal Energy
V	In-Cylinder Volume
V_c	Clearance Volume
V_d	Displacement Volume

W_{net} Net Indicated Work

Greek Letters

η_c Combustion Efficiency

η_{glh} Degree of Constant Volume

η_i Indicated Efficiency

η_{Otto} Otto Cycle Efficiency

γ Ratio of specific heat capacities

λ Air-Fuel excess ratio

ω Eccentric Shaft Rotational Speed

ϕ_w Wall heat loss ratio

ψ N/O Ratio

τ Compression Ratio

θ Eccentric Shaft Angle

Notations

$-$ Mean Value

$\dot{}$ Rate Of Change With Time

$\sim$ Value Per Mole

Introduction

The rising global population and better living standards have increased energy demand. Fossil fuels, historically the main energy source, worsen environmental damage and contribute majorly to global warming. Today, there is an urgent need to reduce reliance on them. The transportation sector alone consumes about 60% of global energy and is responsible for over 25% of CO_2 emissions from fossil fuel burning. A move to cleaner energy alternatives is vital to counter the environmental harm caused by fossil fuels. [20, 21].

Sustainable development, while aligned with the aspirations of the Green Deal, calls for energy strategies that reduce carbon emissions, highlighting the need to shift to alternatives like hydrogen fuel. Hydrogen's unique properties and varied production methods - potentially green methods - make it an eco-friendly energy option, potentially replacing fossil fuels. The automotive industry is really looking into how to use its advantages. However, most hydrogen is still derived from fossil fuels rather than renewable sources. While hydrogen holds promise, its large-scale adoption is still in the beginning stages. Despite challenges, hydrogen's potential for a sustainable, low-carbon energy future is clear [20, 21].

Hydrogen Internal combustion engines (HICE) offer distinct emission advantages. Benefiting from hydrogen's carbon-free nature, these engines align well with clean energy goals. They also hold cost benefits over fuel cells. Hydrogen offers numerous physicochemical advantages, such as wide flammability limits, minimal quenching distance, low ignition energy, exceptional diffusivity, high flame velocity, and a high auto-ignition temperature[22, 23]. However, it also brings challenges like severe abnormal combustion, heightened heat flux, and reduced power output [14, 24]. When considering the Wankel rotary engine (WRE), a synergistic relationship with hydrogen emerges. The distinct four-stroke locations in the WRE, devoid of heat sources like valves, minimizes the risks associated with hydrogen's susceptibility to back-fire and pre-ignition. While the WRE design might traditionally result in reduced efficiency and greater emissions, hydrogen's attributes, such as its minimal quenching distance and high flame velocity, counteract these drawbacks, facilitating

more complete combustion. The WRE high-speed operation, though potentially leading to uneven air-fuel distribution, is balanced by hydrogen's superior diffusivity. Despite hydrogen's low volumetric heat value, the high power density of the WRE serves to mitigate the differences in power output compared to gasoline engines [20, 23].

As the potential of Hydrogen Wankel Rotary Engines (HWRE) gains attention, it is important to consider how these engines fit into the larger picture of sustainable transportation. To answer this, one turns to Life Cycle Assessment (LCA), a tool that evaluates the viability of HWRE-based vehicles alongside other promising technologies for the future, like another hydrogen-powered technology such as Fuel Cell Vehicles (FCVs) and Battery Electric Vehicles (BEVs). LCA considers the complete lifecycle of vehicles, from production to disposal, providing a comprehensive view of their environmental impact. By comparing HWREs to other options, it can be determined whether their integration makes ecological sense in the evolving landscape of automotive technologies. This assessment will guide decisions towards achieving a more sustainable and environmentally friendly future.

While hydrogen presents solutions to earlier challenges in vehicles, its integration with internal combustion engines (ICE) leads to severe abnormal combustion [14] and increased in-cylinder heat flux [24]. While the WRE is a good match for hydrogen, its higher air-volume ratio can lead to increased heat loss. To reduce the heightened heat fluxes and heat loss, lean mixtures are essential. However, such mixtures have a drawback—they reduce the engine power output. The air-to-fuel ratio, a significant parameter in ICE, plays a crucial role in balancing efficiency and power. When operating lean, efficiency is enhanced by reducing heat loss, but power might decrease.

In this research, the most advantageous technology is identified and the operational details of the air-fuel ratio variation of the HWRE are delved into.

Chapter 1

Literature review

In a time deeply marked by environmental concerns and the pressing realities of global warming, the search for sustainable energy alternatives has gained urgency. One promising direction in this quest is the exploration of hydrogen as an alternative fuel.

This literature review offers an insightful journey into the domain of hydrogen as a sustainable fuel. It starts with an overview of hydrogen's intrinsic characteristics and its production methods. As the review unfolds, the focus shifts to hydrogen's integration into ICE, specifically highlighting the distinctive WRE. Subsequent discussions delve into the importance of heat loss inherent to combustion processes, and the broader panorama of hydrogen-fueled vehicles, encompassing HICE vehicles, hybrids (both composed of a HWRE), and those powered by fuel cells.

The aim is to provide a foundational knowledge base, enabling readers to understand the significance and potential of the HWRE in addressing today's environmental challenges.

1.1 Hydrogen

1.1.1 Hydrogen fuel characteristics

Hydrogen, with its unique properties, holds significant potential as a fuel source, offering numerous benefits for a sustainable energy future. Its efficacy and versatility in various applications are highlighted by several key characteristics gathered in Table 1.1.

Firstly, when considering environmental impact, hydrogen stands out as a champion

of near-zero carbon emissions. As a clean-burning fuel, its theoretical combustion produces only water vapor, excluding all carbon based products such as CO, CO_2 and HC. However, Nox emissions are still present and will be discussed later [22, 25].

Flammability limits are an essential consideration when utilizing hydrogen as a fuel. With an exceptionally wide flammability range of $\lambda = 10 - 0.14$ in air, hydrogen exhibits a broad spectrum of combustible air-fuel ratios. In this context, λ represents the actual ratio of air to fuel compared to the stoichiometric ratio for a specific mixture. A value of λ greater than 1 indicates a lean mixture, while a value less than 1 signifies a rich mixture. This flexibility allows for efficient combustion across a diverse range of conditions, reducing fuel consumption since combustion is ensured even with poor mixture [22, 15, 25].

The quenching distance refers to the distance between the flame front and a surface where the flame extinguishes or becomes significantly weakened. The quenching distance plays a crucial role in the combustion characteristics of different fuels. Hydrogen fuel exhibits a small quenching distance of 0.6 mm, significantly shorter than the 2 mm quenching distance of gasoline [26].

Another significant feature lies in the minimum ignition energy required for hydrogen to ignite. With an exceptionally low ignition energy threshold of 0.02 mJ, hydrogen can ignite easily under various conditions but also lead to severe abnormal combustion as discussed later [22, 25].

Hydrogen's impressive diffusivity further contributes to its suitability as a fuel. It disperses rapidly in the air, facilitating efficient mixing with oxygen for combustion. This property ensures an even distribution of the fuel-air mixture. Furthermore, in terms of safety, the hydrogen high diffusivity enables a quick dispersion preventing unsafe conditions [22, 27].

Moreover, hydrogen high flame velocity over a large range of air-fuel mixtures [28, 15] significantly influences the engine combustion process. It can improve efficiency as it approaches more of a thermodynamic ideal cycle [22] and reduce time for heat transfer. Furthermore, its rapid flame allows ICE to run at higher speeds and thus can increase the power output [22, 15].

Hydrogen exhibits a high auto-ignition temperature, which makes it difficult to ignite by only a rise of temperature by compression [29]. An external source of energy is thus required to start ignition [25], which makes this fuel more suitable for spark ignition engines. This feature also enables to use higher compression ratios, ul-

timately increasing the efficiency [25]. The high auto-ignition temperature and fast flame speed both suggest hydrogen to be more resistant to knocking [30]. Knocking is an abnormal combustion process that occurs when a part of the mixture auto-ignites due to high temperature before it gets reached by the flame front generated by the spark plug discharge. It results in uncontrolled combustion creating high-pressure waves, damaging the engine due to high thermal and mechanical stress [14].

When talking about density, hydrogen has a very high energy per mass density of 120 MJ/kg but a very low mass density of 0.08 kg/m^3, resulting in a low thermal value on a volume basis of 10 MJ/m^3. The mass air-fuel ratio for a stoechimetric combustion is 34.2/1 compared to 15/1 for gasoline [25]. The low density and the relatively high stoichiometric air-fuel ratio result in hydrogen taking about 30% of the combustion chamber volume at stoichiometric conditions, compared to the very low 1 to 2% for gasoline. This observation suggests that the volumetric efficiency of an HICE decreases especially in pre-mixed engines [25]. As a matter of fact, it gives rise to a diminution of the amount of O_2 available for the in-cylinder combustion followed by a decrease of the power and torque output [15, 25].

Property	**Hydrogen**	**Methane**	**Iso-octane**
Chemical formulation	H_2	CH_4	C_8H_{18}
Molecular weight (g/mol)	2.016	16.043	114.236
Density (kg/m^3)	0.08	0.65	692
Mass diffusivity in air (cm^2/s)	0.61	0.16	~ 0.07
Minimum ignition energy (mJ)	0.02	0.28	0.28
Minimum quenching distance (mm)	0.64	2.03	3.5
Flammability limits in air ($vol\%$)	$4 - 75$	$5 - 15$	$1.1 - 6$
Flammability limits (λ)	$10 - 0.14$	$2 - 0.6$	$1.51 - 0.26$
Flammability limits (φ)	$0.1 - 7.1$	$0.5 - 1.67$	$0.66 - 3.85$
Lower heating value (MJ/kg)	120	50	44.3
Lower heating value (MJ/m^3)	10	34	216
Air-to-fuel ratio[a] (kg/kg)	34.2	17.1	15.0
Air-to-fuel ratio[a] ($kmol/kmol$)	2.387	9.547	59.666
Laminar burning velocity[a,b] (cm/s)	290	48	45

Table 1.1: Properties of Gasoline, Methane, and Hydrogen at 1 atm and 300K ([a] at stoichiometric conditions, [b] at 360 K). Adapted from [14] and [15].

1.1.2 Hydrogen production

Hydrogen can be generated through various processes. Depending on the approach, hydrogen is classified into different colors, each indicate its origin and environmental impact. From grey hydrogen, obtained through steam reforming or coal gasification, to blue hydrogen, obtained through steam reforming or gasification coupled with carbon capture and storage, to pink hydrogen, which is generated via electrolysis using non-renewable energy sources, and further to green hydrogen, which is obtained from electrolysis powered by clean energy, the main production methods of hydrogen are going to be explained in details.

Steam methane reforming

There are many possible ways by which hydrogen can be produced, including thermochemical conversion of fossil sources, such as natural gas [31]. One of the most important methods is steam methane reforming (SMR), which represents nearly 60% of global hydrogen production [32].

Before the process begins, the natural gas feedstock is desulfurized and pre-treated with steam. The reason for this is to break down higher hydrocarbons into methane, and to maintain a pre-set steam-to-carbon ratio at the pre-reformer inlet [32, 33]. This is represented in 1.1, in the ZnO (zinc oxide) Bed block. Indeed, ZnO is commonly used as a desulfurization agent in order to remove sulfur-containing compounds from the natural gas. This step is important to prevent undesirable by-products to be produced at the end of the entire process.

The SMR process consists of three main steps. Once the natural gas has been pre-treated, the first step is basically a reaction between methane (CH4), the main component of natural gas, with steam (H2O), to form a synthesis gas (syngas). Syngas contains carbon monoxide and hydrogen [34, 32, 33]. This reaction is endothermic, it consumes energy. Therefore it needs heat which is generally provided by an external industrial furnace (usually fueled by natural gas, as it is shown in 1.1) [32, 33].

$$CH_4 + H_2O \longrightarrow CO + 3H_2 \tag{1.1}$$

The second step of the process is the water gas shift section. It consists in sending the hot syngas that resulted from the previous step through high and low temperature shift reactions. This entails the reaction of the carbon monoxide contained in syngas with left steam, in order to produce more hydrogen, producing carbon dioxide as a by-product [1, 34, 32, 33].

$$CO + H_2O \longrightarrow CO_2 + 3H_2 \tag{1.2}$$

The last step in SMR consists of the separation of the products of the last reaction (hydrogen and carbon dioxide). This is done by chemical adsorption. Indeed, hydrogen is purified in a pressure swing adsorption (PSA) unit. Finally, the offgas from the PSA unit is used to preheat the natural gas before step 1 begins once again [1].

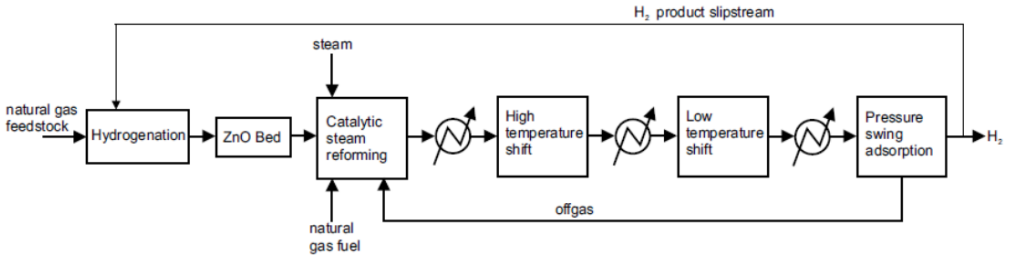


Figure 1.1: Steam Methane Reforming process [1]

The SMR process is considered to be highly efficient, with heating value efficiencies above 70%, reaching over 80% with the secondary utilization of waste streams (using the offgas to pre-heat the natural gas). The overall conversion efficiency of SMR without secondary steam utilization is about 79.2% (or 67% based on lower heating value) [34].

It is important to note that after the third step of SMR, after hydrogen's purification, the carbon dioxide that was produced from the high and low temperature shift reactions is separated from hydrogen, and therefore this by-product is released into the atmosphere. However, the implementation of carbon capture and storage (CCS) is an important advancement in SMR technology. This technology allows the emissions of CO_2 to be reduced, by being able to capture up to 95% of CO_2 produced during the process. The captured CO_2 can then be compressed, transported through pipelines, and stored in depleted gas fields [34]. Efforts to enhance efficiency and reduce carbon footprints are crucial steps in making hydrogen production more environmentally friendly [34, 35].

Partial oxidation and auto-thermal reforming

As it has been stated, SMR is the most spread hydrogen production method, responsible for around 60% of global hydrogen production [32]. However, there are other ways of producing syngas (that can be treated afterwards in order to obtain H_2) coming from natural gas. Among these other methods, there are auto-thermal

reforming (ATR), and partial oxidation (POX) [31].

ATR and POX are similar processes to SMR, where one of the the key differences is the use of high purity oxygen in ATR (in order to minimize the amount of gas that must be treated afterwards) Therefore, this makes these technologies more favorable to CCS, the CO_2 removal process being easier than for SMR [35, 36].

Regarding POX, the idea is that hydrocarbons are partially oxidized to produce hydrogen. Raw materials are gasified during this process, by the means of oxygen and sometimes steam. Compared to SMR, more CO is generated in this way. As it is done in SMR, in the water gas shift section, this CO is going to react with steam in order to produce H_2 and CO_2. Compared to SMR, POX has the advantage that it does not require the desulfurization of the natural gas feedstock. The thermal efficiency of POX reactors using methane as fuel typically lies in the range of 60–75%. POX is not very common, due to the higher production cost associated with the requirement for pure oxygen, as it has already been stated [33, 36].

On the other hand, ATR is as well a catalytic partial oxidation process, with the particularity of the addition of steam. It combines therefore two processes: steam reforming (that is endothermic) and partial oxidation reactions (that are exothermic). This process, is one of the most cost effective solutions to produce low-carbon hydrogen at scale if in its process both the CO-Shift reaction explained in the SMR process is included as well as CCS [37]. It is often stated to be most technological and economic advantageous. Furthermore ATR has several advantages: it does not require external heat, it is simpler, less expensive, and it can quickly be shut down and started, while producing more hydrogen than partial oxidation alone [35].

Coal and biomass gasification, with syngas reforming

Gasification stands out as a prominent method for solid fuels like coal and biomass [31]. The gasification process involves reacting coal or biomass with oxygen and steam to produce syngas, which is further processed through water gas shift reactions and pressure swing adsorption processes, in the same way that it has been described for SMR [1].

Coal, even though it is not very popular in today's environmentally aware world, is still a very important source of energy, especially for power generation. Coal gasification is initiated by introducing dry and pulverized feedstock into the gasifier, where it is gasified with steam and purified oxygen. In the gasification chamber, the feed material gets converted into volatile compounds that combust in the presence

of oxygen, generating heat that enables the gasification of the remaining char as steam is injected. Due to the high temperature inside the gasification chamber, syngas must be cooled down before being treated in order to obtain hydrogen [1, 34].

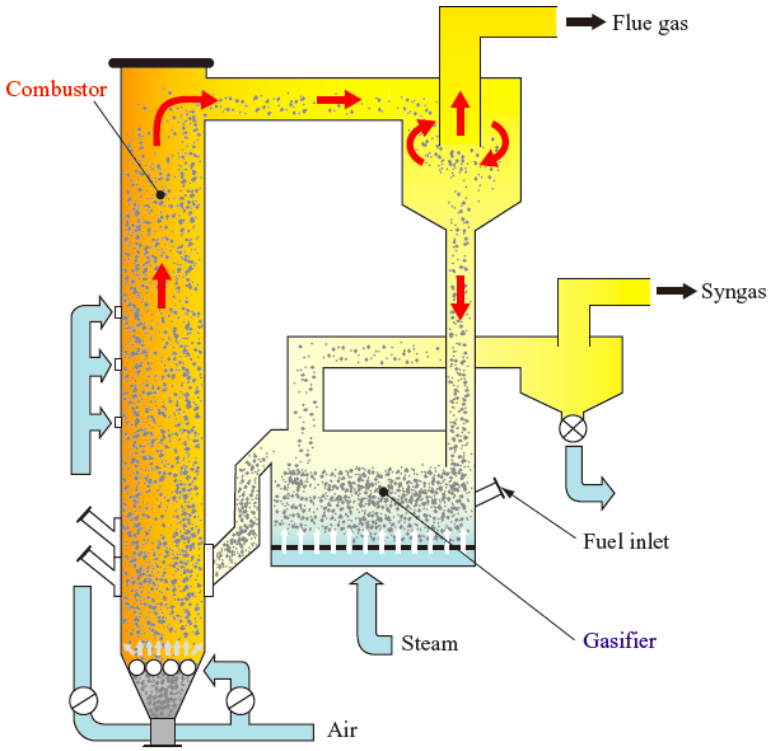


Figure 1.2: Gasification [2]

This technology is considered as an important hydrogen production method mainly because coal is very abundant, because gasification is an efficient and reliable process, and because, in the seek of a greener production, all of the emitted CO_2 is available for capture and can therefore be treated with CCS. The LHV efficiency of the complete process is 72.7% and results in purified H_2 with an output pressure at the PSA unit of 30kPa [1].

Regarding biomass gasification, one of its particularities is that the gasification zone is indirectly heated thanks to the combustion of bed material in a separate chamber. Because of this, air (and not purified oxygen) can be used to feed this combustion. In this way, nitrogen and tar contamination of the product gas is reduced. This reduces nitrogen and tar contamination in the product gas. The cold gas efficiency if this process is of around 73.6% at a temperature of approximately 850°C. After gasification, the product gas is cleaned up, and particles are removed

using methyl ester from rape seed. The cleaned gas then follows the same steps of reforming, water gas shift reactions and pressure swing adsorption that have been described for SMR. This step has efficiency of about 76.3%. The overall LHV efficiency of the biomass gasification process is therefore approximately 56% [1, 34].

Water electrolysis

Electrolysis is an established process for producing hydrogen by splitting water into hydrogen and oxygen using electrical energy [33, 38]. Indeed, it is currently the primary method for producing hydrogen that does not come from direct reforming of carbon carrying fuels. This method is responsible for approximately 4% of the total hydrogen production in the world [1, 3]. It is a crucial process for hydrogen production, most of all in the scope of moving towards a greener alternatives [39, 38].

Regarding how the water electrolysis process works, it basically consists in splitting water molecules into H_2 and O_2. This takes place in what is called an electrolyzer. A basic electrolyzer is composed of an anode and a cathode, covered by a conducting electrolyte, connected through an external power supply. A direct electric current is passed between the electrodes. In this way, electrons flow from the anode to the cathode. The process could be summarized by saying that the hydrogen ions go to the cathode, where therefore H_2 is formed thanks to the electrons that arrive due to the electricity flow (see eq. 1.4), and the hydroxide ions go to the anode, where O_2 is formed (see eq. 1.3). The electrodes are separated by an ion exchange membrane [1].

$$2\mathrm{H}^+_{(\mathrm{aq})} + 2\mathrm{e}^- \longrightarrow \mathrm{H}_{2(\mathrm{g})} \tag{1.3}$$

$$\mathrm{H_2O}_{(\mathrm{l})} \longrightarrow \frac{1}{2}\mathrm{O}_{2(\mathrm{g})} + 2\mathrm{H}^+_{(\mathrm{aq})} + 2\mathrm{e}^- \tag{1.4}$$

The functioning of this basic electrolyzer is summarized in fig 1.3.

This basic electrolyzer is further developed into two main types of electrolyzers: The first one is the alkaline electrolyzer. In alkaline electrolyzers the electrolyte is a strong base. These could be unipolar or a bipolar electrolyzers. The first one is constituted of a tank with alternate positive and negative electrodes. Electrodes of the same sign are all connected in parallel. These alternate positive and negative electrodes are separated by a membrane that separates H_2 and O_2, and lets ions pass through (like in the basic electrolyzer) [33, 3]. This assembly forms a "unit cell", which is afterward connected in series in order to make a plant-scale electrolyzer. The voltage that is applied to the whole assembly of cells connected in series will be the sames as the unit cell voltage with this configuration. As for the bipolar

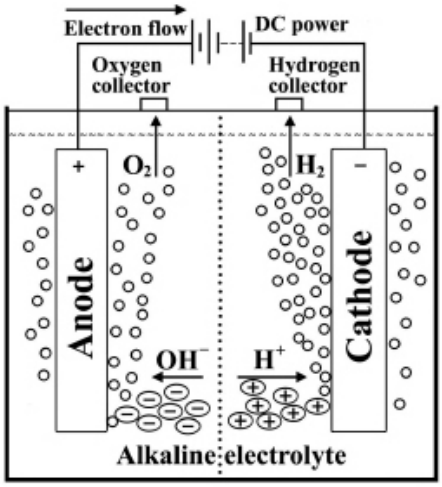


Figure 1.3: Basic electrolyzer [3]

alkaline electrolyzer, a bipole connects electrically adjacent cells in series, provoking the total cell voltage to be the same as the sum of the voltage of each unit cell [3].

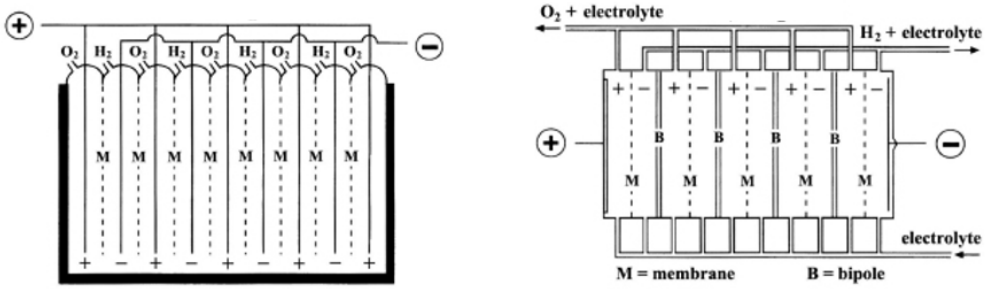


Figure 1.4: Unipolar (left) and bipolar (right) alkaline electrolyzers [3]

Finally, the second main type of electrolyzers is the Solid Polymer Electrolyte (SPE) electrolyzer. This technology is also known as PEM electrolysis, standing for proton exchange membrane. A solid ion conducting membrane is used, and not an aqueous solution [33].

Another technology is the high-temperature electrolysis (HTE) of water at 1100–1250K, that is typically accomplished using yttria-stabilized zirconia (YSZ) as an electrolyte [38]. Its advantages are mainly that it works with a lower voltage and that it has a high current density [38].

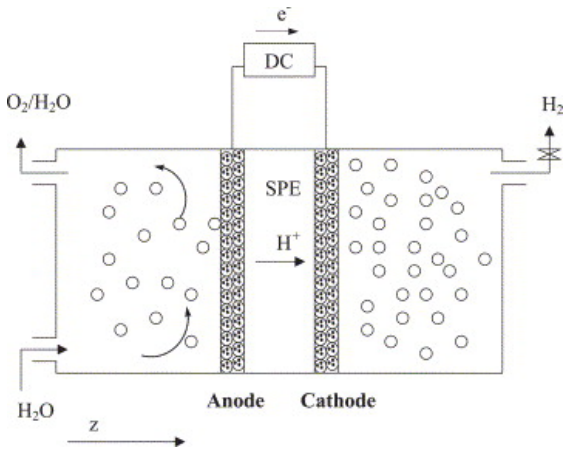


Figure 1.5: Cross-section of SPE water electrolyzer [4]

The efficiency of electrolysis is a very important factor to consider in the context of seeking a more sustainable process for producing hydrogen [34, 1]. When assuming hydrogen as a fuel, the efficiency of the whole electrolysis process depends of course on the electrolyzer's conversion efficiency (the efficiency of converting electricity into hydrogen), but also on the primary energy conversion to electricity and the conversion of hydrogen to motive force by the vehicle for which hydrogen is used as fuel [34, 1]. Current efficiency figures for alkaline electrolyzers fall into the range of 62 to 70%, with potential for improvements through advancements in technology [34, 1]. Efforts are being made to improve the efficiency of electrolysis, and there is potential for further enhancements in the future with technologies like solid oxide electrolysis cells (SOEC). The adoption of high-temperature electrolysis is expected to lead to efficiency improvements. Along with improving electricity utilization and efficiency, efforts are also being made in order to reduce water consumption, which is very high [1].

Electrolysis is a process that has as advantage its modularity. This can be seen in fig.1.6, where the different components forming the process of hydrogen production with electrolysis are shown. Thanks to this property of electrolysis, hydrogen can be produced in a decentralized way, and therefore production facilities can be set up near the market. In this way, investment in hydrogen distribution can greatly be reduced [33, 1]. The choice of technology for electrolysis includes alkaline cells and PEM, with alkaline electrolysis being suitable for larger scales and onshore applications, while PEM offers advantages for offshore use [31]. This is especially beneficial for locations with access to renewable energy sources, such as the North Sea. Indeed, in such locations the production of hydrogen from the electrolysis of desalinated sea water, using electricity coming from wind is a very promising

option [31].

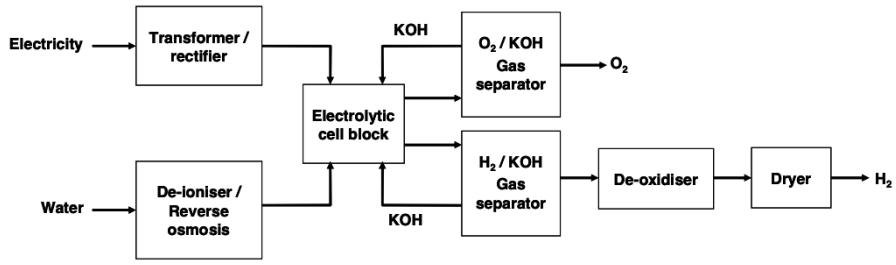


Figure 1.6: Schematic diagram of on-site electrolysis [1]

An important aspect of electrolysis is indeed its potential to use electricity coming in renewable sources (such as wind or hydropower-generated electricity) and in this way reduce environmental impacts and greenhouse gas emissions [33, 39].

1.1.3 Hydrogen in internal combustion engines

The present description explores the combination of hydrogen as a fuel with spark ignition ICE, taking into account its unique characteristics and the challenges associated with this integration.

Firstly, the Nox emissions are still an important drawback of the use of hydrogen as it is present even at a higher rate than gasoline at stoichiometric operations [26]. Indeed, the fast combustion produces high in-cylinder pressure and temperature, promoting the formation of NOx as air is mainly composed of O_2 and N_2. However, its wide flammability limit, its great diffusivity, and its low minimum ignition energy enable the use of lean or even very lean mixtures, reducing the peak temperatures at the end of combustion. Thus the Nox critical threshold of 1800 $[K]$ is not reached, dramatically decreasing its formation in the exhaust gases. [25, 14]. Smaller Nox emissions than engines running with other fuels can even be achieved by running on lean operations [22, 15, 27]. Moreover, even though hydrogen has a carbonless composition, its combustion in an ICE still produces a small amount of carbon-based produced from the combustion of oil on the in-cylinder surface [25].

Furthermore, the low minimum ignition energy can cause abnormal combustion, which is one of the major challenges of using hydrogen in ICE. Indeed, the very low ignition energy can provoke the fuel auto-ignition when in contact with hot spots, hot gases, or even hot remaining particles [25, 14]. Back-fire and pre-ignition

happen respectively during the intake and compression strokes, when the fuel-air mixture comes into contact with those hot spots, causing the mixture to combust in an uncontrolled and undesired manner before the spark plug discharge. It results respectively in an abnormal pressure rise in the intake manifold and in the cylinder, decreasing the power output and causing important damage to the engine. Thus, hot spots should be avoided and the choice of spark plugs is a great deal, where it should be cooled down to avoid abnormal combustion and use specific materials which avoid hydrogen oxidation [22, 25]. An effective means to control these anomalies is to run HICE with lean mixtures. The excess of air present in-cylinder acts as an inert gas reducing the mixture temperature and thus the engine temperature [14].

As can be seen, using hydrogen as a fuel in ICE is a promising technology. However, hydrogen implementation in ICE still comes up with technical issues such as abnormal combustion and Nox emission, promoting the use of lean mixtures, and overall power output decrease of 14% compared to gasoline-based pre-mixed ICE [14].

1.2 Wankel rotary engine

The WRE is a four-stroke spark ignition engine aimed to convert chemical energy stored in fuels into mechanical energy, to finally power an output shaft. This conversion resides in the combustion of an air-fuel mixture in the combustion chamber initiated by a spark, increasing pressure and temperature and finally generating the rotational motion of the output eccentric shaft.

The design of the WRE is simpler than a classical Reciprocating Engine (RPE) in the way that it is made of fewer parts: there is a housing inside which a rotor rotates and transmits the rotating motion to an eccentric shaft. Compared to an RPE, the rotor corresponds to the piston and the connection rod, while the housing corresponds to the cylinder. The rotor rotates around a stationary gear which is fitted to the rotor gear and controls the rotation motion (Figure 1.7). As the rotor moves on, the apex of the rotor draws a peritrochoid shape that corresponds to the inner part of the housing (Figure 1.8). The working chamber lies between the inner part of the housing and the rotor's surface, sealed by the apex seals, and moves as the rotor rotates. Finally, the housing contains intake and exhaust ports directly controlled by the rotor's motion [5, 40].

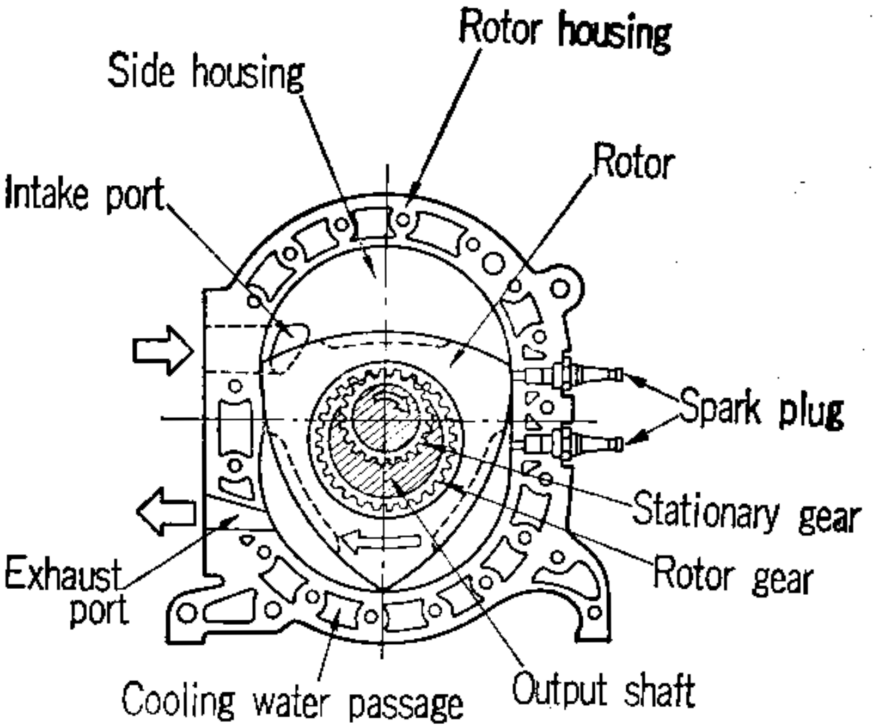


Figure 1.7: Basic construction of WRE [5]

Advantages

The Wankel engine offers a significant advantage by eliminating reciprocating parts that move back and forth in a linear manner. Its unique architecture, with only the rotor and eccentric shaft in motion, generates a smooth rotary movement without the need to convert linear motion into rotary motion. As a result, vibrations are dramatically reduced and it enables faster rotation. Furthermore, the rotor, housing and eccentric shaft design allows eliminating the need for additional components like connecting rods, valves, and camshafts. The absence of reciprocating movement and fewer parts allows for higher rotational speed and makes the engine lighter. Furthermore, as the rotor and eccentric shaft rotate, the working chambers execute the four strokes. Once one of these working chambers has completed the four strokes, the entire cycle has been repeated three times. Indeed, the rotor is made of three faces forming three different chambers with the inner part of the housing, all of them undergoing the four strokes cycle simultaneously, with a phase shift of 120° of the eccentric shaft. Thus, as the eccentric shaft rotates three times for one rotor rotation, there is one power cycle per shaft rotation. Then, focusing on one combustion chamber, the four-stroke cycle lasts 1080° of the output shaft

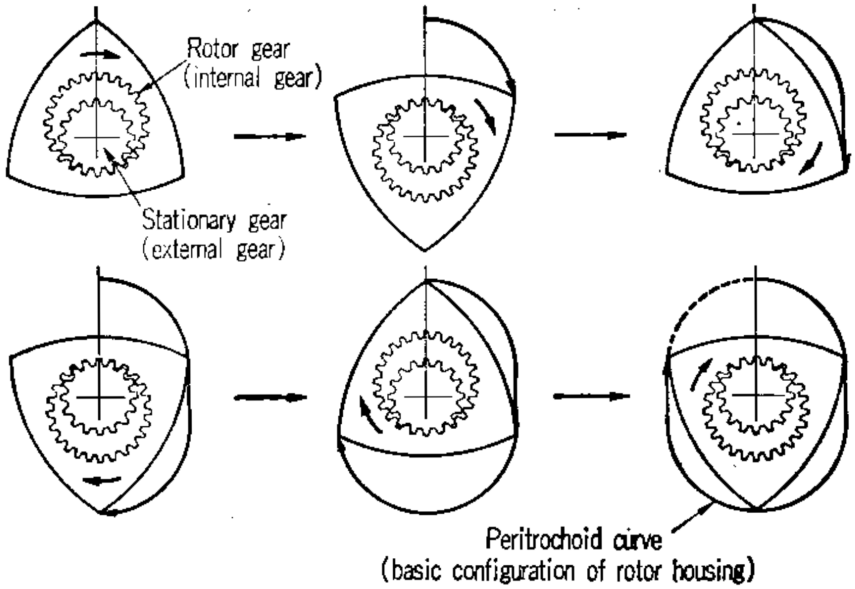


Figure 1.8: Rotor motion and peritrochoid generation [5]

resulting in a duration of 270° per stroke, compared to 180° for a RPE as shown in Figure 1.9. At constant and high rotational speed the WRE will thus have 1.5 times more time to breathe during the intake stroke which can be translated as higher volumetric efficiency. Finally, the architecture of this engine leads to the separation of the 4 strokes process. Indeed, intake, compression, expansion, and exhaust strokes happen all in different areas of the engine. Compared to a RPE, this advantages the Wankel to be more resistant to pre-ignition and backfire as the fresh and cold mixture is less likely to come into contact with hot spots, hot gases or hot residual particles. All these advantages combined lead at the end to a high power-to-weight and high power-to-volume ratios which are the main advantages of the Wankel engine [5].

Disadvantages

The typical geometry of the WRE also brings disadvantages which made the engine disappeared today. The long and narrow combustion chamber shape is at the origin of a lot of those disadvantages. Indeed, it features a higher surface-to-volume ratio, and severe quenching effects[23]. Moreover, as mentioned here above the longer strokes of 270° leads to prolonged exposure of the combustion gases to the chamber walls. Both larger ratio and longer combustion stroke increase the heat transfer loss

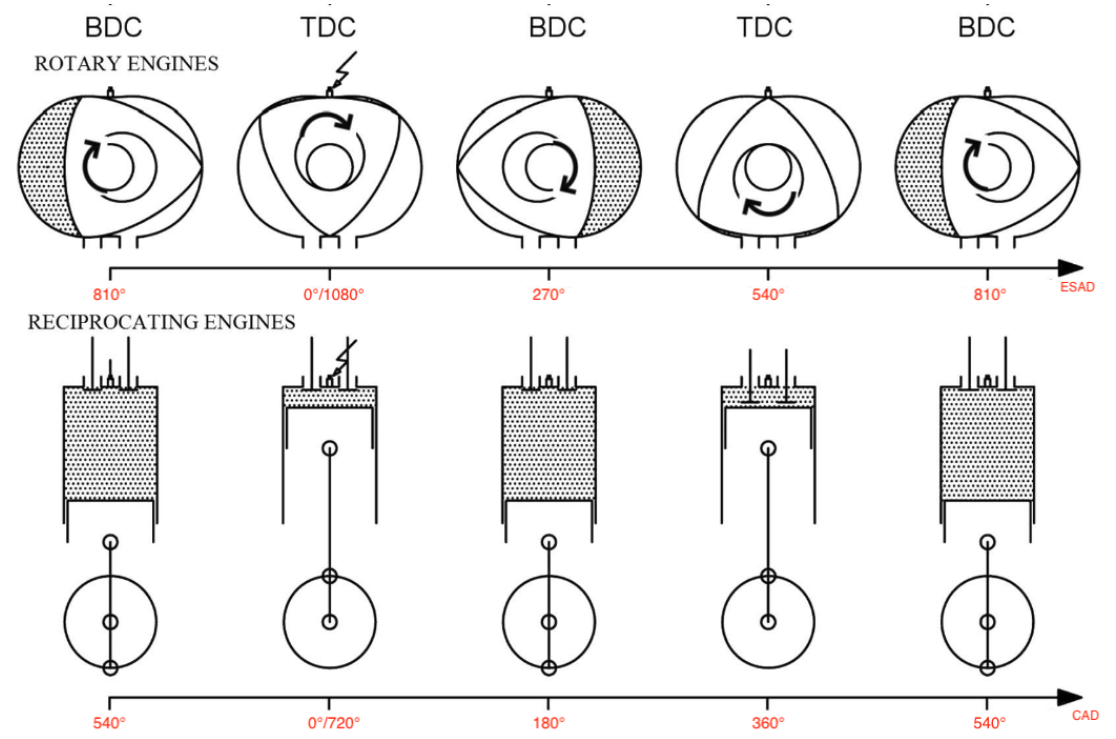


Figure 1.9: WRE and RPE strokes. Adapted from [6]

through the walls. The quench effect along those long walls also induces unburned gases and increasing emissions. The WRE also suffers from gas leakage due to weak seals between the combustion chambers [5]. These leaks cause two main problems. Firstly, some not fully burned gases moves from the combustion chamber to the exhaust stroke, increasing emissions. Secondly, some gases leak from the combustion chamber to the intake stroke, decreasing the combustion efficiency. At the same time, those apex seals need to be lubricated and thus implies a direct injection of oil into the combustion chamber which increases hydrocarbon emissions when burning. Finally, the rotating motion of the rotor implies a main flow field in the direction of rotation. This makes the complete combustion of rear mixture more difficult and increases HC emissions [23]. All these phenomenons led the WRE to feature high emissions, poor thermal efficiency and thus poor fuel consumption[41, 5, 42, 43].

Advantages	Disadvantages
• No reciprocating motion • Less vibration • Higher rotational speed • Fewer parts • Smaller and lighter • Better torque fluctuation • Longer stroke • One power cycle per shaft rotation • Higher power-to-weight ratio • Higher power-to-volume ratio	• Long and narrow shape • Higher surface to volume ratio • Longer stroke • Higher emissions • Lower thermal efficiency • Higher fuel consumption • Leakage • Burns oil

Table 1.2: Advantages and drawbacks of the Wankel rotary engine

1.3 Hydrogen Wankle rotary engine

Initially, employing hydrogen in ICE shows potential, though it comes with significant technical challenges. On the other hand, while the WRE has fallen out of favor due to substantial drawbacks that make it impractical today, there appears to be a notable compatibility between hydrogen and the WRE.

A first notable synergy emerges when pairing the WRE with hydrogen. In the Wankel engine, the four-stroke locations are physically distinct, and there's an absence of potential heat sources like valves. This configuration prevents the fresh hydrogen mixture, which is susceptible to back-fire and pre-ignition, from interacting with hot spots and residual particles [44, 45].

Furthermore, as mentioned earlier, the WRE has a small thermal efficiency due to its narrow and long combustion chamber shape, including large quenching effects and thus high HC emissions. However, hydrogen allows to counterbalance those negative effects with its small quenching distance, enabling a more complete combustion along the walls and in small areas. Hydrocarbon emissions are set to near-zero from the carbon-free characteristic of hydrogen.

The WRE inherent high-speed capability complements the rapid combustion characteristics of hydrogen. However, this high-speed feature can shorten the intake charge mixing time, potentially leading to non-homogeneous air-fuel distribution. However, with hydrogen's enhanced diffusivity, it can achieve effective mixing even within this reduced mixing time [23].

It has been mentioned that the rotating motion of the rotor implies a flow filed in the direction of the rotation, making complete combustion more difficult by the rear of the combustion chamber. However, hydrogen fuel having a high flame velocity, makes its propagation possible by the rear area. It thus results in a more complete combustion [23].

Although hydrogen has a high power-to-mass ratio, its low mass density results in a diminished volumetric heat value. Additionally, the use of hydrogen favors lean mixtures, which further reduces the power output. Consequently, pre-mixed Hydrogen Rotary Piston Engines (HRPE) produce lower power outputs than their gasoline-based counterparts. However, the inherent high power density of the WRE can offset this difference [23].

In the end, the use of hydrogen in the WRE reduces dramatically emissions, increases thermal efficiency, and is less prone to abnormal combustion. Stutenberger et al.

concluded that the HWRE is capable of providing similar power density and thermal efficiency as gasoline-based RPE with a dramatic decrease in Nox emissions [46].

1.4 Heat loss in internal combustion engines

As the combustion progresses within the cylinder, both the pressure and temperature within the cylinder increase, leading to a heat exchange between the cylinder's mixture and the combustion chamber walls. These heat transfers act as parasitic processes, removing a substantial portion of the fuel's energy as thermal energy from the cylinder, which decreases efficiency. This is an inherent occurrence in ICE, given that the peak temperature of the combusted gas can reach a high of 2,500 Kelvin. When dealing with a specific amount of fuel, an increased level of heat transfer will lower the cylinder's temperature and pressure, causing a decrease in piston work. This effect has a direct impact on both the engine's power and its efficiency [40].

Shudo et al. investigated the degree of constant volume and heat loss in a four-stroke four-cylinder HICE in [47]. They observed that the reduced quenching distance of hydrogen can lead the fuel to burn nearer to the cylinder walls and consequently increase heat loss. Furthermore, the rapid combustion process of hydrogen may enhance convection between the mixture and the cylinder walls, thereby increasing heat transfer. These effects ultimately degrades thermal efficiency.

Demuynck et al. conducted a comparative analysis of heat loss across hydrogen, methane, gasoline, and methanol in a single-cylinder four-stroke engine in [24]. Their findings revealed that hydrogen fuel exhibited a higher heat flux measurement and peaked at values approximately three times higher than other fuels. A similar heat flux measurement of hydrogen to that of other fuels can be reached when using lean mixtures. They emphasized the importance of operating HICE with lean mixtures to reduce heat flux and maintain good efficiency. Their data showed that when the air-fuel ratio was reduced from 2 to 1, the indicated efficiency decreased from 29% to 23%, and heat loss increased from 23% to 37%.

1.5 Hydrogen fueled vehicles

As it has been explained, the Wankel engine seems to be the ICE that best suits with hydrogen as a fuel. Therefore it is important to see the history of this application. Mazda has done a lot of research in this field and has already produced concept cars, as well as cars that were allowed to circulate using this technology.

1.5.1 Hydrogen Wankel rotary engine vehicles

The first hydrogen rotary engine vehicle was introduced in 1991 by Mazda, under the name of HR-X. This car was declined for other trials like the Mazda RX-8 Hydrogen RE and the Mazda5 Hydrogen RE Hybrid.

After further research, 1993 was a great year since a more developed version of the HR-X was introduced, the HR-X2. This same year, a new vehicle was developed and tested: the hydrogen fueled MX-5. Opposed to the original MX-5, having a 1.6 liters RPE, this vehicle was composed with a two-rotors 1.3 liters hydrogen rotary engine, the same one as the one in the RX-7, but this time fueled with hydrogen. The hydrogen tank filled up the trunk of this car, making it therefore unusable. Not only the tank took all of the space in the boot, but also the driving range of the car was only of 100km. It is also a much heavier vehicle than the classic model, weighing 1224 kg whilst the latter weighted 975kg.

A decade later, in 2003, the hydrogen fueled RX-8 was introduced, having more or less the same range as the hydrogen fueled MX-5, with an autonomy of 96.6km. What was witnessed after its introduction was that some of the measurements were less efficient than the low-power petrol version of the original RX-8. Since petrol is much denser than hydrogen, both the power of the vehicle and the torque decreased with the latter version. In the petrol one, there was a power of 189 hp and a torque of 220 Nm. Both of these measures dropped to 105 hp and 140 Nm with the introduction of the hydrogen as a fuel. The following year after its development, in 2004, Mazda got the MLIT approval for the vehicle to be tested on the public roads, for it to be successfully commercialised from 2006, leased as the Mazda RX-8 Hydrogen RE. This made Mazda the first company worldwide to get such an achievement with a hydrogen rotary engine.

1.5.2 Hydrogen Wankel engine in hybrid vehicles

Another application where the HWRE has been employed was in hybrid vehicles. There are three different types of hybrid vehicles: the parallel ones, for which wheels are being simultaneously driven by the engine and the electric motor, the series-parallel, for which wheels are driven either by the engine, the motor or both, and the series, for which the wheels are driven by the motor and the output of the engine is always converted into electricity.

Mazda started with the commercial leasing of its Premacy Hydrogen RE Hybrid in 2009. It was composed of a series hybrid system. Mazda chose series because they claimed that this configuration allowed to take benefits from the semiconductor transformers as well as the magnetic motors which were of high performance. It all resulted in very efficient energy transfer [48].

In this vehicle, having a series configuration, the wheels are driven by an independently-developed motor which consumes electricity produced by the generator. A particularity of the engine in this hybrid vehicle was that it made use of the dual-fuel system: it could run on hydrogen and on gasoline. In order to compensate the drawback of the hydrogen fueled RX-8, having its tank occupying all the trunk, this vehicle was a minivan composed by three rows of seats, where the last row area is replaced by the location where the hydrogen tank is placed [48].

The efficiency of energy conversion in such vehicles is crucial, since the energy from the engine's output is firstly converted into electricity, and afterwards this electricity is the one that must be converted back in order to produce a torque. This vehicle seemed as a great opportunity, since not only the performance results compared to the hydrogen fueled RX-8 were greatly enhanced, but also there was still potential for developments, since generators and motors with a more important efficiency will surely be produced in the future. Indeed, the Primacy Hydrogen's range was improved by twice compared to the RX-8: going from almost 100km to up to 200km, even though the weigh of the Primacy Hydrogen is much heavier. Not only the range improves but also the power is much increased by 40%. The overall efficiency is also related to the gear's efficiency, but there is less room for improvement in that sector [48].

Lastly, an important feature of series hybrid vehicles, is that, since the engine is not directly connected to the wheels, but is only there in order to produce electricity, it can always run at the same speed, at the one for which its operation is the most efficient. However, this was not the case in this Mazda vehicle, since they wanted to keep a feeling as if the engine powered the wheels directly, and therefore as the driver accelerated, the engine ran at a higher speed [48].

It is interesting to point out the fact that Mazda is bringing back the rotary engine, with a vehicle with this powertrain configuration. Indeed, in its new MX-30 e-Skyactiv R-EV, a single rotor Wankel engine is included, acting as a range extender in a series hybrid configuration. It is however a gasoline fueled engine. It has a tank storing 50 liters of gasoline, that allows its range to be extended by about 500 km.

1.5.3 Fuel cell vehicles

Nowadays, the predominant use of hydrogen as a fuel in the automotive sector is found in FCVs. Fuel cells are devices where an electrochemical process takes place, which converts energy between chemical and electrical forms, converting hydrogen-containing fuels into electricity and thermal energy [49, 50].

There exist different fuel cells, using different fuels. In this type of cells, the ones being fueled by hydrogen, as electricity is produced, the only by-product coming out of the chemical reaction between hydrogen and oxygen is water.

The functioning of hydrogen-oxygen cells is very similar as the one that has been explained for water electrolysis, but it is reversed. Indeed, the cell is composed of two electrodes, that are one at each side of the electrolyte (where ions move). The anode and the cathode are connected, and electricity will flow between them. Opposed to electrolysis, here, the anode is negative and the cathode is positive. The electrodes are made of porous carbon, containing tiny holes, which contain a catalyst in order to speed up the reaction. The outer side of the cell is composed of the anode and cathode compartments, with an inlet at top of each one. Hydrogen enters in the inlet of the anode, whereas oxygen enter at the inlet of the cathode compartment. As the reaction is completed, water and heat leave by the outlet of the cathode compartment.

In the anode, the oxidation of hydrogen takes place. Indeed, an electron is removed from each atom, giving as product two hydrogen cations (two protons) and two free electrons.

$$H_2 \longrightarrow 2H^+ + 2e^- \tag{1.5}$$

These free electrons will move towards the cathode, passing through the wire that connects both electrodes. In this way, electricity is produced.

On the other hand, in the cathode, the reduction of oxygen takes place. Indeed, ions move through the electrolyte, from the anode to the cathode. There, they react with oxygen that entered through the cathode compartment's inlet, producing water.

$$O_2 + 4H^+ + 4e^- \longrightarrow 2H_2O \tag{1.6}$$

To sum up, fuel (hydrogen) enters the cell through the anode's compartment inlet. Once inside the cell, the fuel becomes oxidized. As this happens, it sets up a

potential difference across the cell, and electricity is produced. Therefore, the overall equation obtained is expressed as follows:

$$O_2 + 2H_2 \longrightarrow 2H_2O \tag{1.7}$$

There are different types of fuel cells. These types are classified according to the combination of type of fuel and oxidant, to the type of electrolyte and to the temperature of operation [50]. Here are some of them:

- Polymer electrolyte membrane fuel cell (PEMFC)
- Phosphoric acid fuel cell (PAFC)
- Molten carbonate fuel cell (MCFC)
- Solid oxide fuel cell (SOFC)
- Direct methanol fuel cell (DMFC)

The most used fuel cell type in today's vehicles is the PEMFC. This choice is justified by their low operating temperature (around 80-100°C), their quick start-up time and their high efficiency. Another advantage for the usage of this type of fuel cells in vehicles is that they have a solid electrolyte. Indeed, their electrolyte is made of a material known as a perfluorosulfonic acid membrane, generally Nafion [51].

This technology looks interesting for replacing ICE, or batteries in vehicles. Indeed, it only requires abundant elements such as hydrogen and oxygen, and on top of that, there is no pollutant waste being produced during its operation. Furthermore, their high energy density and their high electrical efficiency motivates this statement. Indeed, the electrical efficiency of PEM fuel cells is around 40%, and when the heat is used the total efficiency of fuel conversion is around 90%. Moreover, this looks even more interesting as it is clear that today's electricity grid around the world is still dirty, and FCVs do not need to be recharged. On top of all of these advantages of FCVs, it is important to note that they include most of BEVs advantages, such as having zero emission at tailpipe, high efficiency, and a silent operation, as well as most of ICEVs advantages, such as having a long lifetime, a long driving range and a short refuelling time [49, 51, 52, 50].

Nevertheless, certain technological challenges exist. The utilization of platinum poses concerns regarding its limited accessibility and environmental consequences. Additionally, PEM fuel cells are sensitive to fuel impurities, necessitating a high level of fuel purity, which increases its complexity and cost. Moreover, they face

similar problems as other hydrogen-powered vehicles, like difficulties in the production and the storage of hydrogen. As it was mentioned, producing hydrogen needs energy, and if this energy is obtained from fossil fuels, the eco-friendly advantages of this technology loose their interest [49, 52] .

PEMFC system is composed of two parts: the power unit or fuel cell stack, and its direct auxiliaries or the balance-of-plant (BoP) [51].

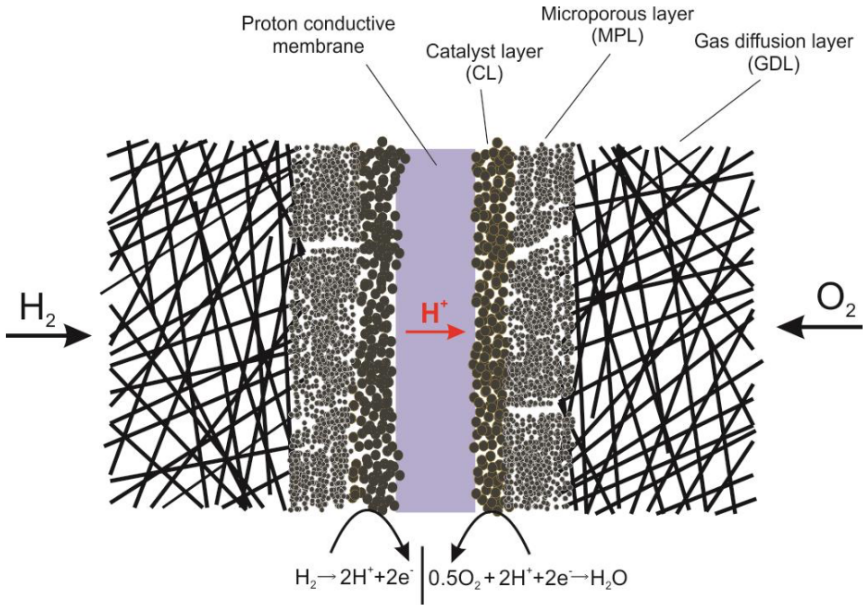


Figure 1.10: Individual PEM cell

Firstly, there is the fuel cell stack, which is composed by several individual cells. An individual cell is composed of an electrolyte (the proton conductive membrane), of a catalyst layer on each side, followed by a distribution layer. This whole assembly is known as the membrane electrode assembly (MEA). At each side of the MEA, there is a contact layer. Thanks to these contact layers, several individual cells can be combined and form a unit with the desired output capacity. This combination of individual cells is then followed by a current collector on each side, a seal gasket and finally an end plate and stack thermal insulation. This whole assembly is basically the fuel cell stack [50].

Secondly, there is the BoP, the auxiliaries of the stack. It is composed of the essential BoP, which ensures all system operating modes. This part of the BoP is composed of the air and the fuel delivery system, as well as the thermal management

system, and the recycle streams. Moreover there is the ancillary BoP, that ensures power management and system control. Lastly, there is the external BoP, that maximizes the energy efficiency, composed of pressure vessels and a waste heat recovery system [50].

1.5.4 Hydrogen storage

Vehicles fueled with hydrogen need what is called a "compressed hydrogen storage system". This system is composed by hydrogen storage tanks, and its base of plant which contains the auxiliary components. There are several kinds of hydrogen storage tanks, they are classified into different types (I, II, III, and IV). Today's FCVs use type IV tanks [53].

Type IV tanks are designed to store compressed hydrogen at 700 bars. They are built with a composite material and do not contain a metal liner. Indeed, they contain a non-metallic internal liner, made of composite materials such as high-density polyethylene (HDPE), followed by an external wrap made out of carbon fiber and other interlaced thermoplastic polymers. With this characteristics, they are up to 70% lighter than Type I tanks. They are therefore great for applications requiring high pressures and low weight, which matches perfectly mobile applications [53].

Regarding its BoP, first it has to allow hydrogen to arrive to the tank. Therefore, it is composed by a filling receptacle and a network of pipelines before arriving to the tank valve. After that, it has to allow hydrogen to arrive from the tank to the fuel cell or to the hydrogen fueled ICE. In order to allow this, it is composed of one or two pressure regulators, which reduce the gas pressure. It is also composed of a gas handling unit which contains ventilation lines, valves, and indicators to monitor the system's temperature and pressure. The aim is to lower the hydrogen pressure and keep it within the needed range for the fuel cell or ICE. If the pressure goes beyond the maximum needed level, excess hydrogen is released through valves [53].

1.5.5 Assessing the vehicle's viability

In order to evaluate the viability of these hydrogen fueled vehicles, their environmental impacts can be calculated and compared by doing a Life Cycle Assessment (LCA). An LCA is a study that investigates the environmental impacts of a product throughout its existence. It is composed of four main stages, being the definition of the goal and scope of the study, the filling of the life cycle inventory (LCI), the calculation of the impacts in several impact categories during the life cycle impact

assessment, and the interpretation of these results.

It is important to point out that LCAs often end up with results that differ and that, at first sight, do not seem to go in the same way. Several aspects play an important role and can influence the study's outcome. One of the reasons can be the way in which the inventories are filled up. These are often simple, and simplify the process that they represent. In other cases, they are completely developed and take into account every aspect to consider, as it should be. Another potential source of disparities related to the inventories is that, for instance, authors consider a stationary applications rather than mobile for the case of a fuel cell LCA, which have very different characteristics. Many times, authors do not publish inventory data (mainly due to reasons of commercial data protection [54]), or if they are shown, this is often done at a very high level of aggregation so it is complicated to evaluate if disparities are due to this [54]. Finally, a last source of problems linked to the inventory could be that a database was not used in order to fill out the inventory. Instead, by not using a database, the author filling out the inventory could neglect many impacts coming from background processes that he did not even think of [49] [51].

Another point from where differences might come from is the environmental impact that a study chooses to assess. Indeed, it is important to evaluate the full range of impacts, in order not to miss out a potential contribution that will lead to disparities in LCAs outcomes [49].

Furthermore, disparities may come from the fact that different temporal scenarios might be considered. Indeed, taking into account the past, the current, or the future performance of a product might lead to great disparities [51]. Also, the fact of assessing different impact categories might lead to confusing results [52].
Another source of difference is the chosen scope. Indeed, for vehicles LCAs for example, many assessments focus on the energy carrier's LCA, only taking into account the production and end-of-life of vehicles approximately. Furthermore, the assumptions made for the analysis might have an impact in the results. For instance, assumptions are often made regarding fuel consumption. The problem with these kinds of assumptions is when they do not match with the chosen vehicle size, or with the kind of powertrain assessed [52]. Finally, if the author lacks informations on crucial aspects of the assessed product, an excess of hypothesis has to be done, which might lead to important disparities [54].

1.6 From literature to inquiry

Hydrogen has emerged as a compelling alternative fuel in ICE due to its numerous advantages. Concurrently, while the WRE faced challenges leading to its decline, its pairing with hydrogen appears to offer new potential.

In the pursuit of a more environmentally friendly automobile industry, from the previous observations, the evaluation of the feasibility of vehicles using the HWRE is motivated. This type of powertrain has shown versatility, being applied in various configurations like traditional ICEVs or series hybrid powertrains. To comprehensively gauge the potential of such vehicles, it becomes crucial to compare them against other promising technologies that could also be the protagonists of a green automotive sector, including FCVs and BEVs. In this context, where do HWRE-powered vehicles position themselves? To address this inquiry, a thorough LCA is conducted to determine where HWRE-powered vehicles stand in relation to their environmental impact and potential contribution to a greener automotive industry.

One significant challenge with hydrogen, as pointed out in the literature review, is the occurrence of severe abnormal combustion and heightened heat flux, necessitating the operation of HICE under lean conditions. However, lean operation inherently reduces power output. The WRE, with its distinct architecture, possesses a higher surface-to-volume ratio and longer strokes. This leads to increased heat loss and diminished efficiency. Furthermore, the air-fuel ratio plays a pivotal role in ICE, influencing combustion behavior, power output, efficiency, and heat loss, making it essential for understanding WRE interaction with hydrogen. Considering hydrogen's inclination towards lean operation, its consequent effects on engine behavior, and the inherent characteristics of the WRE, a question arises: What is the optimal trade-off between efficiency, as limited by wall heat loss, and power output in HWRE, considering variations in the air-to-fuel ratio as a means to control heat transfer and combustion characteristics?

After delving into an LCA to ascertain the position of the HWRE within the industry, the intricacies of how varying the air-fuel ratio influences engine operations, power output, efficiencies, and heat loss are examined. This dual-pronged approach is pivotal: the LCA offers insights into promising technologies worth further exploration, while the air-fuel ratio analysis provides guidance on optimal engine operations. Through this comprehensive study, the aim is not only to pinpoint the most promising technology but also to understand the operational nuances that could enhance the application of such a technology.

Chapter 2

Methodology

This section outlines the methodology adopted to probe the chosen subject. It describes the precise methods and techniques employed for data collection and analysis, providing readers with clarity on the derivation of conclusions.

Initially, emphasis is placed on the big-picture perspective and develops a methodology relative to the viability of vehicles. Subsequently, emphasis is placed on the small-picture perspective and develops the methodology relative to the performance of the HWRE.

2.1 Viability of vehicles

In this section, emphasis is placed on the big-picture perspective. The procedure adopted to ascertain the viability of vehicles is comprehensively articulated. This methodology captures every phase of a LCA, from defining the goal and scope, to elaborating on inventory-filling methods, clarifying impact assessment techniques, and framing the approach to normalize results while gauging their sensitivity to diverse factors.

2.1.1 Life cycle assessment

The aim is to evaluate five different vehicles, in order to explore the potential of the HWRE, to gauge its feasibility in the automotive industry.

The initial vehicle under consideration is a series hybrid vehicle, utilizing a rotary engine as ICE, as it is the case in the new Mazda MX30 R-EV (however in this case the engine is going to be fueled with hydrogen). This vehicle is going to be called

HEV_A throughout this study. The second vehicle that is going to be considered is also a series hybrid vehicle, containing a HWRE. However, for this vehicle, the battery is going to be much smaller, and the hydrogen storage tank considerably bigger. In this way, there will be a 0 km full-electric range, the total autonomy of the vehicle being dependent in the electricity generated by the generator linked to the HWRE. This vehicle is going to be called HEV_B throughout this study. The third vehicle to be evaluated consists of another promising technology that uses hydrogen: it is a FCV. Additionally, the assessment will include a Battery Electric Vehicle (BEV), sharing the same range as the hybrid vehicles. This comparison between the BEV and hybrid will offer valuable insights. Lastly, a fifth vehicle will be examined, an Internal Combustion Engine Vehicle (ICEV) with a HWRE. This ICEV's unique characteristic lies in its requirement to function at various speeds, unlike the hybrid vehicle, where the engine can operate always at its optimum operation point, since its aim is specific to generating electricity.

2.1.2 Software and tools

In this research, the Activity Browser software, which is an open-source tool designed for LCAs was used. This user-friendly software allows a simple comparison of reference flows and a representation of their impacts among different categories. Furthermore, this software offers advanced analytical features, such as results categorized by impact categories, visual representations like Sankey diagrams, Monte Carlo simulations, and Global Sensitivity Analysis. These analytical results provide valuable insights into the problem being studied. For example, the user can examine the Sankey diagram, and in this way it becomes easier to understand where the contributions of the impacts for one product come from [55].

The version 3.9 of the Ecoinvent database is used in order to fill out an important part of the Life Cycle Inventory. The detailed explanation of what the LCI is and how it is completed comes in the following subsections.
Based in Zurich, Switzerland, Ecoinvent is a non-profit organization globally known for its provision of high-quality environmental data used to fill LCIs. Ecoinvent actively engages in collaborative projects and initiatives aimed at promoting best practices in LCI data creation and utilization. This organization is also known for its commitment to transparency, traceability, and data disaggregation. Ecoinvent's participation in partnerships and projects helps enhancing global standards for LCA methods [32].

This database comes with different system models. Understanding these system models is crucial in order to get a relevant result for the desired scope, that is going to be explained later. Among the possible models, the "allocation, cut-off by

classification", the "allocation at the point of substitution", or the "substitution, consequential, long-term" can be found.

Among their differences, one can find:

- The way by-products are handled (the way in which the problem of multi-functionality is solved)
- The way burdens for waste treatment are considered
- The way consumption mixes are supplied

For the first point, the multi-functionality problem refers to the fact that an activity is going to deliver a reference product, but it can produce several by-products as well. In both allocation models, burdens are shared among all the co-products. However, in the substitution model, the reference product will be burdened with the full impact of the activity.

For the way burdens for waste treatment are considered, allocation, cut-off by classification and the substitution model do the same thing: they give full responsibility to the producer of the waste. On the other hand, in the allocation at the point of substitution model, burdens associated to treatment of the waste will be shared between all possible valuable products generated. Indeed, if the treatment of waste has a valuable product, there is a "system expansion" in order to allocate it together with the reference product.

For the last point, for both allocation models, all suppliers supply the market. However this is not the case for the substitution model, where only those who can adapt to changes in the demand from the market can supply. These suppliers are called "unconstrained" or "marginal suppliers".

In order to make the long story short, it is crucial to understand that in the cut-off by classification model, the use of secondary materials is motivated, but there is no credit for useful products in waste treatment, since waste treatment burdens were given to waste producers. There is therefore no encouragement towards waste treatments that would produce beneficial products - towards improving technology around waste treatment. On the other hand, in the allocation at the point of substitution model, waste producers are motivated to assess recycling (this is due to the partial allocation of impacts to useful treatment products).

2.1.3 Goal and scope

At the start of an LCA, before collecting any data, goal and scope must be defined. As explained in the ISO 14040 and 14044 standards, this step is more than just a simple introduction to the LCA. Indeed, it is a very crucial step, because it is in this step where the way that the whole study will be approached is decided [56]. If the goal and scope are not well defined, two LCAs that were supposed to study the same product will end up with findings that finish by being different and insconsistent [8].

According to ISO 14040, a proper goal definition should state the reasons for carrying out the study, the intended audience, and whether the results are intended to be used in comparative assertions intended to be disclosed to the public [56]. In other words, it should be clear from this definition why the LCA study is being undertaken, what the application areas of the results are and who the potential audience is [57].

Based in the statements explained by this standard, the goal for this study is defined as follows: the main goal of this LCA study is to find environmentally friendly applications for the Wankel engine in the automotive sector by using hydrogen as a fuel. The motivation behind this research is the urgent need to reduce carbon emissions. Switching to hydrogen as a clean fuel is crucial, and the Wankel engine is a promising match for this purpose. This LCA study aims to propose two potential applications for the Wankel engine using hydrogen as its fuel: one in a HEV and the other in an ICEV. The objective is to compare the environmental impacts of these applications between them and with other promising sustainable technologies, such as FCVs and BEVs. By assessing the entire life cycle of these vehicles, including manufacturing, operation, and end-of-life, the study will identify each application's impacts and discuss which is more sustainable. The results will be helpful for decision-makers, policymakers, and the public to understand the environmental benefits and trade-offs associated with different vehicle technologies. To recap, this LCA seeks to contribute to a greener automotive sector, aiming to address the challenge of carbon emissions by proposing cleaner and more sustainable options, based on the idea that Wankel engine makes a great match with hydrogen as a fuel.

Regarding the scope definition, the following items should be defined. Firstly, the product that is being assessed has to be clearly identified [57]. In this case, the product is composed of five vehicles: the HEV_A, the HEV_B, the ICEV (the three of them having a HWRE as ICE), the FCV, and the BEV. The abbreviation that is going to be used foe each one of these vehicles is detailed in table 2.1.

After that, the product's system boundary should be defined. The system boundary

Notation	Description
BEV	Battery Electric Vehicle
HEV_A	Series Hybrid Vehicle
HEV_B	Series Hybrid with no Full-Electric Range
FCV	Fuel Cell Vehicle
ICEV	Internal Combustion Engine Vehicle

Table 2.1: Vehicles assessed

defines which processes to include for the assessment [57].

There are three main types of LCA boundaries:

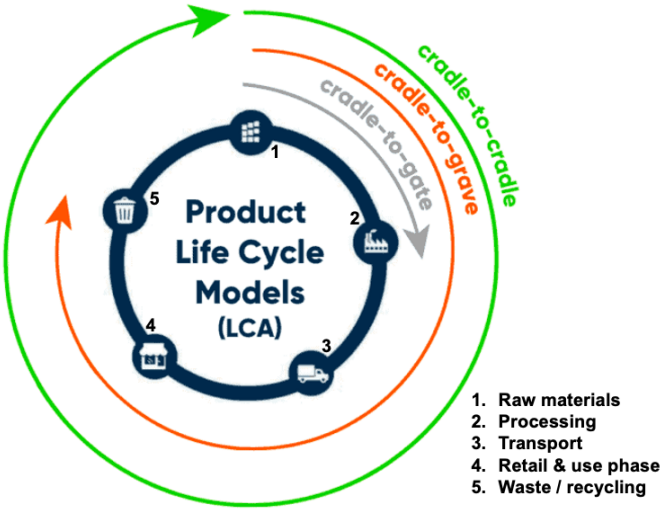


Figure 2.1: Life Cycle Models in LCA [7]

- **Cradle-to-gate** : Evaluation of a product's impacts until it is ready to leave the factory and go to the consumer (it includes steps 1 and 2 of fig.2.1).
- **Cradle-to-grave** : The assessment looks at all five stages of the product's life, giving a full picture of its impacts from the beginning to when it is completely used (including steps 1 to 5 of fig.2.1).
- **Cradle-to-cradle** : It is similar to the cradle-to-grave model, but replacing the waste stage with a recycling/upcycling process, so that materials can be used again in another product.

In this case, the LCA will follow the model of cradle-to-grave. Therefore, the system model of allocation, cut-off by classification will be used. Indeed, in this model there is no encouragement towards waste treatment. The allocation at the point of substitution would have been chosen in a case of cradle-to-cradle assessment, in order to consider recycling possibilities. A simplified view of the complete life cycle scope is shown in fig 2.2.

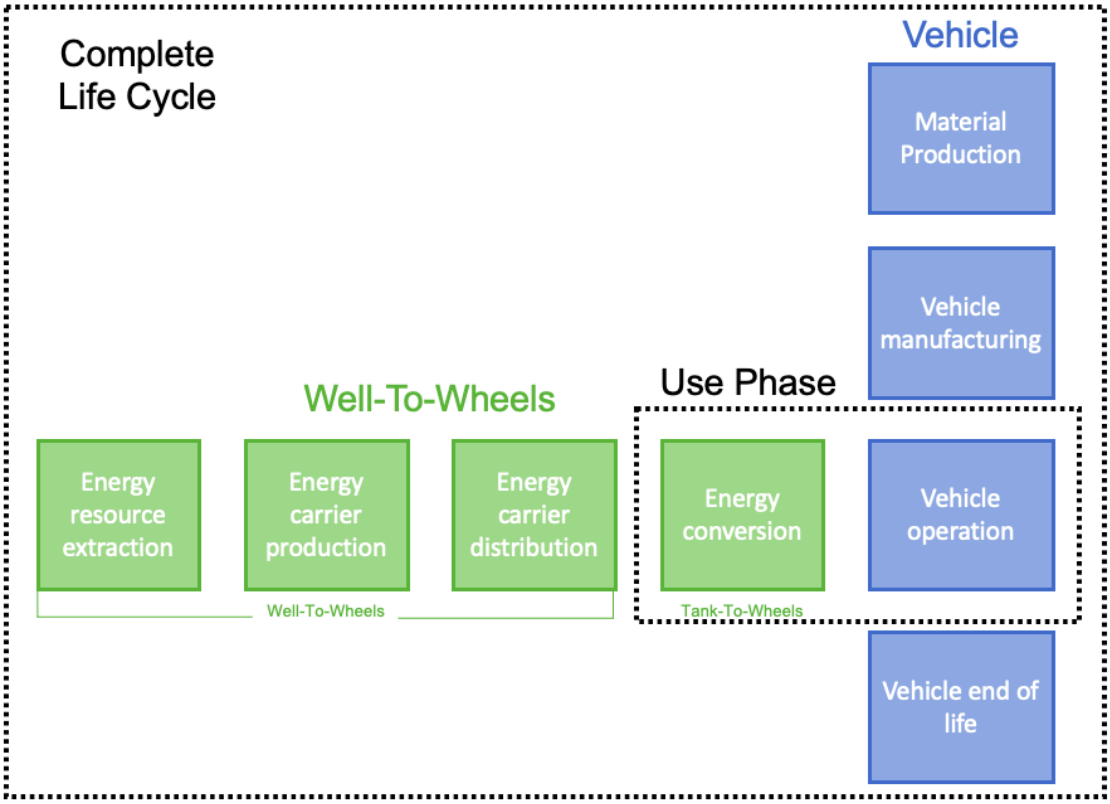


Figure 2.2: Simplified view of this LCA [8]

Finally, in order to complete the scope definition, the "functional unit" of the LCA should be clearly defined as well. The functional unit is a measuring tool that helps to quantify the function of the assessed products [57]. Here, the functional unit in order to assess the function o the vehicles is "1 km driven by one vehicle".

2.1.4 Life cycle inventory

ISO14040: "phase of life cycle assessment involving the compilation and quantification of inputs and outputs for a product throughout its life cycle" [58].

The Life Cycle Inventory for this study is created through the development of a new database using the Active Browser software. This database allows for the addition of new activities, incorporating both biosphere and technosphere flows. Biosphere flows represent natural inputs directly obtained from nature and are filled using the *biosphere*3 database. On the other hand, technosphere flows are acquired from activities present in the 3.9 version of the Ecoinvent database.

Completing an activity involves conducting a literature analysis to assemble various flows from the Ecoinvent database accurately. This process results in the creation of new activities specific to this study, such as specific vehicle components, or activities that are not available in the database, like hydrogen production through electrolysis or type IV hydrogen storage tanks. Detailed explanations for these new activities will be provided in the following subsections.

Production phase

To generate inventories for the production phase of the five different vehicles, a specific vehicle category is chosen for modeling. It is essential for the vehicles to belong to the same category to ensure they have similar curb weight and power performance, making a meaningful comparison possible. The inspiration behind the first vehicle in this comparative LCA was the Mazda MX30 R-EV. Therefore, the subcompact crossover SUV category (the category to which this vehicle belongs) will be considered.

For the FCV and BEV, existing reference vehicles available in the market are used as models. Specifically, the Hyundai Nexo represents the FCV, and the Kia Soul EV 2020 represents the BEV, both being subcompact crossover SUVs. However, neither the ICEV nor the HEVs have any available market vehicle using these technologies. There are no ICEVs powered with a HWRE, nor are there HEVs where the ICE is a HWRE (the MX30 R-EV uses a gasoline-fueled WRE). As a result, technical data from various vehicles are employed to model these unique configurations. To model the HEVs, data from the FCV (Hyundai Nexo), the MX30 R-EV, and the Premacy Hydrogen are used. Similarly, for the ICEV, data from the FCV and the RX8 Hydrogen are utilized in the modeling process.

The way in which all of the vehicles are modelled is by their weight. In the database that is created for this study, the chosen unit of the activity is "kilogram". Therefore, for instance, when modeling the BEV in accordance to its reference vehicle, instead of adding each component of the vehicle by its real weight, it is

added by considering the %age of weight relative to the total weight of the vehicle that each component will consist of.

Glider production

In order to properly model the four vehicles, firstly the assumption that all of the vehicles have the same glider is made. A good way to start is to follow the criterion of Althaus and Gauch [59]. They propose to estimate the glider's weight as being 74% of the mass of a gasoline-fueled RPE ICEV. However, in this case the ICEV is powered by a Wankel engine. This engine being more compact, having a higher power density than reciprocating engines, this criterion is not quite relevant. Furthermore, since a subcompact crossover SUV HWRE powered ICEV does not exist in the market currently, there is no available data of a reference curb weight from which a certain %age could be deducted.

Since this approach can not be used, the glider's mass is estimated by a similar approach. In the comparative LCA performed by [16], the approach used to estimate the glider's mass is to use Althaus and Gauch's criterion in order to model an ICEV with an RPE as ICE. After obtaining the glider's weight, they considered that the BEV's glider will be the same. With this glider, they got a certain weight distribution for the BEV, that is going to be used in this study. The results are summarized in table 1.

BEV Components	**Weight Distribution (%)**
Glider	73.12
Powertrain	6.04
Battery	20.84

Table 2.2: Weight distribution of components in a Battery Electric Vehicle (BEV) based on [16]

Therefore, by considering the reference BEV, the Kia Soul EV 2020, that has a curb weight of 1757 kg, the glider is modelled as weighting 1284.7kg, for all of the vehicles that are modelled. In order to add the glider to the inventories, the Ecoinvent flow "glider, passenger car" is considered. The main inputs that this flow accounts for are "tap water", "heat, district or industrial, natural gas", "electricity, medium voltage", "reinforcing steel", and "sheet rolling, steel".

Hydrogen tank production

In order to store the hydrogen that all of the modeled vehicles except for the BEV are going to use as fuel, it is assumed that they will use type IV tanks, where hydrogen will be stored at 700 MPa. Firstly, for the FCV vehicle, the storage will be done in the same way as in the reference vehicle: there are 3 tanks, storing in total 156.6 liters - or 6.33 kg - of hydrogen.

Regarding the HEV_A, a first assumption will be to assume that it will have a tank size identical to the MX30 R-EV, which is a 50-liter tank. Although the reference vehicle's tank differs from the modeled vehicle, since the tank stores gasoline and not hydrogen, the choice to maintain this assumption for the time being is made. Since, from the FCV's reference vehicle, 6.33 kg of hydrogen at 700 MPa can be stored in a volume of 156.6 liters, it is known that the 50 liter tank can store 2.31 kg of hydrogen. A second possibility will be to consider that the HEV will have the same storage tanks as the reference FCV. That is what it is done for the HEV_B.

For the ICEV, the same storage as in the FCV is assumed. Indeed, it is assumed that this compact engine is going to occupy roughly the same space as the fuel cell stack and its base of plant occupies in the FCV, therefore it is assumed that there will not be any problem of volume arrangement. This assumption is pretty rough and not calculated in details. For now this assumption can be accepted, based in the scope of this study.

The hydrogen tanks are assumed to be of Type IV. The inner liner material is made of high-density polyethylene (HDPE), and it is modeled with the available Ecoinvent flow "polyethylene, high density, granulate". Meanwhile, the carbon fiber wrapping is modeled using the Ecoinvent flow "carbon fiber reinforced plastic, injection molded". Additionally, an outer rigid foam layer is considered in the model, modeled by the flow "polyurethane, rigid foam". To accurately model the tank, information from table 2, coming from [17] is used.

Storage System	**Type IV 700-bar Single Tank (kg)**
Stored Hydrogen	5.8
HDPE Liner	8.0
Carbon Fiber Composite	91.0
Dome Protection	4.0
BOP	18.7

Table 2.3: Predicted mass of a Type IV 700-bar compressed hydrogen system [17]

Regarding the HDPE liner, carbon fiber composite, and dome protection (rigid foam), it is assumed that these components can be proportionally scaled based on the required amount of stored hydrogen. For instance, if the FCV requires 6.33 kg of hydrogen, the HDPE liner will weigh 8.73 kg, the carbon fiber composite will weigh 99.32 kg, and the dome protection will weigh 4.37 kg accordingly. According to this weight distribution, the hydrogen tank for the HEV modeled with a capacity similar to the one of the gasoline tank in the MX30 R-EV will consist of a 3.19 kg layer of polyethylene, a 36.24 kg layer of carbon fiber, and a 1.59 kg layer of rigid foam. Regarding the method for producing the tank, only the blow moulding of the HDPE liner is considered. It has to be noted that in the Ecoinvent flow for this activity, 1 kg of this activity represents the moulding of 0.997 kg of the moulded material. Therefore, since the HDPE liner consists of 7.77% of the storage tank without the BoP, for 1 kg of storage tank without the BoP, the activity "blow moulding" represents 0.078 kg.

Regarding the BoP, it is composed of various components, including safety devices, regulators, electronic controllers, sensors, and all the necessary onboard conditioning equipment to facilitate hydrogen storage (such as pumps, filters, etc.). It is assumed that the BoP remains constant and consistent for all modeled hydrogen tanks, independently of the stored hydrogen amount. The estimated weight of the BoP is 18.7 kg for all vehicles utilizing hydrogen as fuel, as it is modeled in [17] for a tank storing 5.8 kg of hydrogen. To model the BoP itself, the approach is based on the model presented in [53]. According to this model, the BoP is categorized into five main sections: Pipes, Valves, Electronics, Instruments, and Miscellaneous.

BoP categories	**BoP weight per category (%)**
Electronics	7
Valves	25
Instruments	24
Piping	29
Diverse	15

Table 2.4: Breakdown of Balance of Plant (BoP) categories and their respective weights (%)

In this model, the composition of instruments consists of 50% stainless steel-316, 16% stainless steel-316Ti, and 28% aluminum 6082/61-T6. In the article's model, stainless steel-316Ti, is added to the inventory by the flow "steel, chromium steel 18/8" available in the Ecoinvent database. The same is done in this study. However, in this study, the same flow is used to model the stainless steel-316, since among

the available Ecoinvent flows, it is the one that matches the best. Therefore, it is considered that 66% of the instruments is made of "steel, chromium steel 18/8". For aluminum, the flow "aluminium alloy, AlLi" is used. Regarding the pipes, the article's model employs 100% stainless steel-316Ti, which is here modeled, again, with "steel, chromium steel 18/8". As for valves, they are modeled as comprising 75% stainless steel-316 (equivalent to "steel, chromium steel 18/8" in this context) and 25% aluminum 6082/61-T6 (replaced with "aluminium alloy, AlMg3" here). In the electronics category, both the article's model and this study adopt the available flow "electronics, for control units". Lastly, the miscellaneous category is modeled to contain 70% stainless steel-316, 25% stainless steel S355 (here modeled as 95% of "steel, chromium steel 18/8"), and 5% polypropylene represented by the Ecoinvent flow "polypropylene, granulate".

Battery production

Four of the five vehicles that are modelled in this study contain a battery in their powertrain. Indeed, the BEV, the HEVs, and the FCV need this crucial element. Most of today's batteries in the automotive world are Li-ion batteries. This is the battery that is chosen for this study's three vehicles. Again, as for the glider production, the battery's weight must be defined. In order to do this, the battery is firstly modelled for the BEV, for which a weight distribution is available (see Table 1). Therefore for this vehicle, the battery's weight is considered to be 20.84% of the reference vehicle of 1757kg, therefore weighting 366.16 kg. The reference vehicle's battery having a capacity of 64kWh, the energy density of the battery must therefore be of 174.78 Wh/kg. The assumption that the batteries in all of the vehicles have this energy density is made. This development had to be done since in the Ecoinvent database the energy density of the available Li-ion batteries are not specified. Among the available Li-ion batteries, the NMC111 is chosen, modeled with the flow "battery, Li-ion, NMC111, rechargeable, prismatic" from the Ecoinvent database. The reason for this is that it is a battery suitable for the automotive industry, and that the calculated energy density falls into the range of the energy densities of this kind of batteries.

As previously mentioned, the objective of assessing the BEV is to compare its environmental impacts with those of a hypothetical HEV, using a HWRE as ICE, having an equivalent range. To achieve this, the BEV based on its reference vehicle, the Kia Soul EV, which features a 64 kWh battery providing an EPA range of 391.1 km.

In order to model the battery of the HEV_A, the required full-electric range must be calculated. To achieve this, it is necessary to first estimate the range that the

vehicle can achieve only by the use of the ICE, by consuming its total amount of stored hydrogen. As it has been explained, the HEV_A stores 2.31 kg of hydrogen with the assumption that its fuel tank has the same capacity as the MX30 R-EV's tank. In order to estimate the driving range that can be achieved with this amount of hydrogen, the hydrogen consumption of the 2007 Mazda Premacy Hydrogen RE Hybrid is considered. This car was able to drive for 200 km consuming a total amount of 3.27 kg of hydrogen. Therefore, the modeled HEV_A is considered to be able to have a driving range of 141.28 km due to its HWRE.

Furthermore, if its full-electric range is considered to be the distance that could be travelled only due to its battery capacity, supposing that it did not include an ICE in its powertrain, this HEV should have a full-electric range of 249.82 km, since the EPA range of 391.1 km is considered. Supposing that the full-electric range is proportional to the battery's capacity, taking the EPA range the consumption would be 163.64 Wh/km. Since the vehicle needs a full-electric range of 249.82 km, the battery needed would have a capacity of 40.88 kWh. From these values, considering the calculated energy density of 174.78 Wh/kg, the weight the battery can be deduced, being of 233.90 kg.

Finally, modelling the battery of the FCV is straightforward. The battery of the reference vehicle, the Hyundai Nexo, has a capacity of 1.56 kWh. Considering the same energy density as the battery of the modelled BEV and HEVs, the weight of the battery for the FCV is modelled to be of 8.93 kg. The same battery weight is going to be considered for the HEV_B.

In the table 2, a resume of the modelled battery for each vehicle is detailed.

Vehicle	**Battery Capacity (kWh)**	**Battery Weight (kg)**
BEV	64	366.16
HEV_A	40.88	233.90
HEV_B	1.56	8.93
FCV	1.56	8.93

Table 2.5: Battery capacity and weight for different types of vehicles

ICE production

Once the battery size for the HEVs has been determined, the next step is to size their ICE. Referring to [60], the weight of each component of a 2 rotor, 2x654cc Wankel engine can be found. For the HEV_A, the same Wankel engine as the one

in the MX30 R-EV is going to be modeled, which is a single rotor engine with a capacity of 830cc. To maintain consistency with the reference engine, most parts and accessories, such as the shaft, stationary gears, oil pan, or air pump, will be kept at the same weight. However, certain components, namely the rear side housing, front side housing, rear rotor housing, and the rotor itself, will have a slightly heavier weight, which will be proportionate to the engine's capacity. Specifically, the rear side housing will increase from 13.15 kg to 16.69 kg, the front side housing from 12.25 kg to 15.54 kg, the rear rotor housing from 6.58 kg to 8.35 kg, and the rotor from 4.54 kg to 5.76 kg.

It is important to note that the transmission weight will be excluded from the engine's total weight. Indeed, the MX30 R-EV is equipped with a "1 gear, automatic transmission" [61], indicating that it uses a single-speed automatic transmission with only one fixed gear ratio. This type of transmission, known as a direct-drive system, is particularly suitable for BEVs and HEVs as it efficiently utilizes the electric motor's torque over a wide range of speeds, eliminating the need for multiple gears and gear shifting in most driving scenarios. Considering these factors, the final weight of the ICE for the HEV is determined to be 113.02 kg.

On the other hand, for the ICEV, the engine will be considered as it is given in [61]. It will therefore be a 2 rotor, 2x654 cc engine, where the 50.8 kg transmission is not removed. It will therefore be a 163.83 kg engine.

It is important to note that the exhaust system is included in the mass stated for both the HEVs and the ICEV engine. The flow from the Ecoinvent database used is "internal combustion engine, passenger car".

Electric powertrain production

Regarding the powertrain, the distribution outlined in table 2.2 is once again followed [16]. Consequently, the powertrain's weight in the BEV amounts to 6.04 % of its curb weight, totaling 106.12 kg based on the 1757 kg curb weight. For the weight distribution of each individual component constituting the powertrain, reference is made to the data provided by the Ecoinvent flow "powertrain, for electric passenger car". According to this distribution, the electric motor accounts for 66.07 % of the powertrain's weight, the inverter takes up 11.84 %, the charger 7.73 %, the converter 5.61 %, the power distribution unit 4.86 %, and the cables 3.74 %. Given that the powertrain activity in the Ecoinvent database comprises the inverter, converter, power distribution unit, electric motor, charger, and cables – all of which are common components between the BEV and HEVs – the same

powertrain is considered for both vehicles.

The powertrain of hybrid vehicles lacks a component that is not present in the Ecoinvent activity - the generator. The activity used to model the generator is going to be the same as the one used for the electric motor that is included in the electric powertrain. The reason for this is because the "generator" activity in the Ecoinvent database is relative to the infrastructure of an existing natural gas cogeneration plant, and if it is used wrong results are going to be obtained.
Concerning the FCV's powertrain, it is considered that all of the powertrain is the same as in the BEV and in the HEVs, except that the FCV does not contain a charger. Therefore the Ecoinvent 'powertrain' flow is not chosen in the inventory, and each component of this flow is taken individually, keeping the same weight for each one of them as in the BEV. From table 2.2, knowing that the BEV's curb weight is 1757 kg, it is known that the powertrain should weight 106.12 kg. Having the powertrain's weight distribution listed in table 2.6, the weight of each individual component can be deduced, and therefore add each one individually in the inventory of the FCV, without including the charger.

Component	**Weight (%)**
Electric Motor	66.07
Inverter	11.84
Charger	7.73
Converter	5.61
Power Distribution Unit	4.86
Cable, Three-Conductor Cable	3.74

Table 2.6: Weight distribution of an electric vehicle's powertrain

Fuel Cell Stack production

For the fuel cell stack, the reference vehicle uses a 95 kW polymer electrolyte membrane stack. In order to model the stack in a suitable way the inventory of [51] is used. That paper provides a detailed inventory for the membranes, the gas diffusion layers (including the micro-porous layer), the catalyst layers, the MEA, the bi-polar plates, as well as the collector and end-plates production, and its BoP. The "fuel cell" activity available in the Ecoinvent database is not used, since this flow is meant to be used for stationary cogeneration applications and not mobile applications. Its use could provoke the results to be mistaken.

Use phase

The inventory components relative to the use phase of the vehicles consist of the non-exhaust emissions, the emissions linked to the production of the energy carrier (Well-to-Tank analysis), the exhaust emissions (Tank-to-Wheels analysis), the vehicle maintenance, the road infrastructure, and the road maintenance.

Non-exhaust emissions

Non-exhaust emissions are differentiated between brake wear, tyre wear, and road wear [9]. These emissions are important because of the particulate matter emissions that they entail.

Ecoinvent has derived emission factors for various vehicle sizes. This was done by considering the lower and upper limits of the PM emission ranges. Eventually, they assumed that the emission factor calculated for medium-sized vehicles could be applied to all sizes. As a result, non-exhaust emissions per kilometer can be directly adjusted based on the vehicle's weight. The calculation procedure with use of parameters is summarised in fig.2.3 [9].

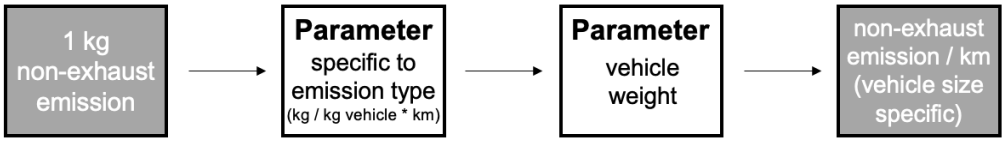


Figure 2.3: Method for calculating size-specific non-exhaust emissions from vehicles [9]

The parameters specific to the emission types are summarized in table 2.7. These parameters are not directly given by Ecoinvent, nor available in the literature that has been found. However they were obtained thanks to their unit expression (kg / kg vehicle*km) that is given in [9] and to the Ecoinvent information. The information that Ecoinvent provides, tells, for instance that for a large sized vehicle, of 2000 kg, carrying a passenger of 97.2 kg, the road wear emissions are 2.0532×10^{-5}. Therefore, by dividing this value by the total weight of 2097.2 kg, the parameter was obtained. This method is confirmed to be correct, firstly because repeating this method for medium or small sized vehicles gives the same parameter, and secondly because for tyre wear emission, [9] gives the value of its parameter, and it is the same that has been obtained for this study.

Non-exhaust emission type	Parameter (kg / kg vehicle*km)
Road wear	$9.790196452 \times 10^{-9}$
Tyre wear	$5.724775892 \times 10^{-8}$
Brake wear	$4.449980927 \times 10^{-9}$

Table 2.7: Non-exhaust emission types and their respective parameters

Because of the regenerative breaking in all of the modeled vehicles except for the ICEV, an extra parameter of 0.20 is going to be multiplied to the result of break wear emissions.

Energy carrier production

Regarding the energy carriers, both electricity and hydrogen have to be assessed. Regarding electricity, two sources are considered. The first one is the electricity available on the high voltage level in Belgium. It is modeled by the Ecoinvent flow "market for electricity, high voltage". It is a "market" activity. Therefore, it takes into account the consumption mix of electricity in the given geography location, Belgium, its transport and its losses. Another source that is considered is electricity from a renewable source. In order to model this, electricity from wind is chosen. It is modeled with the activity "electricity production, wind, 1-3MW turbine, onshore", that considers electricity production in Belgium in 2012. Regarding the location (Belgium) the activity is modeled by Ecoinvent by adapting wind hours to local condition [62]. This activity takes into account operation, maintenance, and infrastructure inputs.

As for hydrogen, as it has been explained there are many production types. It is important to note that only local production at the refueling station have been considered in this study. This assumption is done following the assumption done in [52]. The reason for this assumption, is that due to the chosen scope of the LCA, conducting a comprehensive cost evaluation of the distribution system required for centralized production was not relevant. The chosen considered production methods are therefore production by SMR and electrolysis, since other production methods must be done in a centralized system. Concerning electrolysis, as it is done in [52], two different electricity sources are considered. The two sources are the ones mentioned above, therefore there would be one coming from mixed source, and one coming from a renewable source.

However, Ecoinvent does not provide an activity representing electrolysis. Therefore, a model had to be built from available literature. In order to do this, information from the inventory in [33] was used. The model was based on an inventory made

in 2003 that analyzed a hydrogen fuelling station from Norsk Hydro assembled in Reykjavík, and it was adapted to make the results more relevant to the situation in Europe at the time the article was written. This inventory accounts for all the activities relative to the electrolyser, the diaphragm, the compressor, the storage module, the walls and foundation, and the operation of the hydrogen production plant, as well as an extra activity relative to "other components" of the plant. Something that must be taken into account is that the compression process in order to obtain hydrogen at 700 MPa was not taken into account. This modeled hydrogen fuelling station delivers hydrogen at 5,394 kg/h at 15 bar.

Regarding green electrolysis, with electricity coming from a renewable source, as stated before, it has been considered that the renewable source is wind. In order to model green electrolysis, a first approach is to keep the previous model, and replace the electricity source by the renewable one.

Concerning SMR, in addition to what has been done in [52] of only considering SMR, in this study SMR with carbon capture and storage (CCS) is also considered. In order to model SMR, the activity "hydrogen production, steam reforming" from Ecoinvent is chosen. For SMR with CCS, there is not an available activity provided by Ecoinvent. Therefore, a simplified model taken from [18] is considered.

Inputs and Direct emissions	**SMR+CCS**
Natural Gas	3.76 kg
Electricity	1.11 kWh
Water	23.70 kg
CO2	1.03 kg

Table 2.8: Input values and direct emissions for SMR+CCS process. [18]

This model is summarized in table 2.8.

Since this model is quite simple, another model was also done. The second model comes from the inventory published in [63].

For the consumption of the ICEV, the same consumption of the hydrogen fueled RX8 has been assumed, being of 0.024 kg/km. For the HEV_B, the same consumption as the hydrogen fueled Premacy is assumed, being of 0.01635 kg/km. For the BEV the same electricity consumption as in the Kia Soul EV is taken, being of 163.64 Wh/km. However, the charging efficiency of 90% is considered, therefore the total electricity consumption is 181.82 Wh/km. For the FCV, the

same consumption as in the Hyundai Nexo is considered, being of 10.34 $\times 10^{-3}$ kg/km.

For the HEV_A, a part of its autonomy is assured by the electricity delivered by the generator linked to the HWRE, and another part comes from its full-electric range. As it has been stated, 141.28 km (36.12% of its range) are going to be assured by the HWRE, and 249.82 km (63.88% of its range) by the full-electric mode. In order to determine the hydrogen and the electricity consumption per km, it is assumed that 0.3612 km are going to be assured by the consumption of hydrogen, having a consumption of 0.01635 kg/km, therefore consuming 5.91 $\times 10^{-3}$ kg of hydrogen. It is also assumed that 0.6388 km are going to be assured by the full-electric mode, which consumes 163.64 Wh/km. Therefore, the total amount of electricity that is consumed in this distance is 104.53 Wh. Considering the charging efficiency of 90%, the electricity consumed will be 116.15 Wh.

Exhaust emissions

Regarding exhaust emissions during the use phase, only emissions from the combustion of hydrogen in the HWRE for the ICEV and the HEVs are considered. Indeed, for the FCV the only direct emission is water, and for the BEV, it is powered only from the electricity stored in its battery, therefore they are both zero-emission vehicle during operation.

Concerning the operation of the HWRE, the only emissions considered are the NOx emissions. These emissions have to be estimated by their weight. In order to do this, the emissions around the stoichiometric point in HWRE compared to the emissions in a GWRE are considered. The engines will probably neve be used at this operation point, but it allows to take a conservative amount of emissions. In the article [64], the NO emissions around the stoichiometric point of these two engines are evaluated, as a function of the engine's speed and the brake torque. In order to take a conservative choice, the highest value is considered. It is seen that the highest NO emission value for HWREs is 3.37 times higher than the one in GWRE. Then, the value of NOx emissions in kg from a gasoline fueled large size car is considered. It is assumed that the NOx emissions in this gasoline fueled engine are the same as in a GWRE (even though it is known that in the wankel engine these emissions should be lower). From this value given, the fuel needed in the entire lifetime of the modeled vehicles is scaled, and the weight of the NOx emissions is found by multiplying the scaled value by 3.37.

Vehicle maintenance

In the context of the vehicles' lifetime, a conservative distance of 150000 km is considered, aligning with the values commonly found in literature, as explained in [65]. During the lifetime of the vehicle, the vehicle has to be maintained, and this activity has to be taken into account in its assessment. Therefore, the Ecoinvent flow "passenger car maintenance" is used to model this. The unit of this flow is "unit". Assigning one unit of this flow represents taking into account the entire maintenance demands over the whole lifetime of the vehicle. The main inputs of this activity are electricity, synthetic rubber, ethylene, lubricating oil, lead and steel. In this way, the replacement of common components such as tyres, motor oil, coolant and battery are taken into account, as well as their disposal after their use.

It is important to note that this flow was modeled by Ecoinvent based on an LCI analysis of a 1240 kg vehicle. Therefore, in this study the unit is going to be scaled for each vehicle, according to its weight. For the BEV and the FCV, the weight of their reference vehicles are considered (1757 kg and 1810 kg respectively). As for the ICEV and the HEVs, the sum of the weight of all of the modeled components in the production phase section are considered (1606 kg for the ICEV, 1869 kg for the HEV_A, and 1704 kg for the HEV_B.

Finally, the amount of this flow required for each vehicle can be computed. In order to do this, the weight of the modeled vehicle has to be divided by the weight of the reference vehicle utilized by Ecoinvent for modeling this activity. This will give the amount of maintenance that is going to be required for the whole lifetime of the given vehicle. However, in order to keep consistency with the functional unit, this amount must be divided by the vehicle's lifetime, by the total amount of kilometers that are going to be driven (150000 km), in order to get a maintenance value per kilometer.

Vehicle	**Maintenance Amount (unit/km)**
BEV	9.45×10^{-6}
FCV	9.73×10^{-6}
HEV_A	1×10^{-5}
HEV_B	9.16×10^{-6}
ICEV	8.63×10^{-6}

Table 2.9: Vehicle Maintenance Amounts

The results obtained are summarized in table 2.9.

Regarding the battery's maintenance in all of the vehicles except for the ICEV, the assessment results will first be presented without taking this into account, and after having presented that case, its replacement will also be considered. The batteries lifetime is assumed to be of 100000km. Regarding the fuel cell stack, its replacement is not necessary, considering it to have a longer lifetime than the vehicle [51].

Road infrastructure and maintenance

The activity used to model the road infrastructure is the Ecoinvent data "road construction". The processes that contribute to the provision of construction, renewal and disposal of roads are represented. Its value is assumed to be proportional to the vehicle's weight. In order to give a value for a specific vehicle, Ecoinvent uses the parameter 5.37×10^{-4} m*y per kg of vehicle per km. This parameter is calculated in the same way as the non-exhaust parameters, and its value is confirmed since it is also given in the Ecoinvent data description.

Since the roads are in permanent use, they must be maintained. To model this, the activity "road maintenance" is utilized. It takes into account aspects of lighting, weed control and line marking [32]. This activity is not related to the vehicle's weight, but rather to the kilometers driven. For a lifetime of 150000 km, Ecoinvent gives the value of 0.0002653 m*y of road maintenance, independently of the vehicle.

End-of-life phase

As a reminder, the chosen system is a cradle-to-grave system, and the system model is the allocation, cut-off by classification. In order to treat the end-of-life of the products, for each activity modeled in the database created for this study, the products that are being disposed are considered as negative inputs, as it is required for this system model. As this system model requires, as it can be seen in figs. 2.4 and 2.5, the products recovered from the treatments of the products that are disposed are not taken into account in the system's boundaries. This would have been different if the system model used was allocation at point of substitution (APOS).

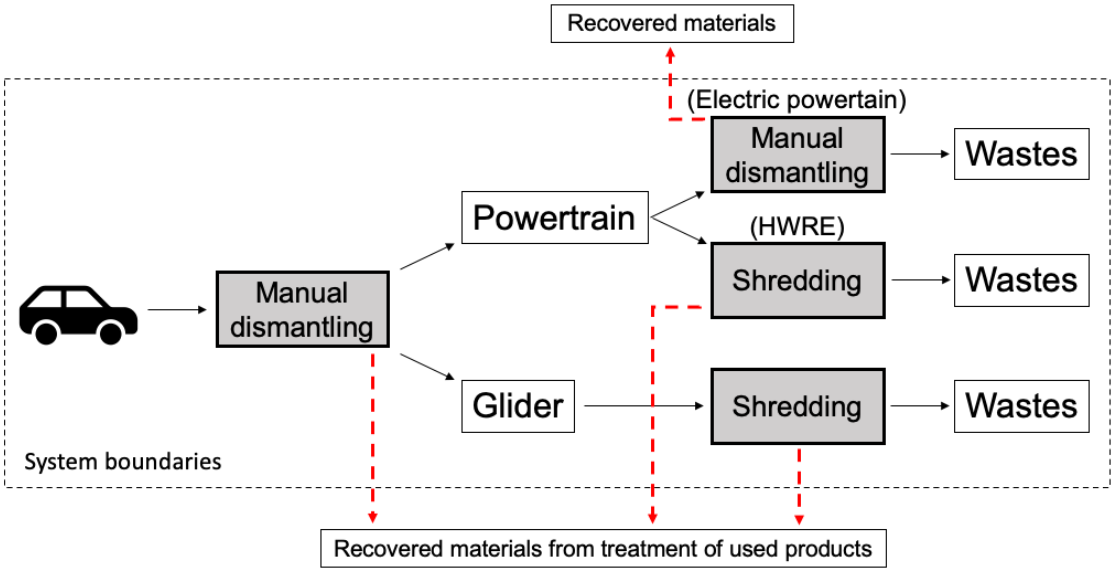


Figure 2.4: Disposal of vehicles [10]

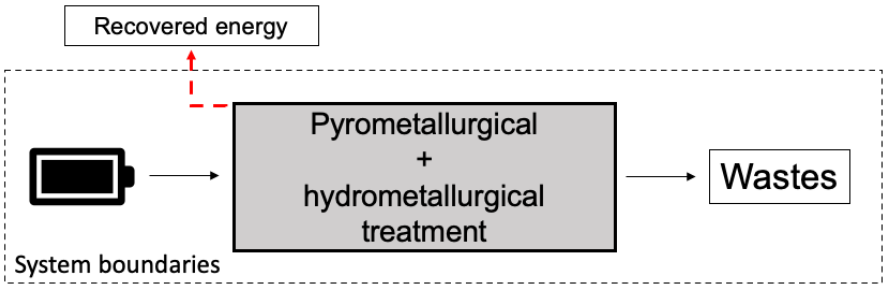


Figure 2.5: Disposal of battery [10]

The end of life of all of the five vehicles (without their battery for the vehicles that have one) firs composed of the manual dismantling of the used vehicle. After this treatment, the glider and the powertrain will be independently treated. The glider will go through a shredding process. Regarding the glider, all of the electric parts of the powertrain (charger, inverter, converter, motor, power distribution unit, cables) will be dismantled manually, whereas the ICE will as well go through a shredding process. Regarding the battery, it will go through a pyrometallurgical and hydrometallurgical treatment.

The end-of-life of the fuel cell stack however is not taken into account, because of a lack of information. Indeed, the inventory provided by [63] contains a disposal phase, but most of the activities that compose that part of the inventory are not available in the Ecoinvent database.

2.1.5 Life cycle impact assessment

ISO14040: "phase of life cycle assessment aimed at understanding and evaluating the magnitude and significance of the potential environmental impacts for a product system throughout the life cycle of the product" [58].

In order to, as the ISO 14040 standard states, understand and evaluate the environmental impacts from the product whose inventory is in this stage completed, a particular method must be followed. In order to do this, the ReCiPe method is employed. This method will allow to obtain a set of indicator ratings from the assessed product's inventory. The method describes 18 midpoints and 3 endpoints, which are described in fig.2.6.

In the case of the study, "Hierarchical" midpoints are studied. This means that these midpoints consider a moderate time horizon, such as a 100-year period, and it typically regarded as the standard model. Other possible choices could have been to consider "Individual" midpoints, which take a near-future perspective, or "Egalitarian" midpoints, which adopts a long-term perspective [66].

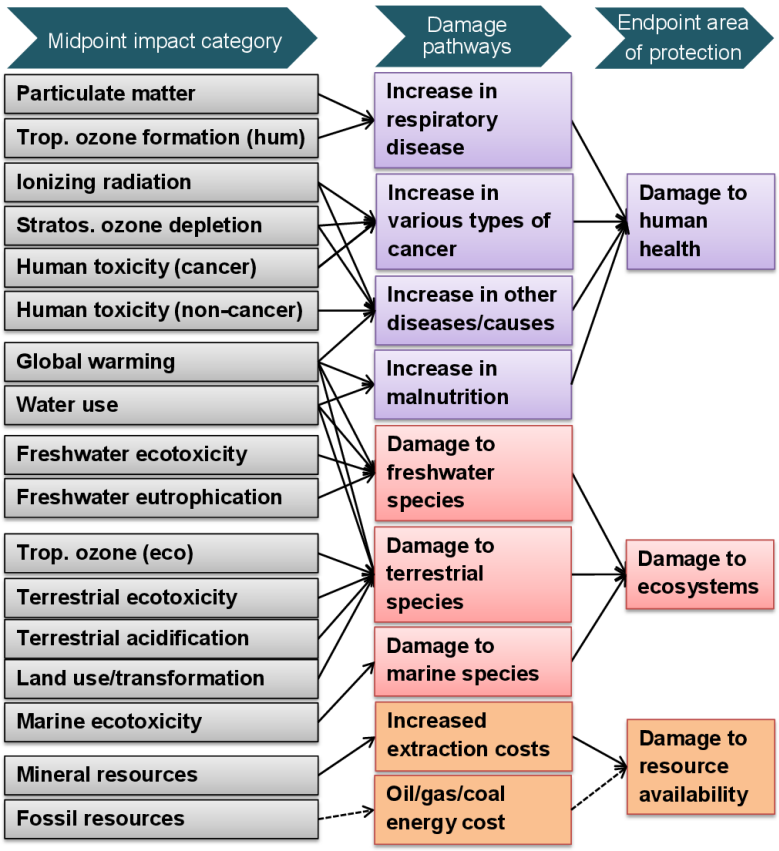


Figure 2.6: ReCiPe midpoints and endpoints

2.1.6 Normalization

In order to better understand the results from the LCIA, it is possible to normalize them. In this way, it is possible to analyze how important the impact in a certain category are, related to the impact in other categories, which are assessed in different units.

ReCiPe normalization and weighting

Two normalization methods have been employed. The first one consists in normalizing the results with normalization factors that are proposed by the ReCiPe method. These factors represent the total impact of a certain region in a reference year. In this case, the factors used correspond to global emissions, and the reference year for which these factors have been provided is 2010. The results from each impact category of the Life Cycle Impact Assessment are divided by their corresponding normalization factors. After their normalization, the obtained indicators must be multiplied by a certain weighting factor. The objective of this weighting step it to assign a certain importance to some categories relative to the others. These weighting factors are also provided by ReCiPe. The normalization factors are take from the ReCiPe 2016 version, and the weighting factors are taken from the 2008 version, that has been updated in 2014.

Impact Category	Unit	Normalization Factor
GWP	kg CO_2-eq./p/yr	7990.4076
METP	kg 1,4-DBC-eq.(to sea water)/p/yr	43.442842
FETP	kg 1,4-DBC-eq.(to freshwater)/p/yr	25.174703
TETP	kg 1,4-DBC-eq.(to freshwater)/p/yr	15200.310
HTC_c	kg 1,4-DCB-eq.(to urban air)/p/yr	10.298306
HTC_{nc}	kg 1,4-DCB-eq.(to urban air)/p/yr	31251.842
TAP	kg 1,4-DCB-eq(to urban air)/p/yr	40.980514
PMFP	kg $PM_{2.5}$-eq./p/yr	25.569594

Table 2.10: Impact Categories and Normalization Factors

The impact categories in the ReCiPe method are divided in three: those regarding the ecosystem, those regarding human health, and those regarding resources. Among the analyzed categories, METP, FETP, TETP and TAP belong to the 'ecosystem' group. On the other hand, HTP_c, HTP_{nc} and PMFP belong to the 'human health' group. As for GWP, it belongs to both 'ecosystem' and 'human health' groups. None of the analyzed categories belong to the 'resources' group. For each group, and for each archetype (individualist, hierarchist and egalitarian)

Impact Category	Method Needed	Unit	Method and Category Used
Global warming	EN15804+A1 (CML v.2012)	kg CO2 eq	CML v4.8 2016, climate change, GWP100
Acidification of land and water sources	EN15804+A1 (CML v.2012)	kg SO2 eq	CML v4.8 2016, acidification, A&B
Human toxicity	USEtox	CTUh	USEtox, human toxicity, carcinogenic
Human toxicity	USEtox	CTUh	USEtox, human toxicity, non-carcinogenic
Particulate matter	RiskPoll	kg PM2,5 eq	ReCiPe 2016 v1.03, particulate matter formation potential
Ecotoxicity	USEtox	CTUe	USEtox, ecotoxicity, total

Table 2.11: MMC method

weighting factors are given. In this study the hierarchist factors are considered. These ones are 400 for 'ecosystem' impact categories, 300 for 'human health' impact categories, and 200 for 'resource' categories. For GWP, since it has impacts on both the 'ecosystem' and the 'human health', the weighting factor that is going to be used is 7000.

Belgian MMC method

Another method that has been employed, in order to validate the previous one, is the Belgian MMC method. In this method, for each impact category, there is a monetisation factor. For example, for the GWP impact category, which is assessed in kg CO_2-eq, the monetisation factor is 0.05 euro/kg CO_2-eq. However, for each impact category, the LCIA method that should be used to get the results is specified. In table 2.11 the specified LCIA methods required, units required, and LCIA methods used are detailed. Since the methods used for each category are different, and are not going to be assessed one by one, but only in total in order to get the MMC method's single score, the contribution from each category in the results from this method are not relevant. Indeed, since in this study this method is only used to validate the single score obtained with the previous method, only the single score result is going to be considered to be relevant, and, again, not from which impact category the contributions came from.

2.1.7 Sensitivity analysis

After the results from the assessment have been obtained, it is interesting to modify the amount of certain components that fill up the inventory of the modeled vehicles, in order to see the level of variation of the results that these inputs' variation provoke. In other words, the goal is to check the assessment's sensitivity with respect to some inputs. The inputs that are going to be modified for this analysis are going to be the lifetime of the vehicles, their hydrogen consumption, the way of modelling the hydrogen production method of SMR with CCS, and the fact of replacing the battery in vehicles that contain this component, considering the battery to have a lifetime of 100000km (therefore shorter than the vehicle's lifetime).

2.2 Performance of the hydrogen Wankel rotary engine

In this section, emphasis is placed on the small-picture perspective. The objective of this section is to demonstrate and justify the methodology employed to assess the engine's behavior using in-cylinder pressure measurements. Initially, the data pre-processing procedure of the in-cylinder experimental pressure trace is outlined. This is followed by an in-depth description of the post-processing methods, which cover areas such as the WRE geometry, in-cylinder combustion modeling, and heat transfer modeling, ultimately providing insights into power and efficiency metrics. Finally, the obtained results will be used to shed light on the impact of the air-fuel ratio on the combustion process, influencing power output, heat loss, and overall efficiency.

2.2.1 Data pre-processing

In order to investigate the HWRE behavior over a range of air-fuel ratios, the initial stage involves collecting and pre-processing data. Researches on HWRE are still not very common and most studies are carried via computer simulations. Thus, this study is based on data provided by Huaiyu Wang et al., 2022 in [19].

The article presents pressure and mass traces for various excess-air ratios, including λ values of 1.4, 1.6, 1.8, and 2.0 for a range of Eccentric Shaft Angle Degree (ESAD) from -90 ESAD to 120 ESAD. Their experiments were realized on an atmospheric dual-rotor WRE where precise specifications are provided in Table 2.12. The engine rotational speed was set to 3000 RPM with fixed ignition timing. The data was

extracted using an online graph digitizer, and a low-frequency filter was applied to remove digitizing noise.

The 0° ESAD in this work is set at Top Dead Center (TDC) and a schematic representation is shown in Figure 2.7. However, for further computations, pressure

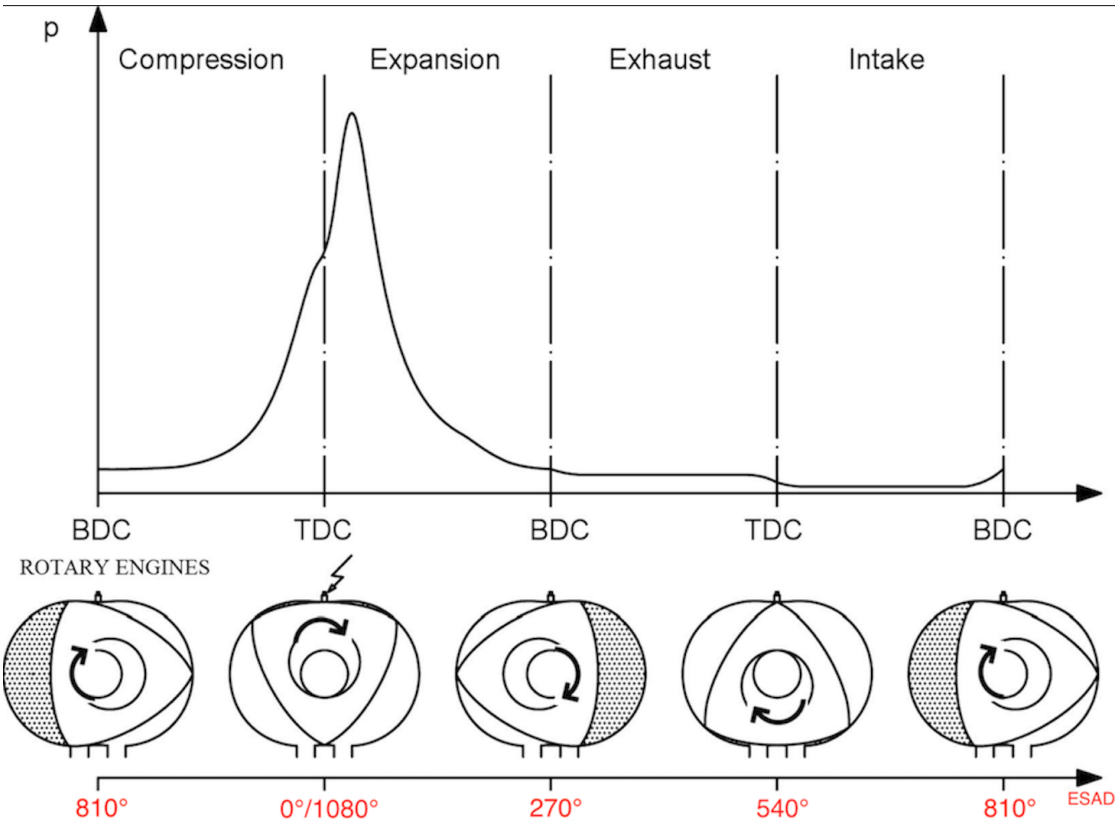


Figure 2.7: Representation of the Wankel Rotary Engine. Adapted from [6]

traces from the intake valve closing (IVC) to the exhaust valve opening (EVO) is required. To achieve this, a polytropic compression is assumed over missing data, and a polytropic expansion is assumed over missing data. A polytropic process is a thermodynamic description that encompasses both expansion and compression while accounting for heat transfer. It can be mathematically represented as follows:

$$pV^n = Constant \tag{2.1}$$

where n is such called the polytropic coefficient. It is possible to compute this coefficient from the input data for the compression and expansion strokes as follows:

$$n = \frac{log(\frac{p_1}{p_2})}{log(\frac{V_2}{V_1})}$$

By using this process, the mean polytropic coefficient can be evaluated and the result can be reused to better estimate the engine behavior over the range of missing data. The final results are shown on Figure 2.8 and Figure 2.9.

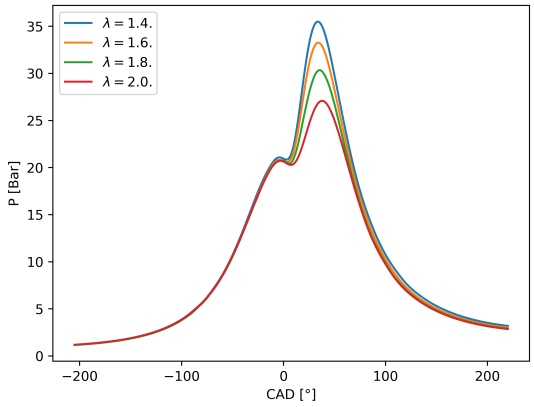


Figure 2.8: In-cylinder pressure trace

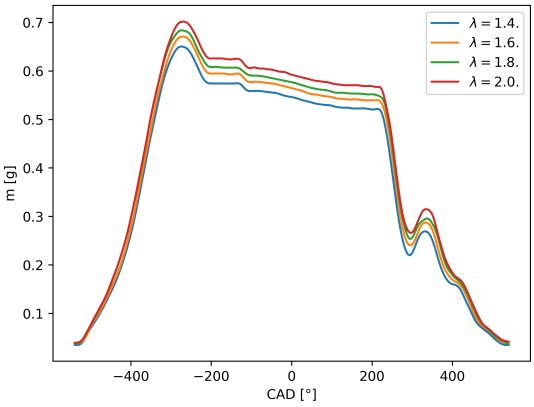


Figure 2.9: In-cylinder mass trace

Specification	Value
RPM	3000
Displacement V_d [L]	0.654×2
Eccentricity e [mm]	15
Generating Radius R [mm]	105
Width b [mm]	80
Compression ratio τ	10.0
Intake Charge Type	Natural Aspiration
Intake Type	Side Ported
Exhaust Type	Side Ported
Intake Close [BTDC]	205 ESAD
Exhaust Open [ATDC]	220 ESAD

Table 2.12: Specification of the Wankel Rotary engine. Adapted form [19]

2.2.2 Data post-processing

This section of the thesis focuses on the post-processing of the collected data. In order to effectively investigate the behavior of the HWRE over a range of air-fuel ratios, it is crucial to develop a consistent data post-process methodology based on the gathered pressure and mass data. By utilizing the pressure trace, various

methods can be employed to analyze the combustion process inside the engine's cylinder. For this study, an approach based on the "Heat Released Rate" and the first law of thermodynamics is adopted.

The in-cylinder pressure change with respect to the eccentric shaft angle is influenced by several factors, such as changes in cylinder volume, combustion, heat transfer to the walls, flow into and out of crevices, and leakage. Since combustion and heat transfer exert the most significant impact, contributions from crevice flow and mass leakage can be disregarded. By simplifying these factors, details about the combustion rate can be derived from accurate pressure measurements [40].

This method provides an approximation of real quantities that cannot be precisely determined. By incorporating a model that represents the significant heat transfer effects within the cylinder, it becomes possible to derive an approximation of the hydrogen combustion behavior inside the cylinder. Although this method relies on certain approximations, it offers a solid approach to analyze the combustion characteristics in the HWRE [40].

The section primarily focuses on three main aspects: analyzing the combustion behavior inside the cylinder, evaluating the associated heat loss, and assessing the overall performance of the engine.

Wankel engine geometry

For post-processing accuracy, it is essential to consider the unique shape of the WRE, as it significantly impacts the determination of volume and air compared to typical reciprocating engines. Due to the engine's distinct design, traditional methods used for volume and air calculations in reciprocating engines may not be directly applicable. Therefore, specialized approaches must be developed to accurately assess these parameters.

First, the side area of the working chamber represented on Figure 2.10 is determined as follows [5]:

$$\begin{aligned} F(\theta) =& \frac{\pi}{3}e^2 + eR\left\{2\cos(\arcsin(\frac{3e}{R})) - \frac{3\sqrt{3}}{2}\sin\left(\frac{2}{3}\theta + \frac{\pi}{2}\right)\right\} \\ &+ \left(\frac{2}{9}R^2 + 4e^2\right)\arcsin(\frac{3e}{R}) \quad [m^2] \end{aligned} \tag{2.2}$$

Where

- e the eccentricity $[m]$
- R the generating radius of the peritrochoid $[m]$
- θ the eccentric shaft angle $[deg]$

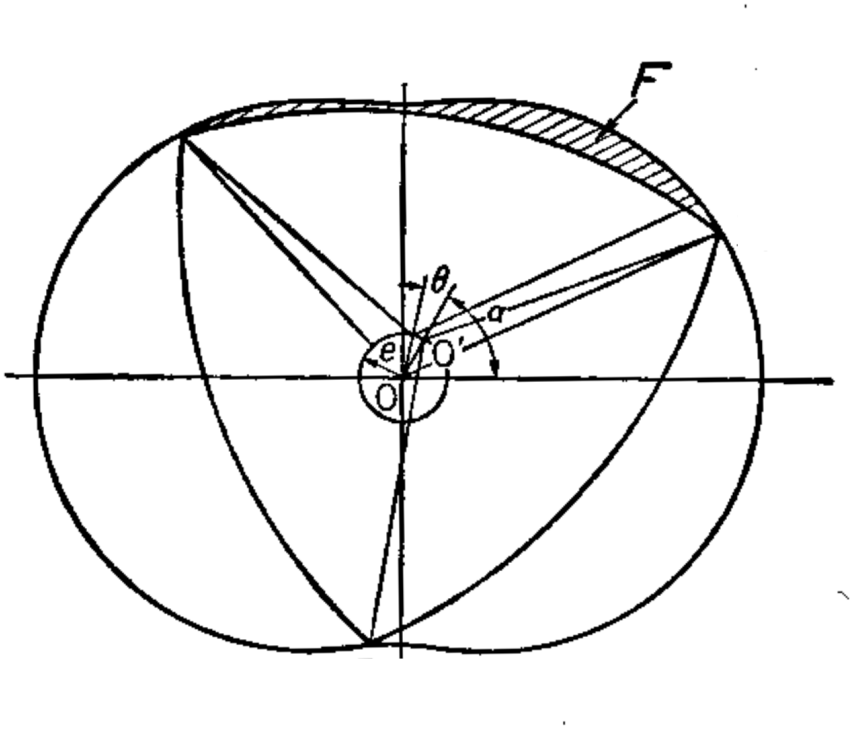


Figure 2.10: Side Area of the working chamber [5]

The working chamber volume can then be determined by multiplying the side area by the rotor width which leads to equation 2.3:

$$V(\theta) = b \cdot F(\theta) = V_c + \frac{3\sqrt{3}}{3} eRb \left\{ 1 - \sin\left(\frac{2}{3}\theta + \frac{\pi}{2}\right) \right\} \quad [m^3] \tag{2.3}$$

Where

- b the rotor width $[m]$
- V_c the clearance volume of the working chamber $[m^3]$

Finally the clearance volume is computed based on the engine's design parameters :

$$V_c = \frac{V_d}{\tau - 1} \quad [m^3]$$

Where

- V_d the displacement volume $[m^3]$
- τ the compression ratio $[-]$

Subsequently, by deriving the volume equation with respect to the eccentric shaft angle, the following expression is obtained:

$$\frac{dV(\theta)}{d\theta} = -\sqrt{3}eRb\cos(\frac{2}{3}\theta + \frac{\pi}{2}) \quad [m^3/s] \tag{2.4}$$

The unique geometry of the Wankel engine necessitates an approximation and division of the working chamber area into three distinctive regions: the constant rotor area, the side area, and the housing area [67, 68].

First, the rotor length can be approximated by a circular arc:

$$L = 2R_x\beta \quad [m]$$

where

- $R_x = \frac{R^2 - 2eR + 4e^2}{R - 4e}$ the radius of the circular arc approximation.
- $\beta = \frac{\sqrt{3R}}{(\frac{6eR}{R-4e}) + R + 2e}$ half the angle created by the circular arc.

The rotor area is constant and is approximated using the rotor's length :

$$A_{Rotor} = Lb \quad [m^2]$$

The sides areas depend on the eccentric shaft angle and is approximated using the volume :

$$A_{Side}(\theta) = \frac{V(\theta)}{b} \quad [m^2]$$

Finally, the housing area depends on the eccentric shaft angle and is approximated using the volume as well:

$$A_{Housing}(\theta) = \frac{V(\theta)}{L} + bL \quad [m^2]$$

The total approximated area of the working chamber is calculated by adding together the individual approximated areas of its components :

$$A(\theta) = A_{Rotor} + 2A_{Side}(\theta) + A_{Housing}(\theta) \tag{2.5}$$

$$= 2[\frac{V(\theta)}{b} + \frac{V(\theta)}{L} + bL] \quad [m^2] \tag{2.6}$$

Combustion reaction

The stoichiometric combustion reaction of any fuel with air excess can be represented with respect to the excess of air λ as follows :

$$\mathrm{C}_z\mathrm{H}_y\mathrm{O}_x + \lambda\left(z + \frac{y-2x}{4}\right)(\mathrm{O}_2 + \psi\mathrm{N}_2) \longrightarrow$$
$$a_0\mathrm{O}_2 + a_1\mathrm{CO} + a_2\mathrm{CO}_2 + b_1\mathrm{H}_2 + b_2\mathrm{H}_2\mathrm{O} + \psi\lambda(z + \frac{y-2x}{4})\mathrm{N}_2$$

By balancing the stoichiometric combustion reaction with hydrogen as a fuel, the resulting combustion equation with air excess is represented as follows :

$$\mathrm{H}_2 + \frac{1}{2}\lambda(\mathrm{O}_2 + \psi\mathrm{N}_2) \longrightarrow \mathrm{H}_2\mathrm{O} + \frac{1}{2}(\lambda-1)\mathrm{O}_2 + \frac{1}{2}\lambda\psi\mathrm{N}_2$$

Where

- $\lambda = \frac{(A/F)_{acutal}}{(A/F)_s}$, the air-fuel ratio
- $\psi = 3.76$, the molar N/O ratio for air

The combustion reaction of hydrogen with air involves the chemical combination of hydrogen gas and atmospheric oxygen. As a result of this exothermic process, hydrogen reacts with oxygen to primarily form water vapor (H2O) while releasing a substantial amount of heat energy. While combustion reactions can lead to the formation of various byproducts, such as NOx, for the purpose of this analysis, the focus will be solely on the lean and stoichiometric reaction leading to $\mathrm{H}_2\mathrm{O}$, O_2 and N_2 as stated here above. Other byproducts and their effects will not be considered in this specific context.

Molar mass

The molar mass of the combustion reaction is derived from the law of conservation of mass, which postulates that the total mass of the reactants must equal the total mass of the products, considering no leakage. Moreover, assuming that the reaction rate of all species involved is identical, the equation can be rewritten for the in-cylinder molar mass, depending on the Mass Fraction Burned (MFB) :

$$M_m(\theta) = [1 - MFB(\theta)]M_m^{Reactants} + [MFB(\theta)]M_m^{Products} \quad [kg/mol] \tag{2.7}$$

Where the molar mass of reactants and products can be found using a weighted sum :

$$M_m^{Products} = M_m^{H2O}\tilde{X}_{H20} + M_m^{O2}\tilde{X}_{O2} + M_m^{N2}\tilde{X}_{N2}$$
$$M_m^{Reactants} = M_m^{H2}\tilde{X}_{H2} + M_m^{O2}\tilde{X}_{O2} + M_m^{N2}\tilde{X}_{N2} + M_m^{Products}\tilde{X}_{RG}$$

Where $\tilde{X}_i$ stats for the mole fraction of each species i and $\tilde{X}_{RG}$ is the mole fraction of residual gas trapped in-cylinder after intake valve closing.

In-cylinder temperature

The in-cylinder temperature during the combustion process can be determined by applying the ideal gas law. Assuming here the in-cylinder content to be an ideal gas at uniform temperature without any mass leakage :

$$T(\theta) = \frac{p(\theta)V(\theta)}{m_{IVC}R(\theta)} \quad [K] \tag{2.8}$$

Where here, m_{IVC} represents the mass of the mixture in-cylinder after the intake valve closing, and where the specific gas constant directly depends on the mass fraction burned :

$$R(\theta) = \frac{\tilde{R}}{M_m(\theta)} \quad [J/kgK]$$

Specific heat ratios

In order to determine the rate of heat released, one of the most important parameters is the ratio of specific heats [69]:

$$\gamma(\theta) = \frac{\tilde{c}_p(T)}{\tilde{c}_v(T)} \quad [-] \tag{2.9}$$

Considering the cylinder content as an ideal gas, the specific heats then depends only on the temperature, and thus γ depends on the temperature as well. It is then crucial to update its value based on the calculated temperature during combustion to achieve the most accurate prediction.

To compute the specific heat for each species, polynomial fits are utilized based on thermodynamic data. The JANFA thermodynamic tables from the NASA equilibrium program offer a valuable resource for determining the heat capacities at a constant pressure of each species present in the mixture as follows [70]:

$$\frac{\tilde{c}_p^i}{\tilde{R}} = a_1^i + a_2^i T + a_3^i T^2 + a_4^i T^3 + a_5^i T^4 \quad [-]$$

By employing these polynomial fits, the specific heats can be computed for further analysis of the mixture thermodynamic behavior [40].
Finally, the mixture heat capacity is computed based on the characteristics of the reactants and products :

$$\tilde{c}_p(\theta) = (1 - MFB(\theta))\, \tilde{c}_p^{Reactants} + (MFB(\theta))\, \tilde{c}_p^{Products} \quad [J/molK]$$

Where the heat capacities of reactants and products can be found with the weighted sum:

$$\tilde{c}_p^{Products} = \tilde{c}_{p,H2O}\tilde{X}_{H20} + \tilde{c}_{p,O2}\tilde{X}_{O2} + \tilde{c}_{p,N2}\tilde{X}_{N2}$$
$$\tilde{c}_p^{Reactants} = \tilde{c}_{p,H2}\tilde{X}_{H2} + \tilde{c}_{p,O2}\tilde{X}_{O2} + \tilde{c}_{p,N2}\tilde{X}_{N2} + \tilde{c}_{p,Products}\tilde{X}_{RG}$$

Where $\tilde{X}_i$ stats for the mole fraction of each species i and $\tilde{X}_{RG}$ is the mole fraction of residual gas trapped in-cylinder at IVC.

Heat released

Having identified and discussed all the requisite parameters, the next step is to delve into the analysis of the net heat release rate. For this, establishing the differential form of the first law of thermodynamics is essential. The analysis will assume that the content within the cylinder behaves as an ideal gas, with no leakage and no crevice volume.

On the first hand, the statement for the first law of thermodynamics can be stated as follows :

$$\begin{aligned} dU &= dQ_{net} - pdV \\ mc_v\frac{dT}{d\theta} &= \frac{dQ_{net}}{d\theta} - p\frac{dV}{d\theta} \\ \frac{c_v}{R}\frac{1}{T}\frac{dT}{d\theta} &= \frac{1}{pV}\frac{dQ_{net}}{d\theta} - \frac{1}{V}\frac{dV}{d\theta} \end{aligned} \tag{2.10}$$

On the other hand, the ideal gas law can be stated as follows :

$$\begin{aligned} pV &= mRT \\ p\frac{dV}{d\theta} + V\frac{dp}{d\theta} &= mR\frac{dT}{d\theta} \\ \frac{1}{V}\frac{dV}{d\theta} + \frac{1}{p}\frac{dp}{d\theta} &= \frac{1}{T}\frac{dT}{d\theta} \end{aligned} \tag{2.11}$$

By combining both Equation 2.10 and Equation 2.11, Equation 2.12 can be written for the rate of heat release [71]:

$$\frac{dQ_{net}}{d\theta} = \frac{\gamma}{\gamma-1}p\frac{dV}{d\theta} + \frac{1}{\gamma-1}V\frac{dp}{d\theta} \quad [J/ESAD] \tag{2.12}$$

One considerable benefit of this methodology is that it directly correlates pressure fluctuations with the quantity of fuel's chemical energy released via combustion. Indeed, the net rate of heat released ($\frac{dQ_{net}}{d\theta}$) can be considered as the difference

between the rate of chemical energy released during the combustion of the fuel ($\frac{dQ_{ch}}{d\theta}$) and the rate of heat transfer from the system to the cylinder walls ($\frac{dQ_w}{d\theta}$) [40][72][73].

$$\frac{dQ_{net}}{d\theta} = \frac{dQ_{ch}}{d\theta} - \frac{dQ_w}{d\theta} \quad [J/ESAD] \tag{2.13}$$

By integrating the net rate of heat released of equation 2.12 over the combustion cycle, a profile is obtained that contains key aspects of the combustion process within the engine's combustion chamber. This profile offers a snapshot of how heat is generated and used throughout the combustion process, serving as a valuable tool for understanding engine operation.

$$Q_{net}(\theta) = \int_{start}^{stop} \frac{dQ_{net}(\theta)}{d\theta} d\theta \quad [J] \tag{2.14}$$

Often, it is useful to normalize this net heat released profile by the maximum value to give unity. This normalization process creates a dimensionless quantity named the Mass Fraction Burned, which offers a relative measure of the heat released throughout the combustion cycle [40].

$$MFB(\theta) = \frac{Q_{net}(\theta)}{Q_{net,max}} \quad [-] \tag{2.15}$$

Mass fraction burned

First, the MFB refers to the proportion of the overall fuel-air mix in the combustion chamber that has undergone combustion at any specific time. As a normative function, the MFB ranges from 0 to 1. At the outset of the combustion process, the MFB is 0, indicating no consumption of the fuel-air mixture. When the combustion is complete, the MFB ideally reaches 1, suggesting the entire fuel-air mix has been combusted.

It's clear at this point that an iterative loop is required when representing the combustion process. This necessity arises due to the interdependent relationship between several key parameters in the process.

Indeed, The calculation of the MFB relies on the heat capacities ratio. This ratio, in turn, is influenced by the temperature within the combustion chamber. Yet, this temperature profile isn't standalone; it is dependent on the molar mass of the in-cylinder mixture. The molar mass of this mixture is dynamic and changes throughout the combustion process, directly influenced by the MFB itself. As fuel-air mixture is burned, the molar mass of the mixture changes, as combustion products replace the original fuel-air mixture.

So, there exists a cycle of dependencies: the MFB affects the molar mass, which influences the temperature, which in turn affects the heat capacities ratio, and consequently, the MFB itself. Therefore, an iterative computational process is required and represented in Figure 2.11. In this process, an initial estimate of the MFB is used to calculate the other parameters, then these results are used to update the MFB estimation, and this process is repeated until the solution converges.

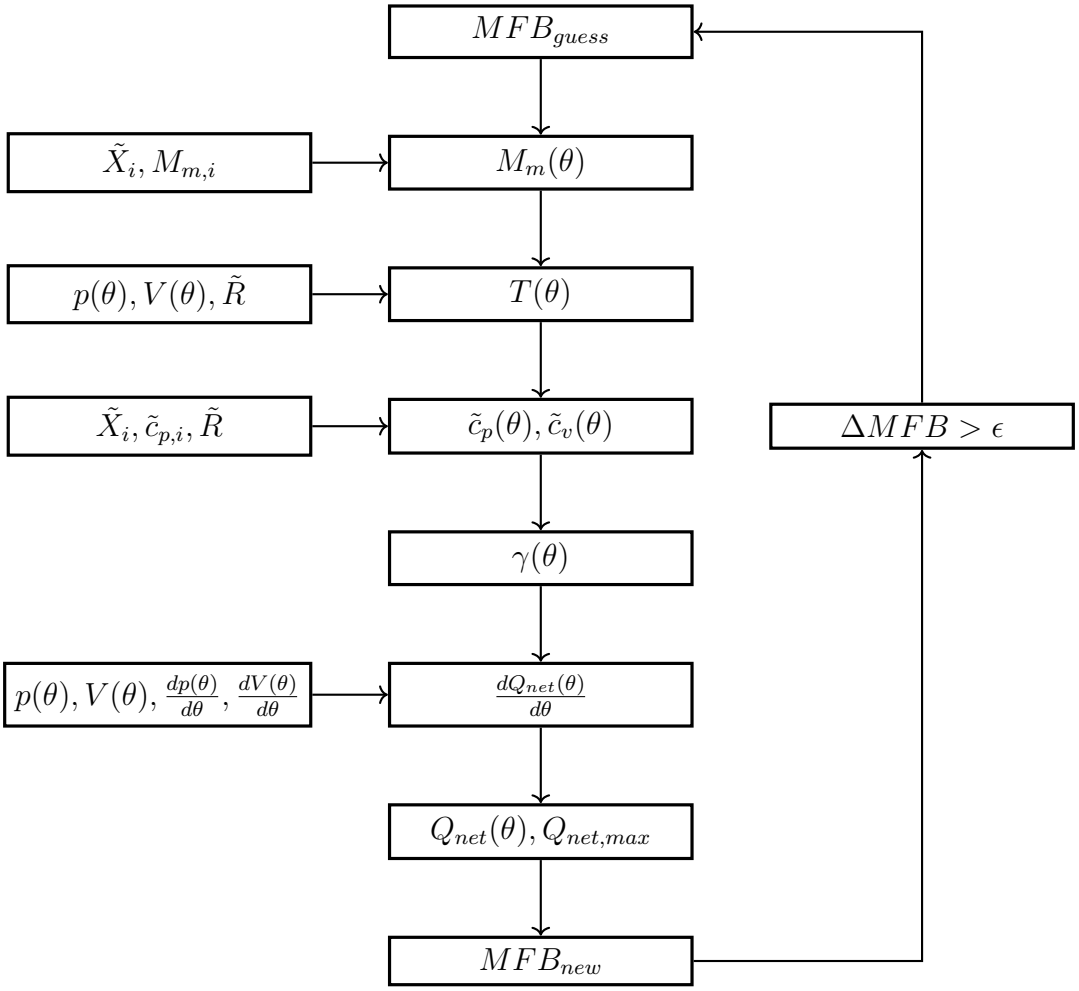


Figure 2.11: Iteration process overview for the MFB determination.

Heat transfer

Within an ICE, heat flux typically involves convective and radiative heat transfer from the in-cylinder contents to the walls, followed by convection from the combustion chamber walls to the engine's cooling system. The conditions for heat transfer - pressure, temperature, velocities, and surface area - vary based on the engine operating cycle. Research has generally determined that for most applications, the assumption of quasi-steady heat transfer is adequate. Furthermore, in the context of a pre-mixed spark ignition engine, where the combustion produces a dim-flame, the contribution of the radiation component is usually so small as to be disregarded [40][74].

Convective heat transfer is typically characterized as the movement of heat through a flowing fluid, and between a fluid and a solid surface. In the context of an ICE, the in-cylinder contents experience a forced motion triggered by the piston's movement, leading to what is called forced convection. For a steady flow forced convection heat transfer scenario, the heat flux transfer to a solid surface, can be computed using Newton's law:

$$\dot{q} = h_c(T - T_w) \quad [W/m^2] \tag{2.16}$$

Where

- h_c the heat transfer coefficient $[W/m^2K]$
- T the in-cylinder mean temperature $[K]$
- T_w the in-cylinder wall temperature $[K]$

The Woschni heat transfer model, established in 1967, is renowned and widely used for computing the heat transfer coefficient in both spark ignition and compression ICE. Unlike other correlations that consider the gas velocity to remain constant throughout the engine cycle, Woschni's correlation offers the most comprehensive approach for estimating convective heat transfer and can be written as follows [47]:

$$h_c(\theta) = 0.013 p(\theta)^{0.8} T(\theta)^{-0.52} d^{-0.2} w(\theta)^{0.8} \quad [W/m^2K] \tag{2.17}$$

Where

- $p(\theta)$ the in-cylinder pressure $[Pa]$
- $T(\theta)$ the in-cylinder mean temperature $[K]$
- $d(\theta)$ the characteristic length $[m]$

- $w(\theta)$ the velocity term $[m/s]$

Woschni stated that combustion's effect mainly increased fluid velocity, thus introducing a unique combustion term proportional to the pressure difference between the fired and motored states. Consequently, he incorporated the pressure difference between fired and motored operations $(p - p_m)$ into the characteristic velocity to reflect the combustion's impact on heat transfer. The magnitude of the gas velocity within the cylinder depends on the engine's operating conditions and can be calculated with equation 2.18 [75][68].

$$w(\theta) = C_1 w_z + C_2 \frac{V_d T_0}{p_0 V_0}(p(\theta) - p_m(\theta)) \tag{2.18}$$

Where

- $p(\theta)$ the firing pressure $[Pa]$
- $p_m(\theta)$ the motoring pressure $[Pa]$
- V_d the displacement volume $[m^3]$
- w_z the average rotor's velocity $[m/s]$
- T_0, p_0, V_0 correspond to a reference point before combustion $[K], [Pa], [m^3]$
- C_1, C_2 Constants

Take into account that for the unique architecture of the Wankel engine, the mean piston speed and the characteristic length require modification [68]:

$$\begin{cases} w_z = \dfrac{R\omega}{3} \\ d = (\dfrac{1}{b} + \dfrac{bL}{V})^{-1} \end{cases}$$

This correlation can now be used to compute the heat transfer losses within the cylinder during the combustion process. By computing the heat flux using Newton's law and Woschni correlation, it becomes possible to calculate the rate of heat loss due to conduction.

This rate of heat loss can be computed as follows :

$$\frac{dQ_w}{d\theta} = \frac{dQ_w}{dt}\frac{dt}{d\theta} = \frac{dQ_w}{dt}\frac{1}{\omega} \quad [J/ESAD]$$

Where $\frac{dQ_w(\theta)}{dt}$ is obtained from Newton's equation 2.16 and thus it can be rewritten as follows :

$$\begin{aligned} \frac{dQ_w(\theta)}{d\theta} &= A(\theta)\dot{q}\frac{1}{\omega} \quad [J/ESAD] \\ &= h_c(\theta)A(\theta)(T(\theta) - T_w)\frac{1}{\omega} \end{aligned} \tag{2.19}$$

Where

- h_c the heat transfer coefficient $[W/m^2K]$
- A the in-cylinder area $[m^2]$
- T the in-cylinder content mean temperature $[K]$
- T_w the in-cylinder wall temperature $[K]$
- ω the rotor's angular velocity $[s^{-1}]$

It's essential to highlight that the wall temperature is assumed to remain constant throughout the combustion process. Given the absence of experimental data concerning the wall temperature and to simplify the model, the wall temperature has been approximated as $450[K]$ as reported in [76] for a HWRE.

Heat transfer model calibration

In the examination, it was observed that the heat transfer model incorporates constants due to its semi-empirical nature. Specifically, Danieli et al. suggested the values $C_1 = 1$ and $C_2 = 0.00324$ for the Wankel engine in [68]. However, Shudo et al. revealed that unfortunately, the current equations using these constants underestimate the cooling loss of hydrogen when compared to experimental data. Therefore, by adjusting these constants, a more precise representation of the heat transfer processes occurring within the engine's combustion chamber can be achieved [77][78].

In order to better represent the rapid combustion of hydrogen, the method proposed is to apply a calibration constant (C_3) to the term representing the increase in gas motion, as all other terms are constant for fixed engine conditions. Thus the Equation 2.18 can be rewritten as follows :

$$w(\theta) = w_z + 0.00324C_3\frac{V_d T_0}{p_0 V_0}(p(\theta) - p_m(\theta)) \quad [m/s]$$

An effective method of calibration, using pressure trace data, consists to ensure that the energy released within the cylinder matches with the sum of the cumulative net

heat released and the heat loss at any eccentric shaft angle [79, 72]. Integrating equation 2.13 :

$$Q_{ch}(\theta) = Q_{net}(\theta) + Q_w(\theta) \quad [J] \tag{2.20}$$

Where the chemical energy released at any crank angle degree should be equal to the energy of the fuel multiplied by the MFB. The fuel chemical energy is computed by the mass of fuel multiplied by its lower heating value (LHV) and the combustion efficiency :

$$Q_{ch}(\theta) = MFB(\theta)\eta_c m_f LHV \quad [J] \tag{2.21}$$

Where here, as no information is available for the exhaust gas analysis, the combustion efficiency is approximated as being equal to unity. Additionally, Lee et al. reported very low combustion loss, reaching a maximum value of 0.32%, over a large range of excess ratios in HRPE [80]. Considering these low values, the combustion efficiency is disregarded.

Using a minimization algorithm, an objective function f can be written as equation 2.22:

$$f = \frac{1}{n_i} \sum_{\theta_i} \sqrt{\left[Q_{ch}(\theta) - (Q_{net}(\theta) + Q_w(\theta))\right]^2} \tag{2.22}$$

After convergence, the minimization algorithm gives the value for C_3 which allows to compute the heat transfer coefficient for any eccentric shaft angle.

Otto efficiency

A spark ignition engine can be described by an ideal cycle known as the constant volume heat addition cycle or Otto cycle. This representation is an idealized model that considers four main stages: isentropic compression, constant volume heat addition, isentropic expansion, and constant volume heat rejection. It serves as a simplified theoretical framework to understand the engine's behavior during its operation.

The efficiency of the Otto cycle, denoted as η_{Otto}, is a key parameter to evaluate the engine's performance. It can be computed using the following expression:

$$\eta_{Otto} = 1 - \frac{1}{\tau^{\bar{\gamma}-1}} \quad [-] \tag{2.23}$$

where τ represents the compression ratio, and $\bar{\gamma}$ denotes the mean ratio of specific heat capacities of the working fluid over the entire cycle.

Real-world engines, however, face various inefficiencies due to factors like heat loss, friction, incomplete combustion, and not constant volume heat addition, resulting in actual efficiencies that are lower than the theoretical values.

Degree of Constant Volume

The degree of constant volume, denoted as η_{glh}, is a critical, parameter used to assess the engine's ability to approximate constant volume heat addition during the combustion process. It can be computed using the net rate of heat released as follows [47] :

$$\eta_{glh} = \frac{1}{\eta_{Otto} Q_{net}} \int \left(1 - \left(\frac{V_d + V_c}{V(\theta)}\right)^{\gamma-1}\right) \frac{dQ_{net}}{d\theta} d\theta \quad [-] \tag{2.24}$$

Where V_d is the displacement volume and V_c is the clearance volume.

Wall heat loss ratio

Considering heat loss and incorporating them into the analysis is a crucial aspect when investigating efficiencies. To quantify the impact of heat loss, the wall heat loss ratio is employed, which measures the significance of heat loss in relation to the chemical energy released. This ratio can be calculated using the following formula:

$$\phi_w = \frac{Q_w}{Q_{ch}} \quad [-] \tag{2.25}$$

Internal thermodynamic efficiency

Finally, considering all these terms the indicated efficiency can be found as follows :

$$\eta_i = \eta_{Otto} \eta_{glh} \eta_c (1 - \phi_w) \quad [-] \tag{2.26}$$

This efficiency gives an idea of quality of conversion of the input energy into useful work done by the engine.

Work, IMEP and power

The net indicated work refers to the work exerted by the gas on the piston inside the cylinder during each engine cycle. It can be computed by integrating the pressure over the variation in volume during the compression-expansion stroke :

$$W_{net} = \int_{IVC}^{EVO} p(\theta) \frac{dV(\theta)}{d\theta} d\theta \quad [J] \tag{2.27}$$

The Indicated Mean Effective Pressure (IMEP) is a significant parameter used to characterize the performance of a reciprocating engine. It provides a measure

of the engine's ability to perform work, independent of its displacement, and is defined as follows:

$$IMEP_{net} = \frac{W_{net}}{V_d} \quad [Pa] \tag{2.28}$$

Ultimately, the net power output of the engine can be determined by multiplying the work done per cycle by the rotational speed (N) of the eccentric shaft and then dividing by the number of power strokes per rotation (n_c) :

$$P_{net} = \frac{W_{net} N}{n_c} \quad [W] \tag{2.29}$$

Note here that $n_c = 1$ for a WRE.

Hypothesis

In order to simplify the engine behavior and streamline the analysis, several assumptions have been made. Firstly, the in-cylinder unburned reactants and burned products are treated as a single mixture. This mixture is modeled to behave as an ideal gas. Furthermore, both the unburned reactants and the burned products are considered frozen, indicating that their chemical composition remains unchanged. It is also assumed that all species within the mixture have identical reaction rates. Factors such as leakage and crevices are not taken into account since combustion and heat transfer are the primary contributors to cylinder pressure changes. Radiative heat transfer is overlooked in this analysis, and quasi-steady heat transfer is assumed to be applicable at any point in the cycle. Additionally, the engine wall temperature remains consistent throughout the cycle, set at $T_w = 450[K]$. Lastly, both in-cylinder pressure and temperature are presumed to be uniform at any given point of the cycle.

General view

To provide a comprehensive understanding of the computational post-processing method, a schematic representation can be found at Figure 2.12.

In the initial phase, inputs are derived from the research paper, which include the pressure trace, the mass of air, and the residual gas mass trapped in-cylinder. Taking into account the specific engine geometry, all related geometric values are computed upfront. Similarly, the fuel characteristics are also determined in advance.

Next, by using the pressure trace and the engine's geometry, IMEP, net indicated work and net power of the engine can be calculated.

Subsequently, the iterative loop described in section 2.2.2 is employed to compute the mass fraction burned, which is highlighted in red. Upon the algorithm's convergence, the molar mass, temperature, and thermodynamic properties (TDP) are known for every eccentric shaft angle, which then permits the resolution of the heat release rate equation.

The next stage involves the calibration of the heat transfer model based on the total chemical energy released, as detailed in section 2.2.2. After calibration, the heat transfer models can be used to calculate the heat loss.

As a final step, the remaining engine's characteristics can now be computed, such as the internal thermodynamic efficiency, the Otto efficiency, the heat loss ratio, and the degree of constant volume.

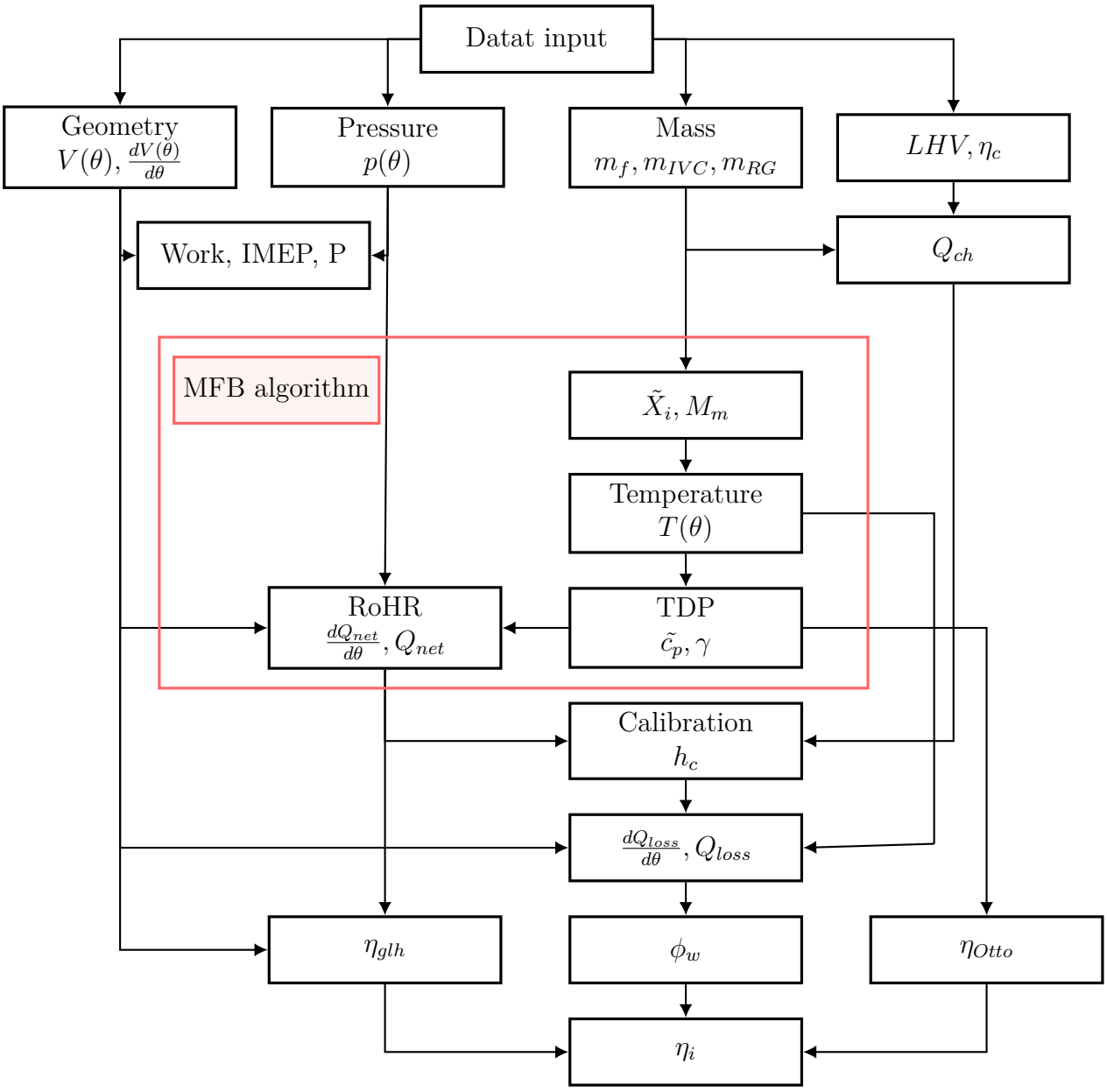


Figure 2.12: Post-processing method overview

Chapter 3

Results

In this section, the results generated will be presented and delved into, in order to identify the most promising technologies while understanding the operational nuances that could enhance the application of such technologies. Initially, emphasis is placed on the big-picture perspective and present results relative to the viability of vehicles. Subsequently, emphasis is placed on the small-picture perspective and develops the methodology relative to the performance of the HWRE.

3.1 Viability of vehicles

In this section, emphasis is placed on the big-picture perspective and present results relative to the viability of vehicles. A detailed exploration of the environmental implications associated with various vehicle technologies is presented. Initially, the Impact Assessment of five distinct vehicle types - two HEVs, an ICEV (the three of them being powered by a HWRE), a FCV and a BEV - is showcased. Their impacts in eight different categories are assessed. To facilitate the comparative analysis, results from these diverse impact categories are normalized. This normalization aids, on the one hand, in identifying the most influential categories, and on the other hand, in assembling all of the impacts from the various categories into one single score, allowing an easy to interpret comparison of the vehicles. Ending the big-picture, a sensitivity analysis is provided, highlighting the degree to which variations in certain inputs can influence the findings.

3.1.1 Life Cycle Impact Assessment results

As it has been explained in the methodology, eight impact categories are analyzed. The comparative assessment is done for five different vehicles, with four

different hydrogen production technologies: technology 1 is SMR, technology 2 is SMR+CCS, technology 3 is water electrolysis based in the Belgian electricity mix, and technology 4 is water electrolysis based in electricity from a renewable source in Belgium (coming from wind). For each of the impact categories that have been assessed, a bar graph is presented indicating the respective impacts for each vehicle, with each of the four hydrogen production methods. The number next to the vehicle's name represents thus the hydrogen production method that is considered.

Global warming potential

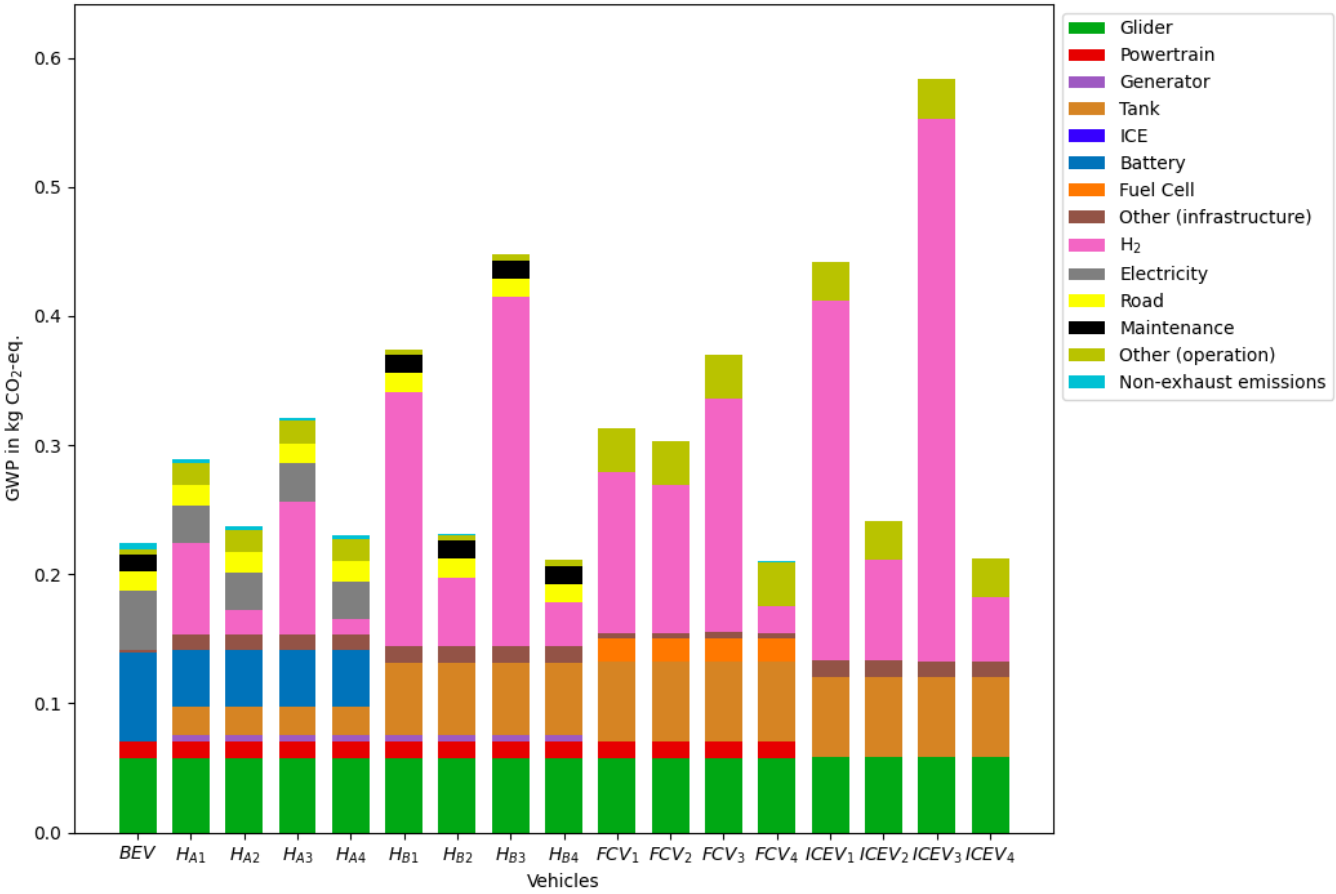


Figure 3.1: Global warming potential

The first thing to point out is that the green electrolysis is the hydrogen production method that has the less impacts for the global warming potential category. It is followed by the SMR with CCS. Moreover, the production method that comes

after is SMR, and finally, the one that has the highest impacts for this category is electrolysis with electricity from the grid.

It is important to point out that if every vehicle fueled with green electrolysis produced hydrogen is compared with each other, and with the BEV, they all have roughly the same global warming potential impact: this value oscillates around 0.21 kg CO_2-eq. If the ICEV is compared to the HEV_B, the ICEV consumes more hydrogen and therefore this has a greater impact, but this difference is compensated by the electric powertrain of the HEV_B. If the ICEV is compared to the FCV, this difference in hydrogen consumption is compensated by the impacts provoked by the fuel cell itself. For the FCV, ICEV, and HEV_B, compared to the BEV and to the HEV_A, their hydrogen storage tank provoke an important impact, which is compensated in the BEV and HEV_A by the impact due to the battery. Finally, comparing the BEV to the hydrogen fueled vehicles, it does not have the impact provoked by hydrogen, but this vehicle consumes electricity, which compensates these impacts.

In this category, there is potential for reduction of impacts for the BEV and the HEV_A, if a green production for the electricity that they consume was considered.

While the hydrogen production methods do not evolve towards a cleaner method such as SMR with CCS or green electrolysis, the ICEV and the HEV_B seem to be vehicles that have the most important impacts. Furthermore, while the hydrogen production does not evolve towards a cleaner method, the BEV seems to be the most interesting vehicle regarding the global warming potential.

As a conclusion, with a dirty hydrogen production method, the BEV is the most viable vehicle. With a clean hydrogen production method, the BEV, the FCV, and the three other vehicles containing a HWRE have the same impact level for this category.

Freshwater ecotoxicity potential

For the freshwater ecotoxicity potential, the hydrogen production method that has the lowest impact is SMR with CCS. It is important to point out that in the way that the inventory of the green electrolysis has been filled, it has even a greater impact for this category than SMR.

In this category, the only vehicle that seems to have an important impact compared to the others is the ICEV with dirty electrolysis produced hydrogen. The most interesting vehicle for this category is the ICEV with SMR with CCS produced

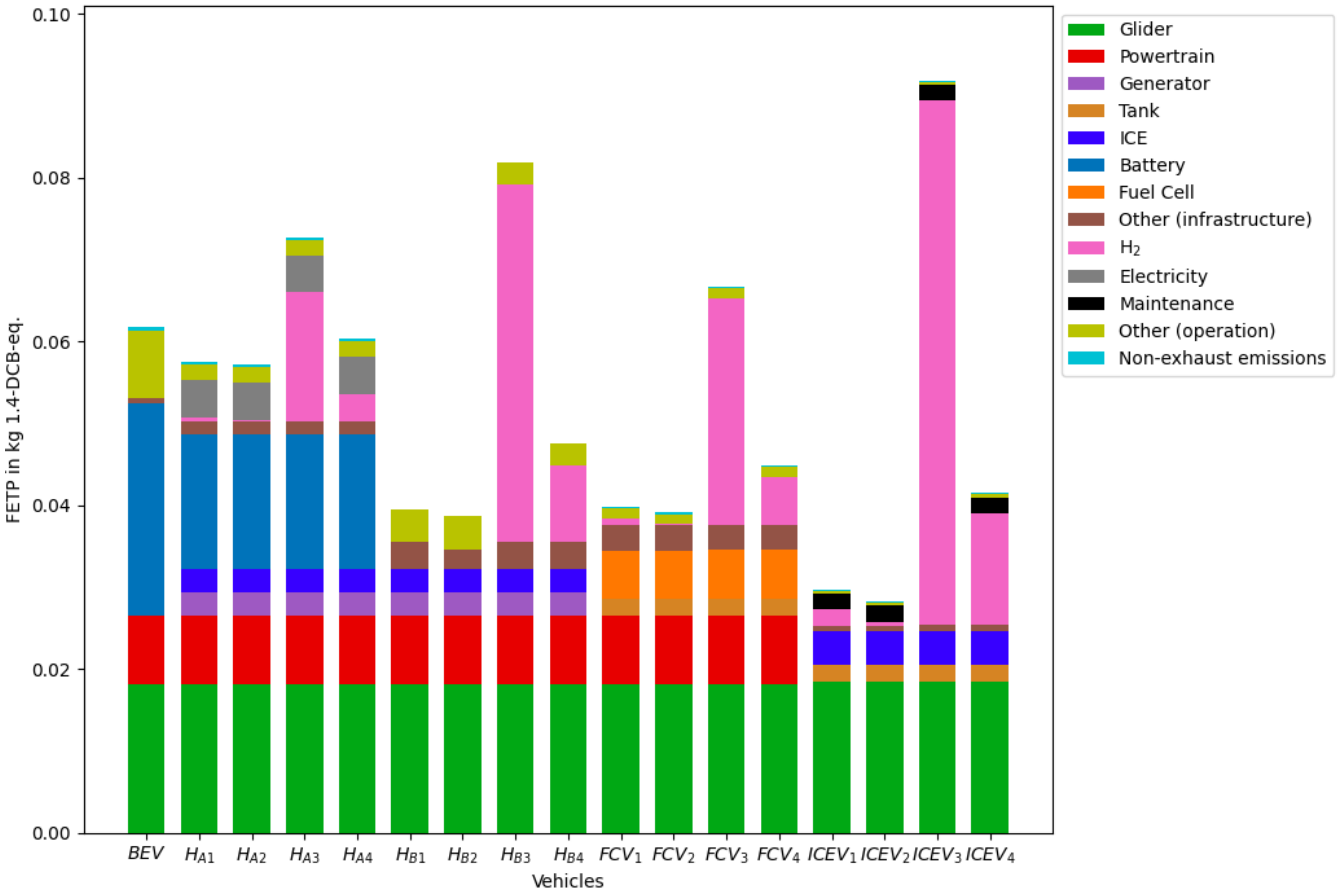


Figure 3.2: Freshwater ecotoxicity potential

hydrogen, where the greatest impact is due to the glider.

Even with a dirty hydrogen production such as SMR, the HEV_B, the ICEV and the FCV have interesting results compared to the other vehicles, with impacts considerably lower than those of the BEV or HEV_A, whose most important contribution is due to the battery.

As a conclusion, regardless of the fact that hydrogen is produced in a clean way (such as SMR with CCS), or in a dirty way (such as SMR), the ICEV is the vehicle with the lowest impacts. Furthermore, the HEV_B and the FCV seem to be interesting to take into account, also having lower impacts than the BEV for this category.

Marine ecotoxicity potential

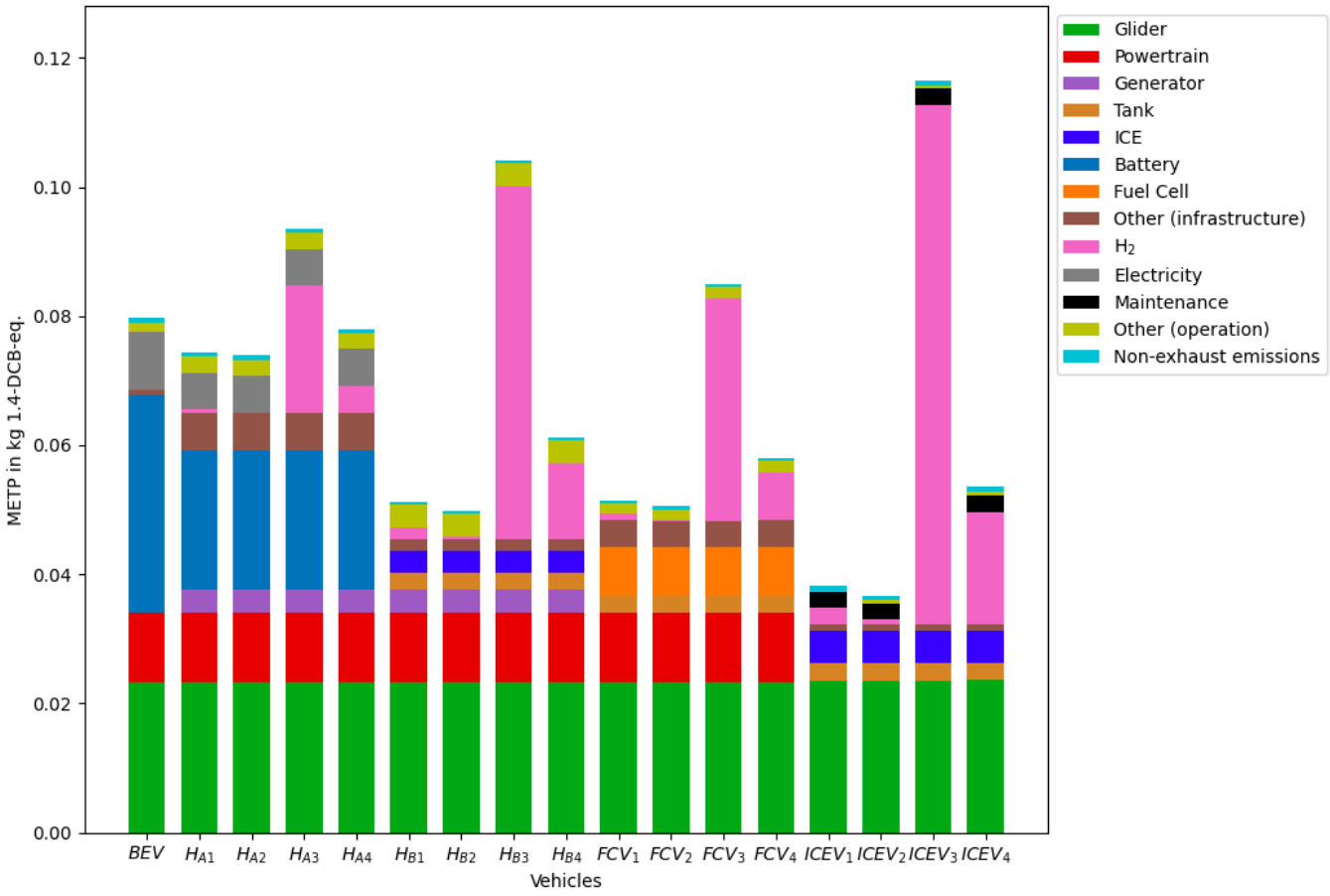


Figure 3.3: Marine ecotoxicity potential

For marine ecotoxicity potential, the observations join those that have been made for freshwater ecotoxicity potential. Indeed, the vehicle that has the less impact for this category is the ICEV, with both SMR or SMR with CCS. Again, the HEV_B, the FCV and the ICEV, have the advantage of being nearly battery free (or totally battery free for the ICEV). Their lower impact is also justified, as it has been said, by the low impacts caused by their energy carrier (SMR or SMR with CCS produced hydrogen), and is furthermore justified by the fact that their hydrogen storage tank does not contribute to a great impact. Even if a green electricity production method was considered for the BEV and the HEV_A's energy carrier, these vehicles would still have a greater impact than the three others.

Terrestrial ecotoxicity potential

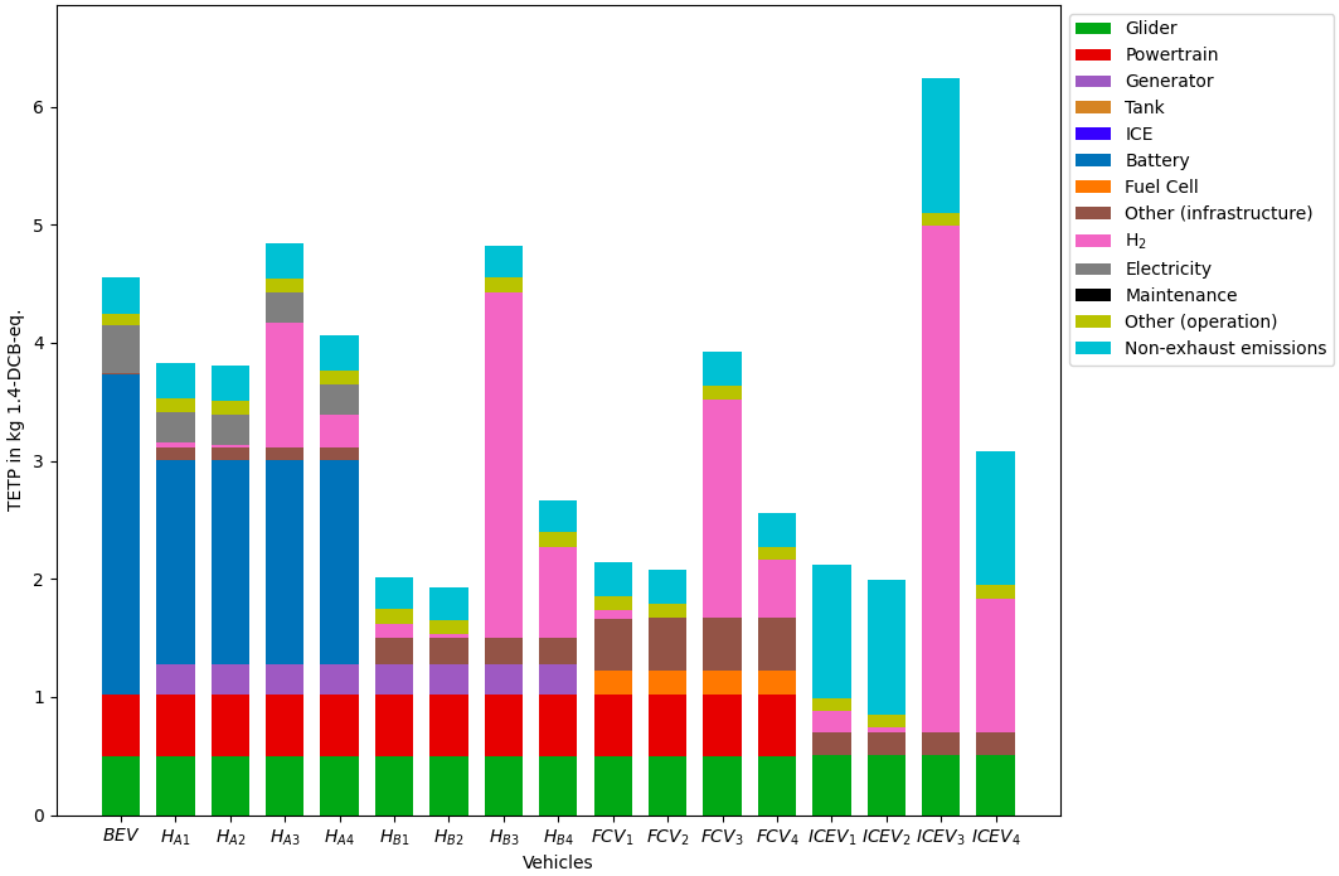


Figure 3.4: Terrestrial ecotoxicity potential

Again, for the terrestrial ecotoxicity potential, as for the freshwater or the marine ecotoxicity potential, the BEV and the HEV_A have a greater impact than the other three vehicles. However for this case it is interesting to point out that the ICEV does not really present better results than the BEV_B and the FCV. Indeed these three vehicles have the same levels of impact. The main reason for the ICEV not being more interesting than the BEV_B and the FCV for the terrestrial ecotoxicity potential is due to the non-exhaust emissions. Indeed, as it has been explained, the inventory of the ICEV has been filled in such a way that the break wear emissions of the ICEV are five times more important than those of the other vehicles, due to the fact that it does not benefit from regenerative breaking.

Moreover, it is important to point out that for the terrestrial ecotoxicity potential, opposed to the freshwater and marine ecotoxicity potential, even with the most impacting hydrogen production method, all of the hydrogen fueled vehicles, except for the ICEV, have impact levels similar to the one of the BEV. More precisely,

the FCV with its worst case hydrogen production method, has an impact that is not only similar, but also lower than the one of the BEV.

As a conclusion, with a clean or dirty hydrogen production method, the HEV_B, the FCV and the ICEV have the lowest impacts for the terrestrial ecotoxicity potential, and even with the most impacting hydrogen production method these vehicles remain viable (except for the ICEV).

Human toxicity potential (carcinogenic)

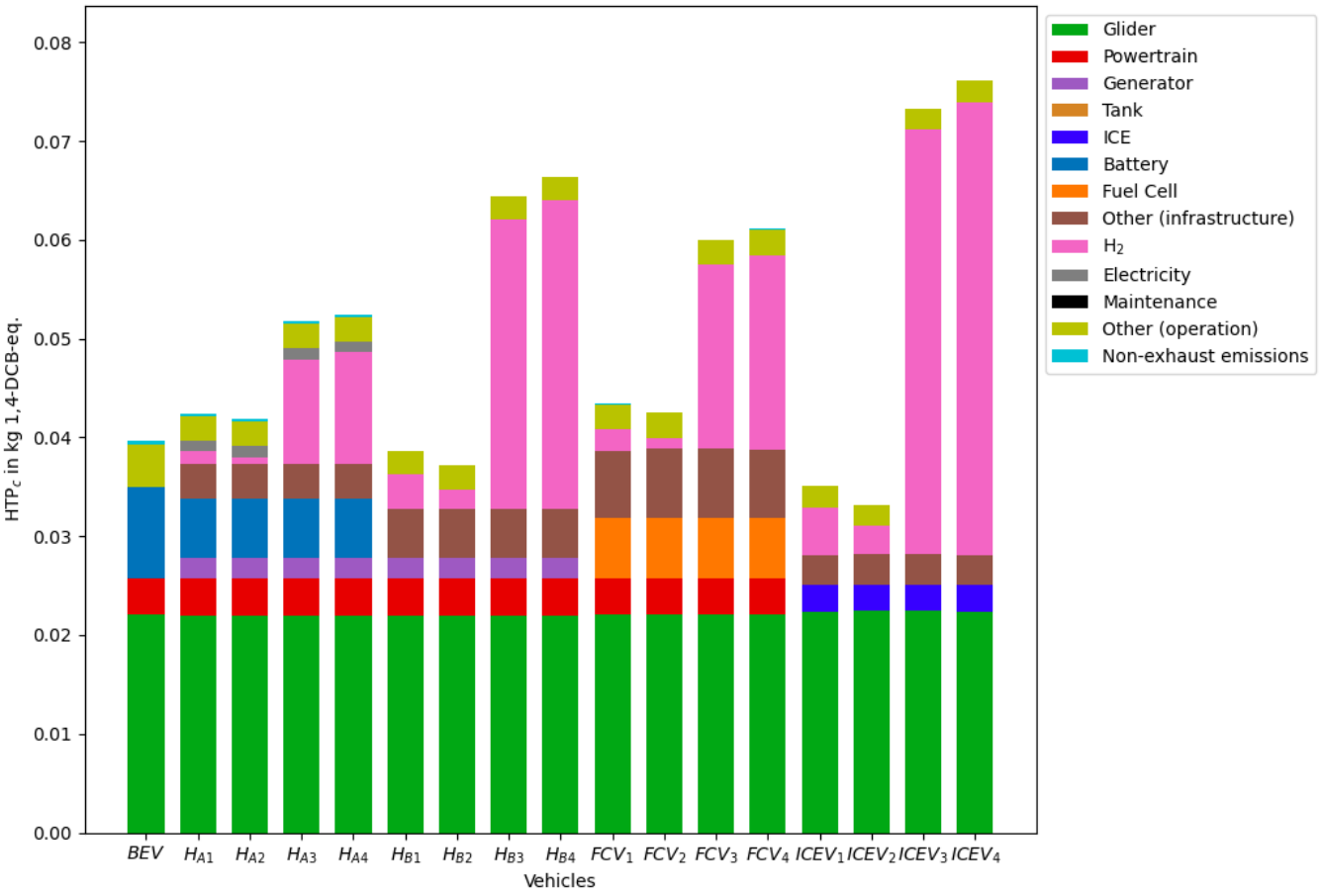


Figure 3.5: Human toxicity potential (carcinogenic)

Regarding the carcinogenic human toxicity potential, the hydrogen production methods with the greatest impacts are electrolysis and green electrolysis. The latter has even a greater impact than regular electrolysis. This is due to the fact that wind electricity production has a great impact in this category. If the electricity

used for green electricity would have been photovoltaic, this impact would be even greater. However, for a green electricity coming from electricity produced in a run-of-river power plant unit, this impact would be greatly reduced. As for the ecotoxicity potential, the carcinogenic human toxicity potential impacts of SMR and SMR with CCS do not have impacts that differ a lot, both being pretty low in comparison to the two other production methods.

For this category, all of the vehicles have comparable impacts, having all (in their optimal case) a similar level of impact. The HEV_B has an even lower impact than the other hybrid vehicle, the full electric vehicle, and even than the FCV. Its benefit comes from the fact that it does not have neither such a big battery as the HEV_A or the BEV, nor does it have a fuel cell of course.

Moreover, the vehicle with the lowest impact for this category is the ICEV, whose impact due to its ICE is lower than the impact of the electric powertrain (including the generator) of the HEV_B. The exceeding hydrogen consumption of this vehicle compared to the HEV_B does not cause a considerable impact.

Human toxicity potential (non-carcinogenic)

For the non-carcinogenic human toxicity potential, the green electrolysis impact is greatly reduced. However it is still greater than the impact of SMR or SMR with CCS. With all of the hydrogen production methods excluding the regular electrolysis, the less impacting vehicle for this category is the ICEV. The most interesting vehicle after the ICEV is the HEV_B, again for all of the production methods excluding regular electrolysis. Particularly, the ICEV with SMR with CCS produced hydrogen, has an impact that is even more than two times lower than the one of the BEV.

The battery in the BEV and in the HEV_A have a great impact in this category. Due to this important contribution, all of the other vehicles, even with the worst case hydrogen production method, have a similar impact level. The FCV has the advantage of not having the impact due to the generator, but on the other hand, the production of its fuel cell increases its impact considerably for this category.

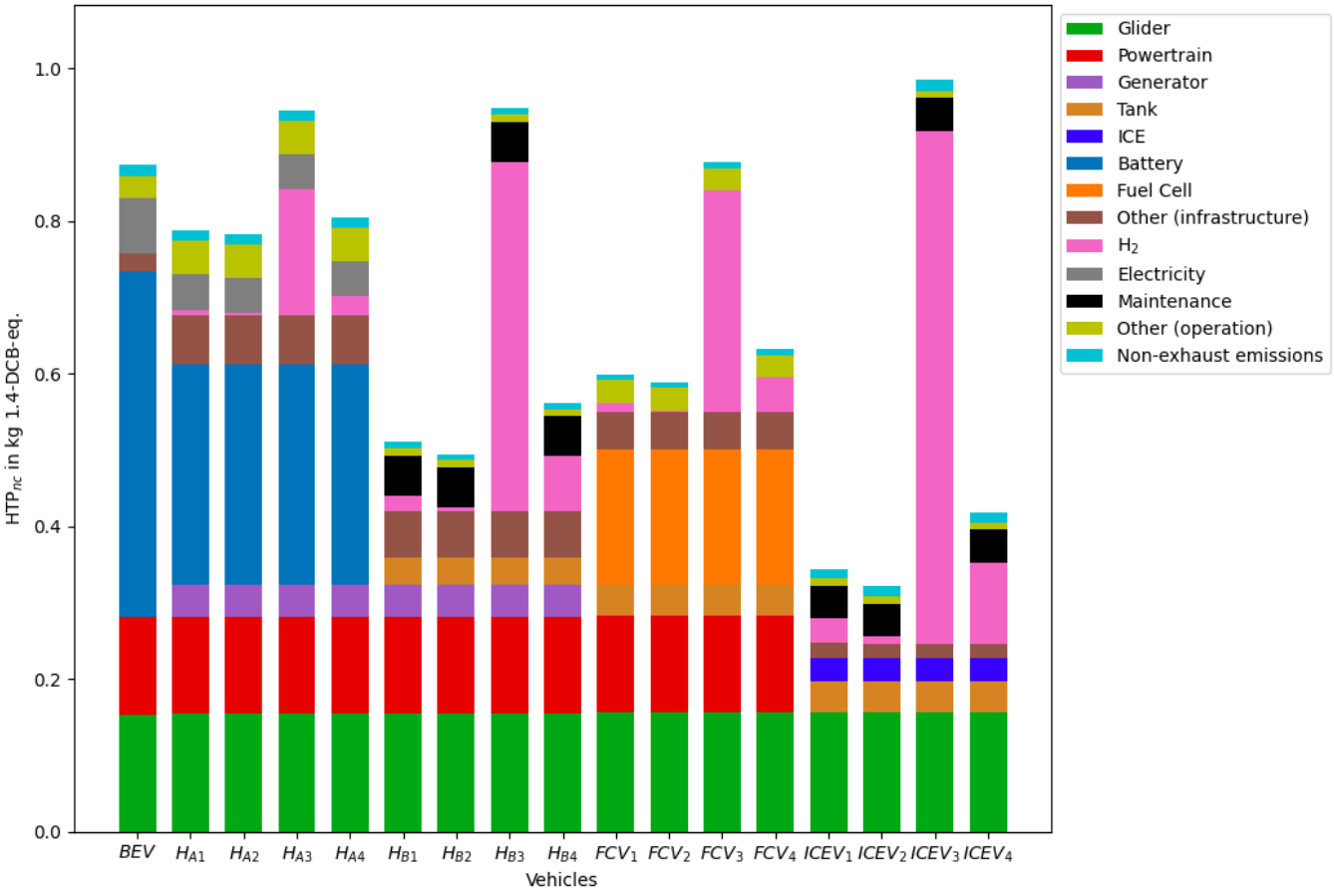


Figure 3.6: Human toxicity potential (non-carcinogenic)

Terrestrial acidification potential potential

For the terrestrial acidification potential, for the hydrogen production methods, the green electrolysis has a greater impact than both SMR methods (with and without CCS).

The most important contributions for this category come from the battery in the BEV and the HEV_A, the hydrogen storage tank in the HEB_B, in the FCV and in the ICEV, the fuel cell, the glider that is common to all vehicles, and hydrogen, in some of its production methods.

The vehicles with the lowest impacts for this category are the HEV_B and the ICEV. These vehicles, even with a dirty hydrogen production method such as SMR, have a considerably lower impact than all of the other vehicles.

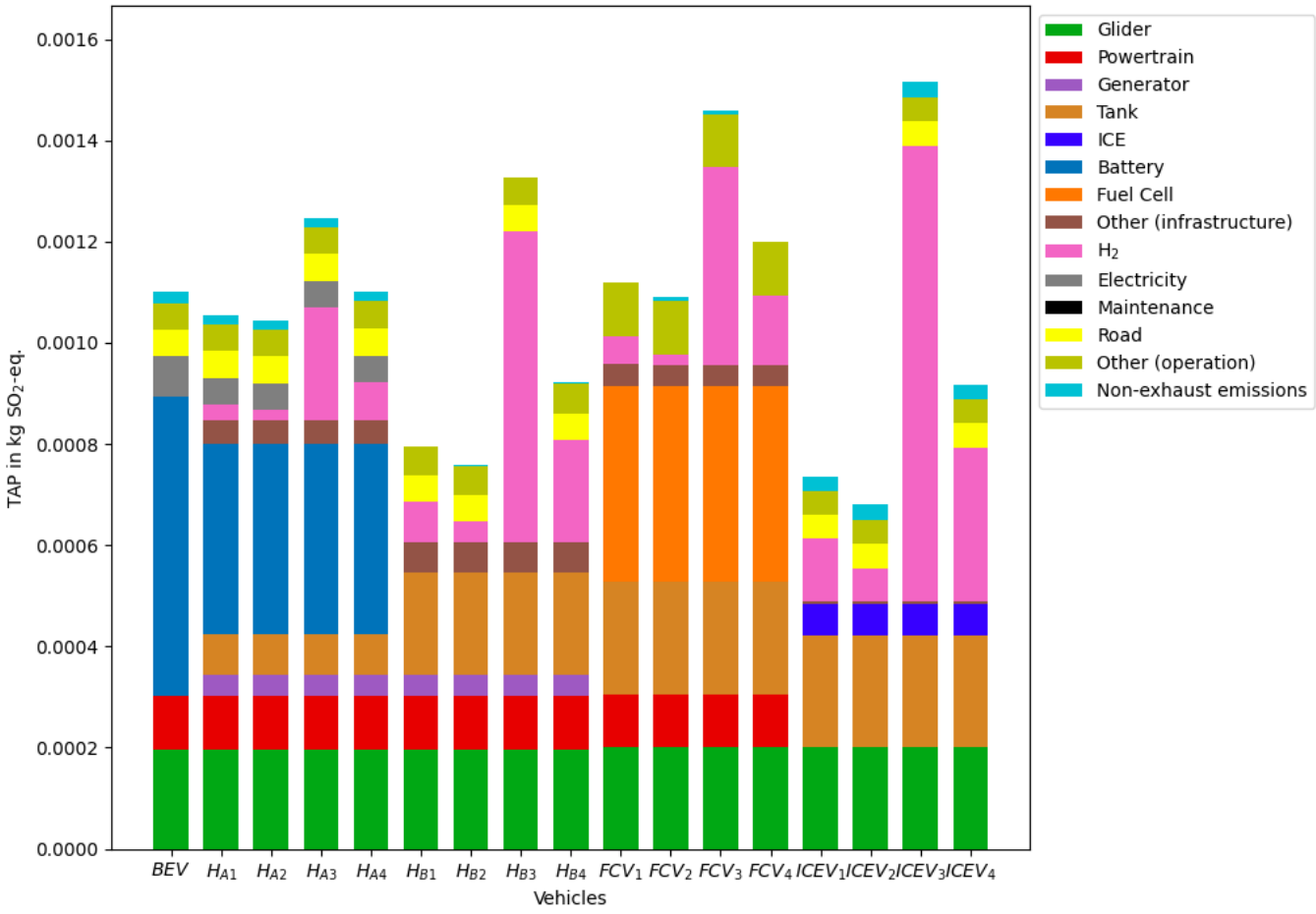


Figure 3.7: Terrestrial acidification potential potential

Particulate matter formation potential

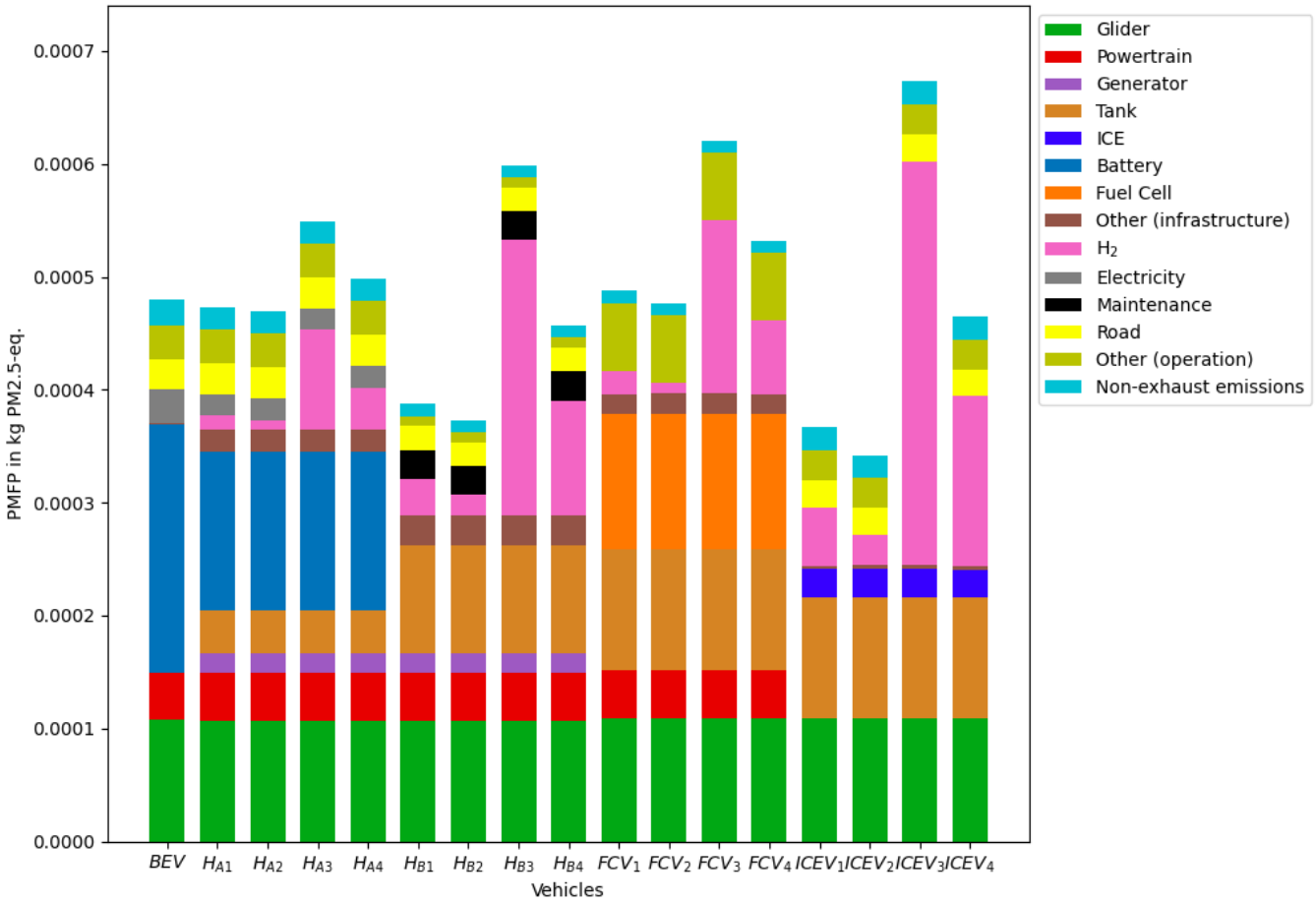


Figure 3.8: Particulate matter formation potential

Regarding the particulate matter formation potential, the green electrolysis hydrogen production method has once again a greater impact than the regular SMR (without CCS). As for the TAP category, the elements with the greatest impact are the battery, the hydrogen tank, the fuel cell, the glider and hydrogen coming from electrolysis (dirty or green).

The vehicles with the lowest impacts are once again the HEV_B and the ICEV with hydrogen produced by SMR (with or without CCS). Excluding these vehicles, and the ones with hydrogen produced from regular electrolysis that have the highest impact, all of the other vehicles have impacts of similar levels.

3.1.2 Normalization

Comparison of impact categories

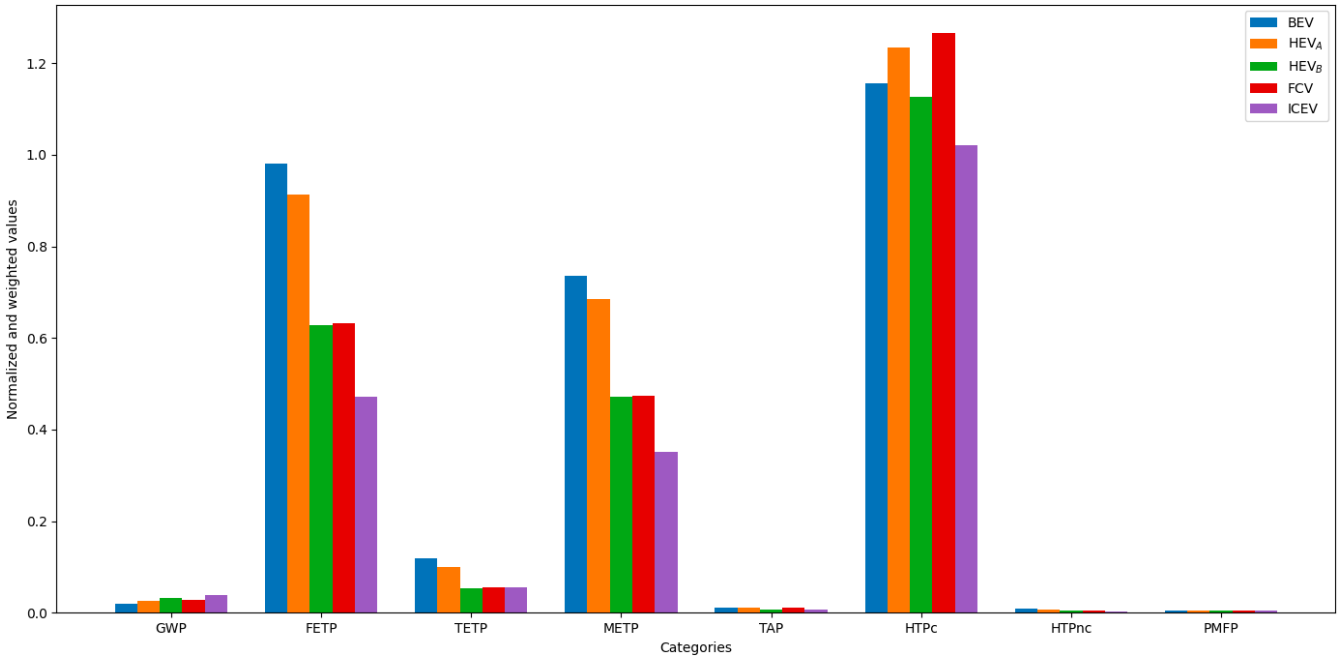


Figure 3.9: ReCiPe normalization results

Firstly, it is interesting to understand which impact categories play the most significant role in shaping the overall impact of the evaluated vehicles. In order to achieve this, the results from the LCIA are normalized.

From the normalization of the results, it is possible to observe what categories have the most important relative environmental impacts. The results of the LCIA are transformed into dimensionless values, representing the significance of each impact category relative to its corresponding global benchmarks, and therefore these dimensionless values can be more easily interpreted. Indeed, they show which impact categories contribute the most to the overall environmental impact of the assessed vehicles. These values are also weighted by their respective weighting factors that ReCiPe 2008 recommends.

From what can be seen in fig.3.9, the impact category that holds the greatest influence on the overall impact is HTP$_c$. It is followed by FETP and METP. Moreover, these categories are followed by TETP and GWP. Finally the three

remaining categories that have been taken into account do not seem to have a significant contribution.

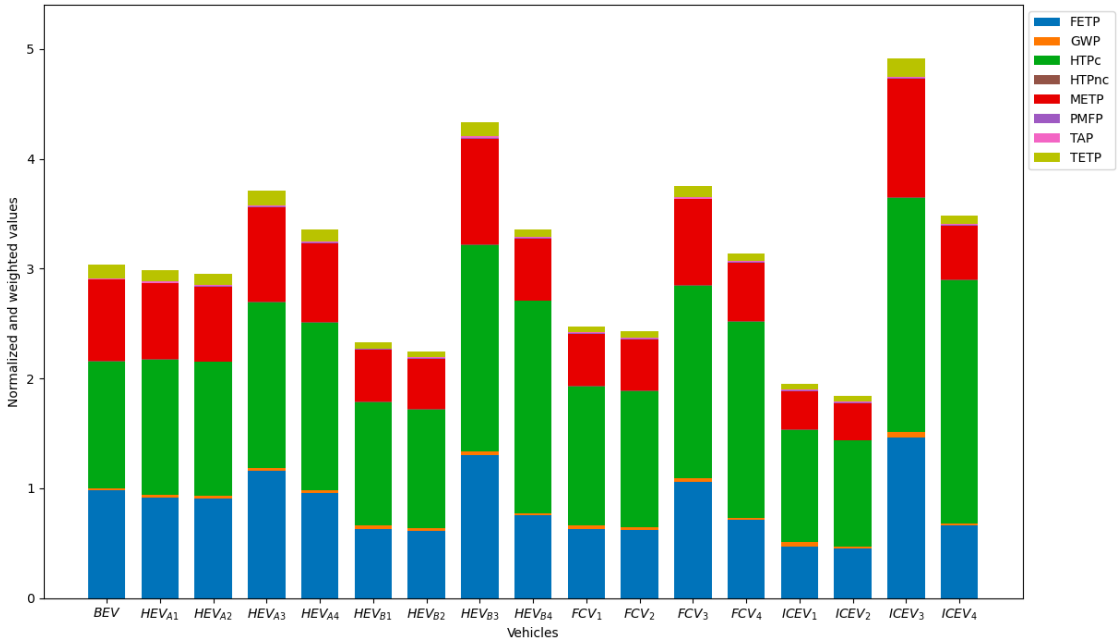


Figure 3.10: ReCiPe normalization and weighting results: single score

Comparison of vehicles

Secondly, not only it is important to understand what impact categories are the most significant compared one another, but also it is crucial to see at the end what vehicles come up to have the lower impacts in general. In order to do this, the normalized and weighted results must be added up, so that each vehicle gets a single score.

From the single scores of each vehicle shown in fig.3.10, it can be seen that the vehicle with the lowest score is the ICEV. This is the case either with SMR or with SMR+CCS produced hydrogen. The HEV$_B$ and the FCV have a score close to the one of the ICEV as well.

The vehicles with the highest scores are the ones fueled by hydrogen produced with regular electrolysis. The vehicles fueled with green electrolysis have a higher score than those fueled with hydrogen produced with SMR. This is mostly due to the high ecotoxicity impacts of the production of wind electricity that is used for the green electrolysis process. However, as is has been explained, for other electricity methods such as hydro-based electricity, the ecotoxicity impacts could be greatly

reduced. Compared to the most optimistic cases of hydrogen production for the HEV_B, for the FCV and for the ICEV, the BEV and the HEV_A do not seem to be interesting vehicles in the seek for a greener automobile industry.

In order to verify the observations that have been done, another normalization and weighting method was performed. The results can be seen in fig.3.11. Here, the main thing to point out is that the vehicles follow pretty much the same pattern as in fig.3.10. However, this method follows a complete different way into getting the single score final results: indeed, as it is explained in the methodology, different LCIA methods have been used for each impact category (instead of using the ReCiPe method). Also, the impact categories do not represent exactly the same thing as those assessed with the ReCiPe method do. Moreover the units measuring the impacts for each category are also different from the ReCiPe method. Finally, the MMG method uses "monetisation" factors, that differ greatly from the normalization and weighting factors that have been used in the previous method. As it can be seen, the impact categories that make up the most important contributions differ greatly from those in the ReCiPe method. However, the reason for having analyzed this further normalization method in this study is to compare the vehicles among themselves, and not to compare the impact categories among them, therefore only the pattern followed by the total bars can be analyzed. As it has been stated, this pattern being similar to the one observed following the ReCiPe method, the results seem to be verified.

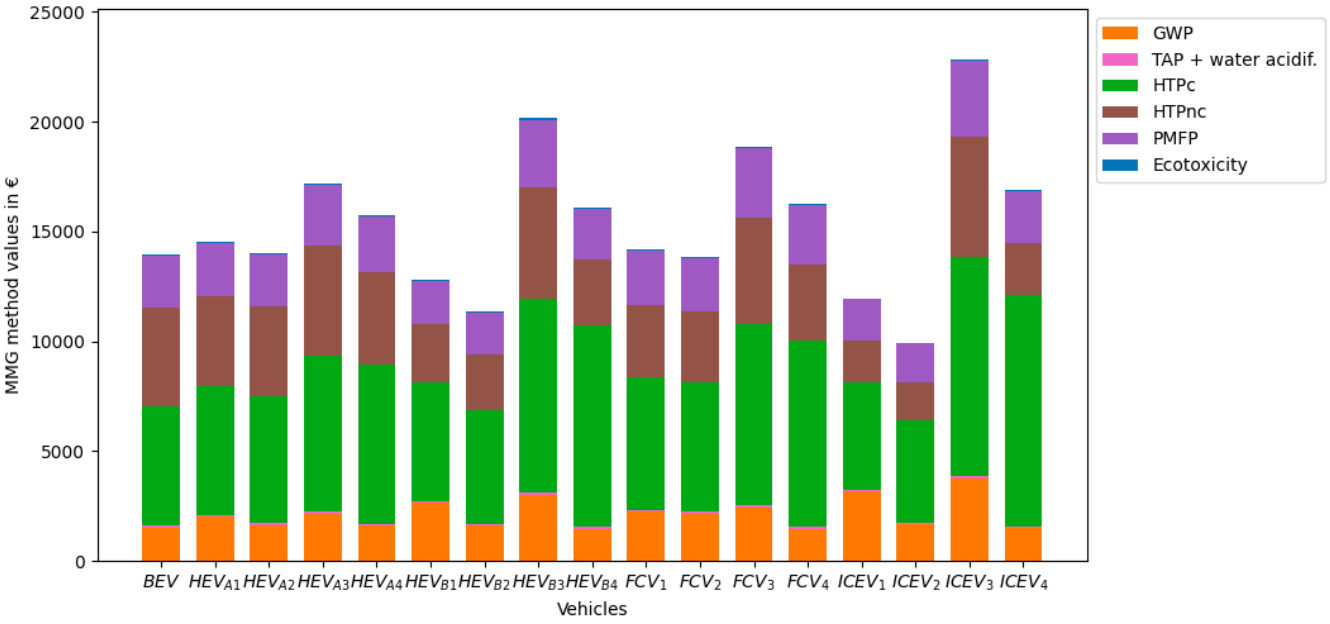


Figure 3.11: Belgian MMG method normalization and weighting results: single score

3.1.3 Sensitivity analysis

In order to see the variation of the results that are due to the variation of the inputs, only the scenario of hydrogen produced from SMR is considered.

The first input that is evaluated is the lifetime of the vehicles. It can be seen in fig.3.12 that the results follow exactly the variation of this input. Indeed, raising this variable to 200000km, the results will be 75% of the base case results. By increasing this value to 250000km, the results will be 60% of the base case. Finally, by doubling the initial lifetime, the impacts will be reduced by half. This is logical since the functional unit is 1 km travelled.

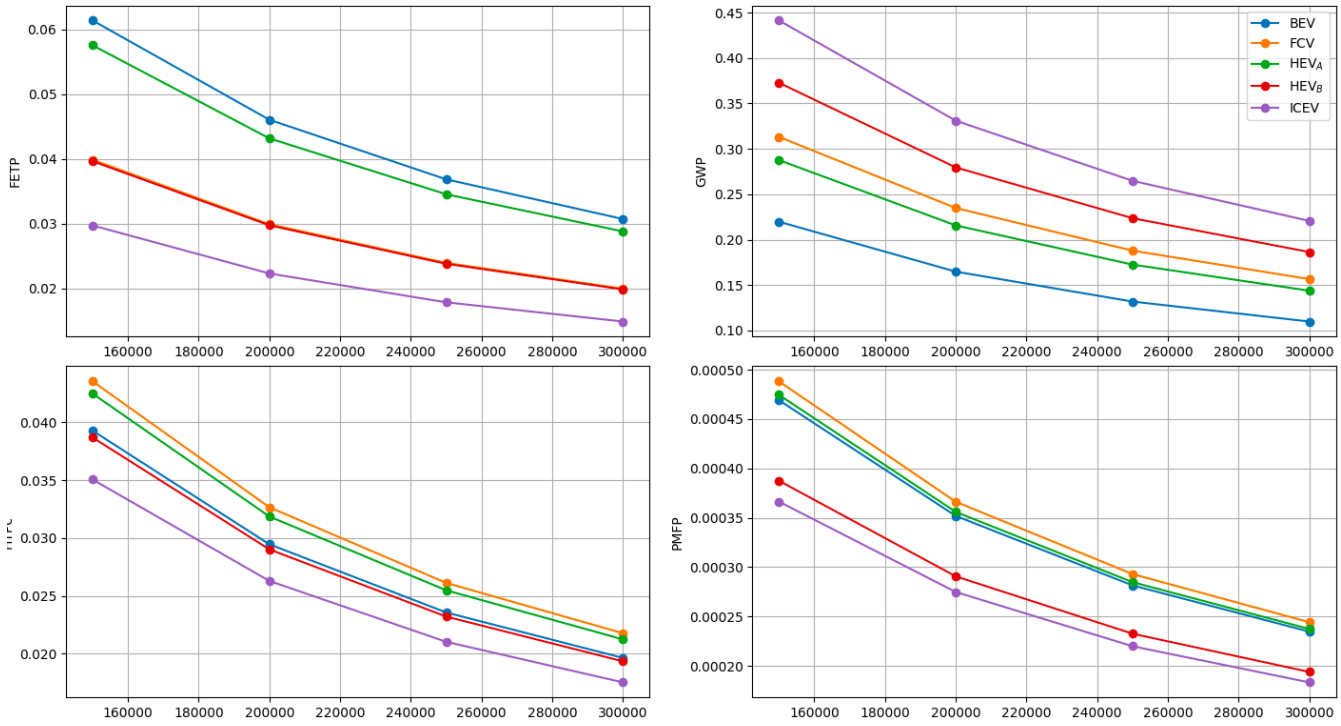


Figure 3.12: Variation of lifetime of vehicles

In fig.3.13, the same analysis is done, but now the replacement of the battery is considered. This figure shows the results obtained for the HTP$_c$ category. For the rest of the categories the same pattern is followed. Since the battery's lifetime is considered to be of 100000km, in the case of a vehicle's lifetime of 150000 km or 200000 km, one battery replacement is considered. For the case where the vehicles' lifetime is 250000 km or 300000 km, two battery replacements are therefore needed. It can be clearly seen that when the replacement of the battery is considered,

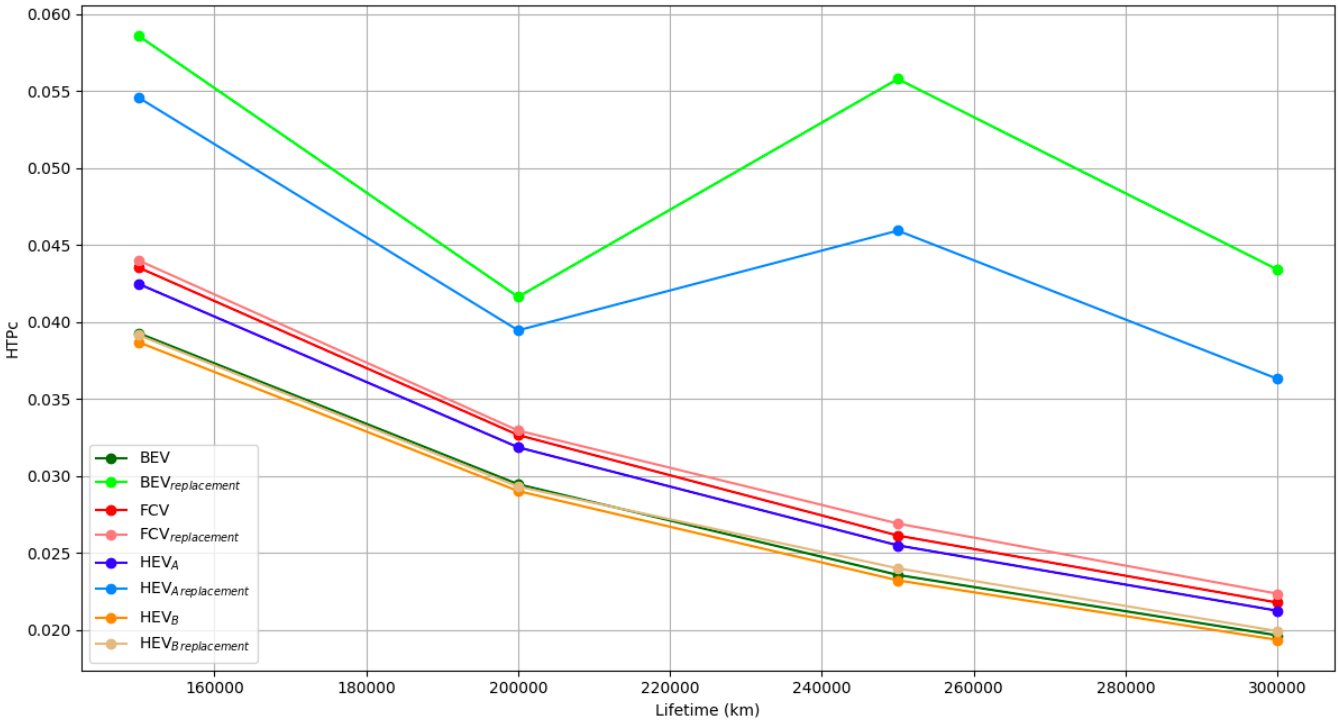


Figure 3.13: Battery replacement considered

the BEV and the HEV_A's impacts are considerably increased. For the vehicles containing batteries of small sizes, such as the FCV or the HEV_B, taking into account the replacement of the battery does not seem to influence the impacts considerably.

In fig.3.14 the input that is analyzed is the consumption of hydrogen in HWRE in the HEV_A, in the HEV_B, and in the ICEV. The first thing to point out is that the shape of the curve of the HEV_A differs from the two others. The two other vehicles have a linear curve, since their autonomy fully depends on the hydrogen consumption. Whereas the HEV_A has a part of its autonomy that is assured by a full-electric mode. Therefore, in order to maintain the same total range, if the hydrogen consumption raises, since the vehicle's hydrogen storage tank is unchanged, the battery will have to be bigger, in order to provide the same total range. The electricity that is going to be consumed is therefore also going to increase.

It can be seen that for the impact categories FETP and PMFP, there is only a consequential modification of the impacts for the HEV_A. Regarding the GWP category however, the modification of the consumption has a greater impact on the other two vehicles. For the HTP_c category, the variation of the consumption

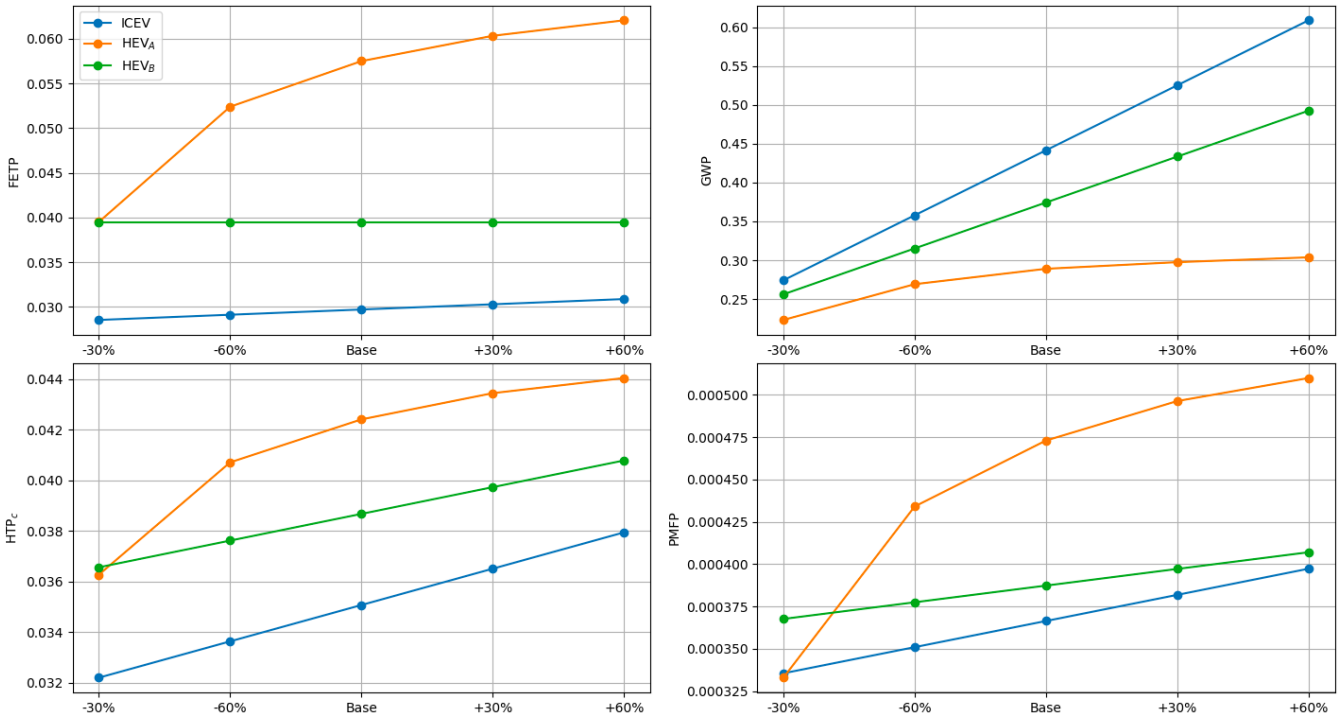


Figure 3.14: Variation of hydrogen consumption

seems to modify the impacts of the three vehicles in a very similar way.

It is important to point out that for the HEV$_A$, a diminution in the consumption will provoke a greater variation of its impacts than an increase of its consumption. For the other two vehicles, since the curves are linear, a diminution or an increase of the consumption will provoke the same modification of the impacts (in opposite ways).

In fig.3.15 the way in which the inventory for the SMR with CCS hydrogen production method was filled up has been questioned. In order to see if it is correct, it is compared to another model of SMR with CCS, coming from another paper, as it was explained in the methodology. The results in the four categories presented show similar outcomes.

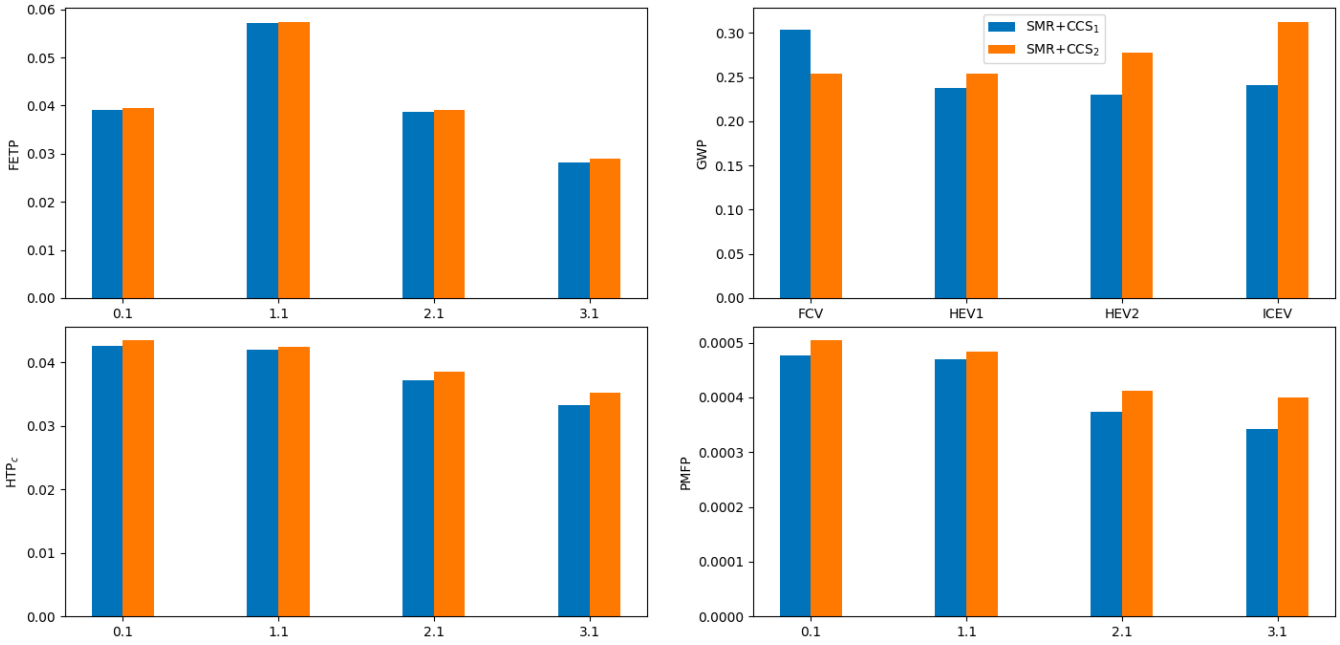


Figure 3.15: SMR+CCS: Comparison of two models of this production method

3.2 Performance of the hydrogen Wankel rotary engine

In this section, emphasis is placed on the small-picture perspective and develops results relative to the performance of the HWRE. This examination will focus on understanding how the engine output power and heat loss respond to changes in the air-fuel parameter, specifically ranging from $\lambda = 1.4$ to $\lambda = 2.0$. Exploration will reveal how variations in this air-fuel impact engine performance and indicated efficiency. This involves observing patterns and trends in the data, and discussing the underlying mechanisms that contribute to these observed behaviors. The objective is to understand the trade-offs between power output and heat loss at different lambda values. This analysis will provide valuable insights into the engine's operation, guiding future adjustments and potential improvements to its design and operating conditions.

3.2.1 Combustion analysis

Analyzing the combustion process is an essential step for gaining an accurate understanding of the dynamics occurring within the engine's cylinder.

Figure 3.16 provides a visualization of the Mass Fraction Burned profile as a function of crank angle, a key indicator of the combustion progression under varying levels of air-fuel ratio. From this visualization, a clear trend is observed: as the air-fuel ratio increases, the duration of the combustion process also extends. This indicates that the combustion process slows down, or becomes less rapid when the mixture becomes leaner.

Flame development is often defined as the time it takes for a small but meaningful portion of fuel to burn, typically represented as ESAD10 (Eccentric shaft angle degree at which 10% of fuel has been burned)[40]. As indicated in Figure 3.17(a), the duration of flame development lengthens as the excess of air, increases. This trend can be attributed to the concentration of the hydrogen-air mixture. As lambda decreases, implying a richer mixture, the concentration of hydrogen in the mixture increases, subsequently leading to an easier flame development phase [81].

Meanwhile, combustion duration, defined as the interval between flame development and the point at which the bulk of the fuel-air mix has been burned (ESAD90 - Crank Angle Degrees at which 90% of fuel has been burned), also shows a dependency on the air-fuel ratio [40]. As shown in Figure 3.17(b), the combustion

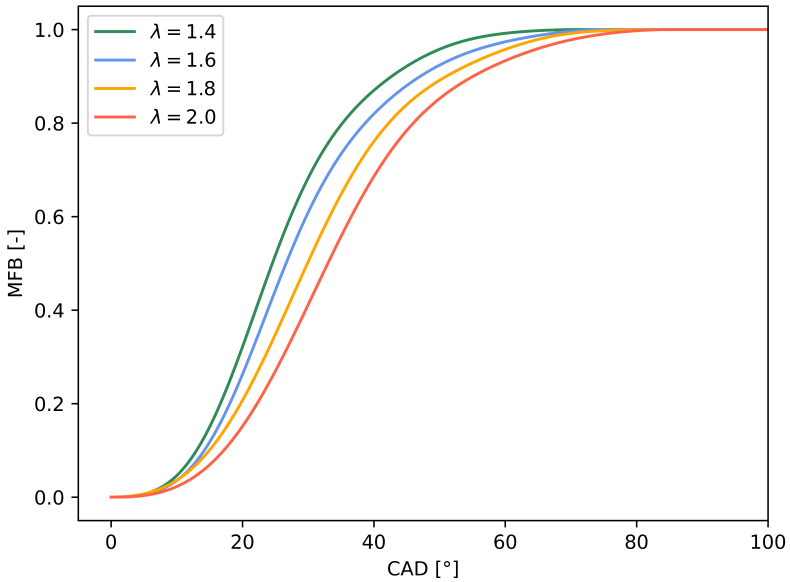


Figure 3.16: Mass fraction burned profile at varying air-fuel ratios

duration lengthens as the air-fuel ratio increases. This behavior can be explained by the rising laminar flame speed of hydrogen as the concentration of hydrogen increases in the mixture. It results in a shortening of the combustion duration [81, 82].

Lastly, examining peak pressures in the context of the combustion process provides additional perspective. As Figure 3.18 illustrates, the intensity of pressure peaks rises and occurs earlier as the excess of air decreases. This trend can be explained as follows: a decrease in lambda means a richer mixture, with more fuel being introduced into the cylinder. Hence, more chemical energy is available for combustion, increasing the peak pressure. Moreover, a richer mixture tends to result in a shorter combustion duration, leading to a more rapid release of heat in a smaller volume, which also contributes to higher and earlier pressure peaks [81]. Finally, it can be noted that temperature profiles depicted in Figure 3.21 show equivalent trends.

3.2.2 Heat loss

The initial investigation into heat loss begins with an exploration of the heat transfer coefficient. As outlined in Woschni's Equation 2.17, the most significant variables are pressure and velocity, each having an exponent of 0.8. This interplay

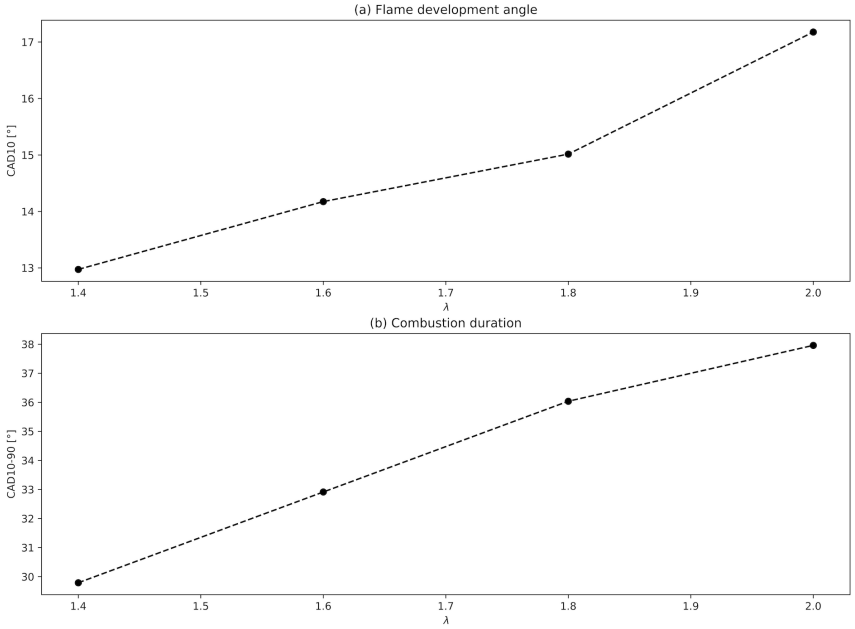


Figure 3.17: (a) The flame development angle and (b) the combustion duration, at varying air-fuel ratios.

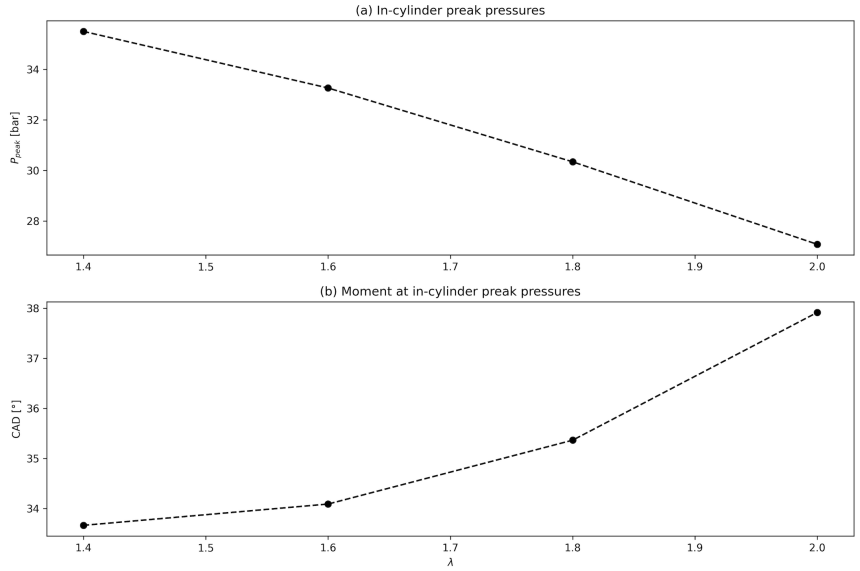


Figure 3.18: (a) In-cylinder peak pressures with (b) their corresponding ESAD moment, at varying air-fuel ratios.

between pressure, velocity, and heat transfer during combustion is a key factor to understand in the dynamics of thermal losses.

To start, in the pre-combustion phase, the increase in the heat transfer coefficient is primarily driven by compression, which in turn results in an increase in pressure and temperature. As highlighted by Figure 3.19, the combustion velocity term (W_c) associated is zero at this point. This is while both the term for mean rotor velocity (W_z) and the characteristic length (d) remain constant throughout the cycle.

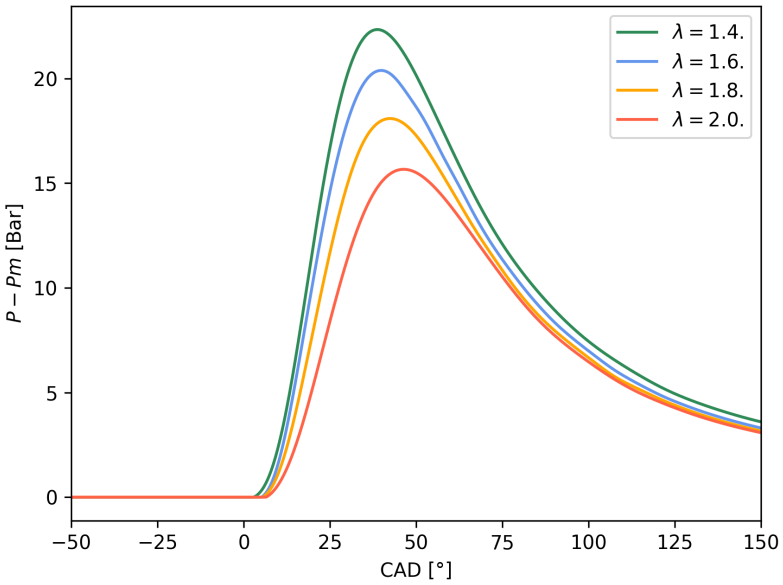


Figure 3.19: Combustion velocity term, at varying excess ratios.

However, during the combustion phase, there's a notable acceleration in the combustion velocity term (W_c) as shown in Figure 3.19. This surge becomes evident as the gap between the in-cylinder pressure and the motored pressure widens. Consequently, there's a corresponding sharp increase in the heat transfer coefficient, as demonstrated in Figure 3.20. This behavior can be explained by the high convection from the high burning velocity and the small quenching distance of hydrogen [47].

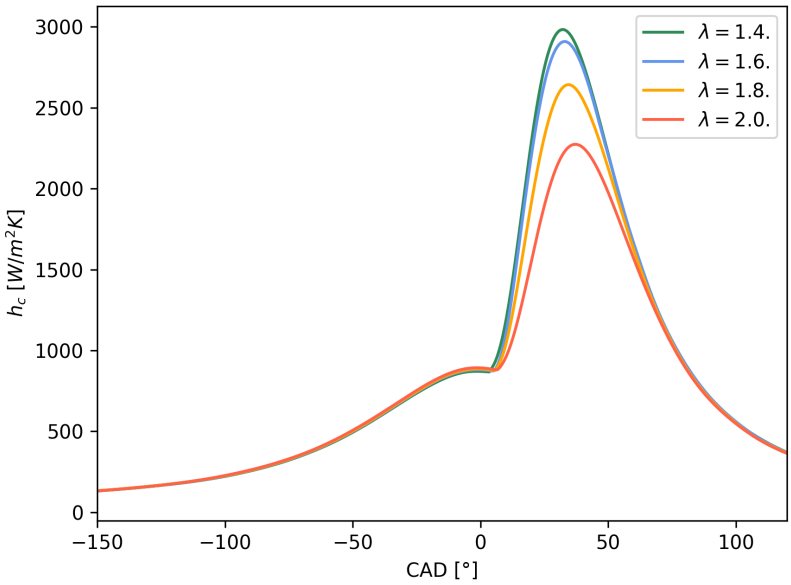


Figure 3.20: Heat transfer coefficient, at varying excess ratios.

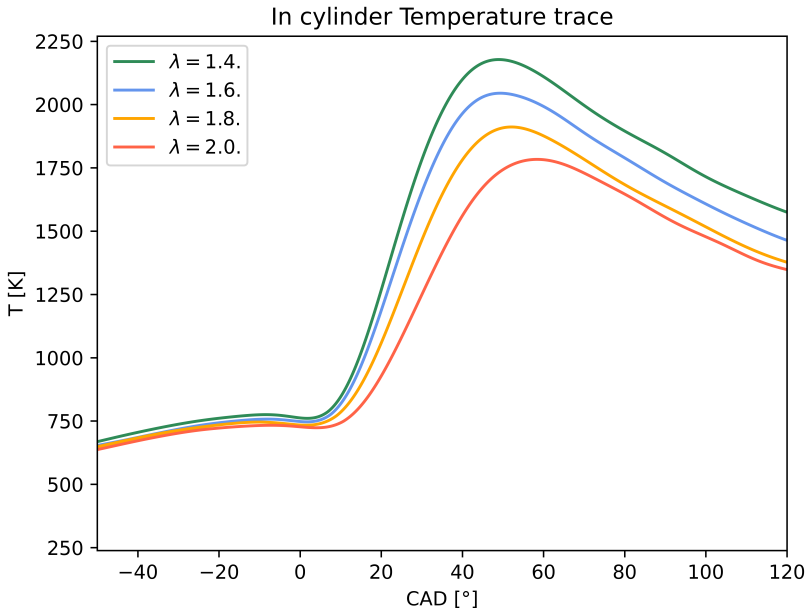


Figure 3.21: In-cylinder temperaturetrace, at varying excess ratios.

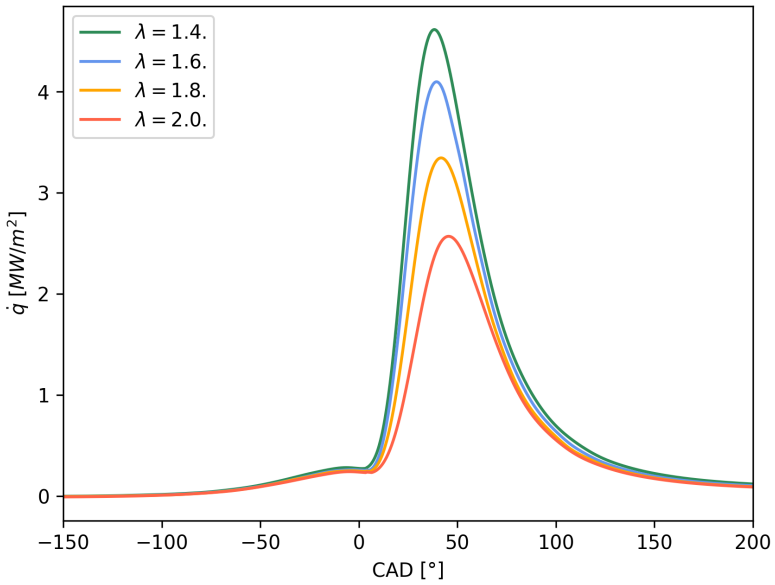


Figure 3.22: Heat flux using Woshcni model, at varying excess ratios.

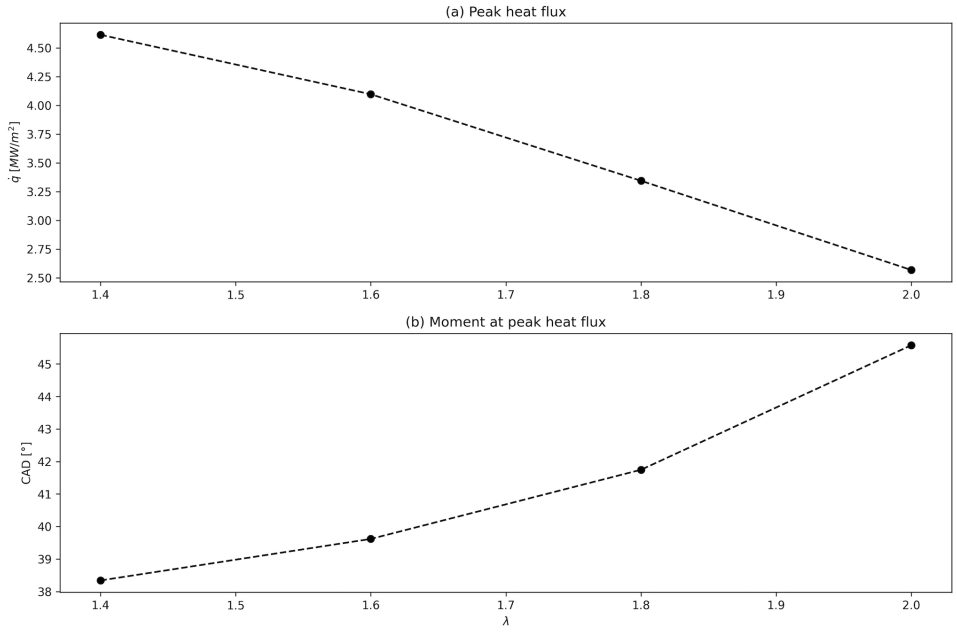


Figure 3.23: (a) In-cylinder heat flux with (b) their corresponding ESAD moment, at varying air-fuel ratios.

Heat flux in the engine cylinder is dynamic and greatly affected by factors such as air-fuel ratio as shown in Figure 3.22. During compression, as the cylinder content is compressed, pressure and temperature rise. This causes heat transfer from the hot cylinder content to the cooler cylinder walls. The start of combustion brings a significant rise in heat flux, peaking around the time of maximum pressure. After combustion, during the expansion phase, cooling exhaust gases cause a decrease in heat flux.

As the changes in heat flux with increasing λ are examined, two distinct trends are noticed: a reduction in peak heat flux intensity and a delay in the timing as observed in Figure 3.23. Indeed, with a larger lambda value, the proportion of fuel in the mixture entering the cylinder decreases. This reduction in fuel quantity leads to a less intense combustion process, which in turn results in a lower peak pressure and temperature and therefore a reduced peak heat flux. In addition, as lambda increases, the duration of the combustion process lengthens. This extension in combustion duration means that the point of maximum pressure and temperature is reached later in the engine cycle. Consequently, the timing of peak heat flux is delayed.

3.2.3 Efficiencies

The analysis of efficiencies reveals intriguing trends. Figures 3.24 highlights the indicated efficiency (η_i), the degree of constant volume (η_{glh}), the heat loss ratio (ϕ_w) and the product of degree of constant volume by the importance of heat loss ($\eta_{glh}(1-\phi_w)$).

Firstly, when analyzing the heat loss ratio, it becomes evident that as the air-fuel ratio increases, this ratio decreases. Consequently, it can be inferred that heat loss become less significant as λ goes from 1.4 to 2.0 as reported in Figure 3.24 and in Table 3.1. This observation can be attributed to the fact that, with an increase in lambda, the peak temperatures decrease, leading to a reduction in heat loss, which positively impacts efficiency.

Secondly, the degree of constant volume indicates how closely the combustion process approaches a constant volume heat addition. As Lambda increases, the combustion duration also increases, as suggested by Figure 3.17 and Figure 3.16. Consequently, there is a decrease in the degree of constant volume, which negatively affects efficiency.

Thirdly, the product of the degree of constant volume and the importance of heat

loss is depicted at the bottom of Figure 3.24. With an increase in the air-fuel ratio, it is observed that the beneficial impact of reducing heat loss outweighs the decrease in the degree of constant volume as the products increases slightly. As a result, a small increase in the indicated efficiency is observed.

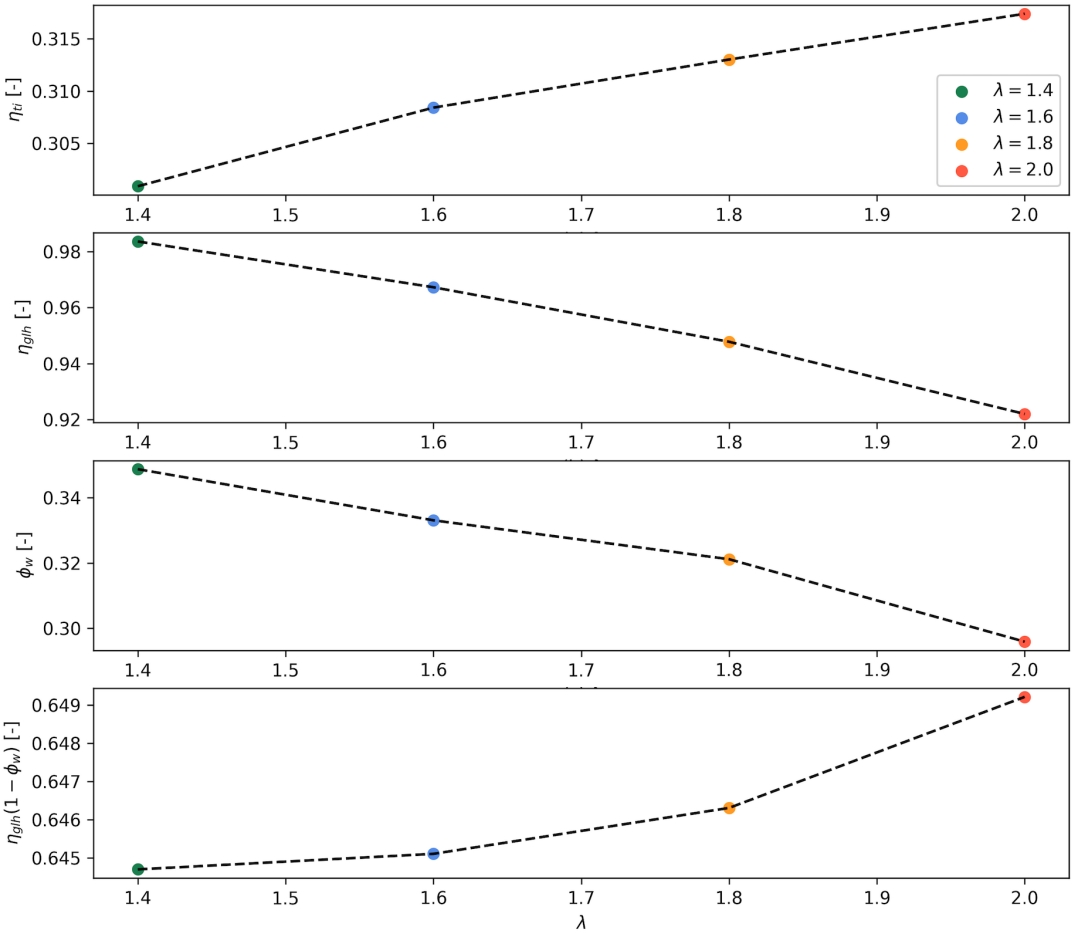


Figure 3.24: Efficiencies, at varying air-fuel ratios.

3.2.4 Power and IMEP

Finally, an analysis of the trends of IMEP and Power is delved into.

Figure 3.25 illustrates the evolution of IMEP at varying air-fuel ratios. Notably, as the lambda value decreases, the work done by the engine also decreases, indicating a reduced utilization of chemical energy within the cylinder.

Moreover, an increase in the air-fuel ratio leads to a decrease in power since less chemical energy is being supplied to the cylinders. However, it is essential to consider the implications highlighted in the previous section. Despite the reduction in power, there is a slight increase in internal thermodynamic efficiency.

Figure 3.26 provides an insightful comparison, taking the engine operation at $\lambda = 1.4$ as the reference point. The relative differences compared to all other cases are demonstrated, showcasing the trade-off between power and internal thermodynamic efficiency. As λ increases, there is a noticeable drop in power and a corresponding increase in internal thermodynamic efficiency. For instance, when transitioning from $\lambda = 1.4$ to 2.0, a maximum power drop of approximately 20.8% is observed. In contrast, there is a gain in efficiency of 4.95%

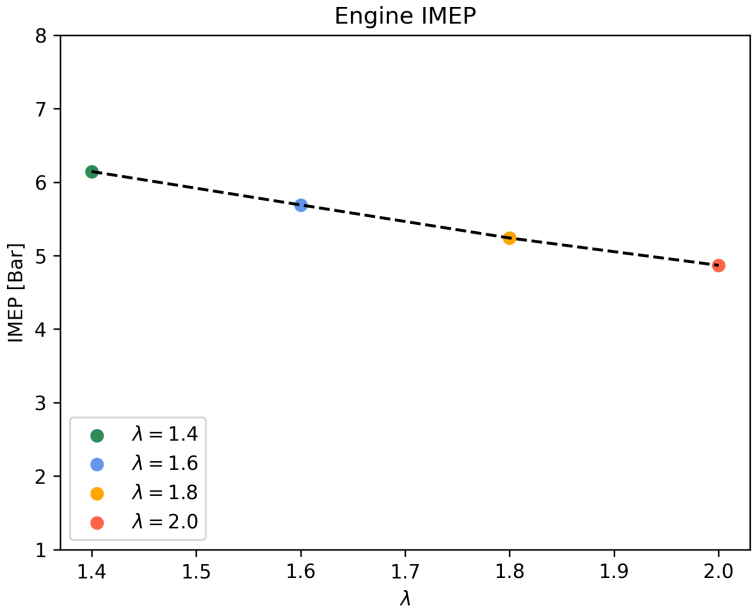


Figure 3.25: Engine IMEP, at varying excess ratios.

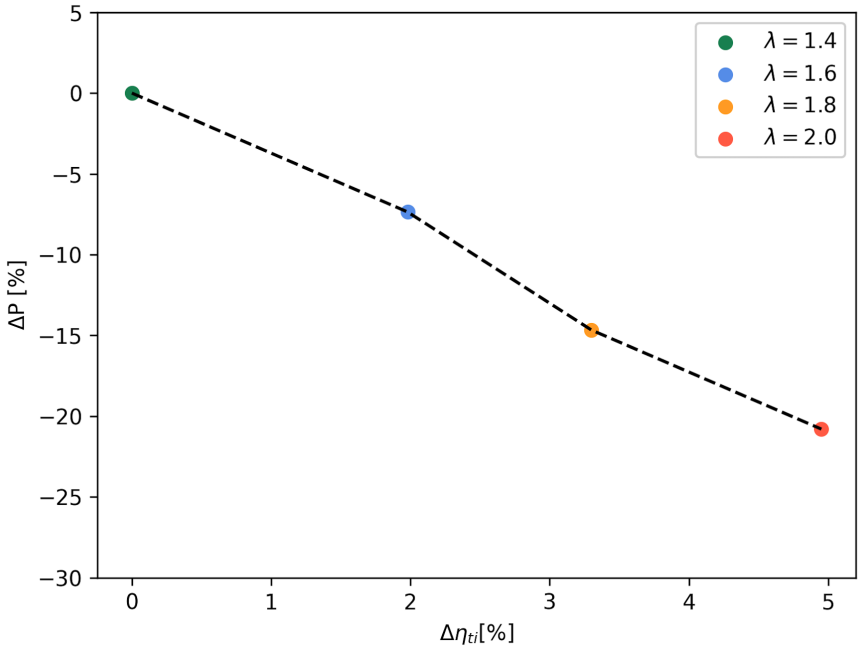


Figure 3.26: Engine power vs efficiency, at varying excess ratios.

λ	**Power [kW]**	$\lvert\Delta P\rvert$ [%]	η_i [%]	$\lvert\Delta\eta_i\rvert$ [%]	ϕ_w [%]	$\Delta\phi_w$ [%]
1.4	39.8	0	30.3	0	34.9	0
1.6	36.7	7.36	30.9	1.98	33.3	4.6
1.8	33.7	14.67	31.3	3.30	32.1	8.0
2.0	31.9	20.8	31.8	4.95	29.6	15

Table 3.1: Summary table

3.3 Discussion

In the realm of environmental concerns, particularly in the context of global warming and the overarching goals set forth by initiatives like the Green Deal, the initial approach to evaluating different vehicles centered on their impact within the category of global warming potential. This evaluation revealed different vehicles to have the possibility to be good viable solutions depending on the powertrain they use and the hydrogen production method considered. Among these vehicles were the FCV fueled by green hydrogen, the ICEV and the HEV_B both powered by green and blue hydrogen and, with battery replacement being omitted, the HEV_A propelled by green and blue hydrogen as well as the BEV. Indeed, they all held

similar impact levels in this category.

However, upon delving into the normalized results, several remarkable observations come to light. Contrary to initial assumptions that global warming potential would serve as a crucial criterion for vehicle comparison, the normalized results underscore the significance of impacts coming from other categories such as freshwater or marine ecotoxicity potential, as well as human carcinogenic toxicity potential. This observation serves as a pivotal reminder, emphasizing the need to consider impacts beyond the conventional focus on CO_2 emissions reduction.

Another pivotal finding emerges when considering hydrogen sources. Green hydrogen's efficacy is cast in doubt, particularly when compared to its grey or blue counterparts in the normalized and weighted single scores obtained. This is especially evident when green hydrogen is derived from wind-generated electricity.

However, a more salient revelation pertains to the vehicles that demonstrate the least environmental impacts. In this regard, ICEVs, FCVs, and HEV_Bs, fueled with grey or blue hydrogen, emerge as the most environmentally friendly options. Indeed the single score of these vehicles is beneath the ones of the other vehicles, even without considering the battery replacement that would yield a much greater difference of the single score compared to the BEV or the HEV_A.

The study also encompasses a performance analysis conducted at an operational point featuring 3000 RPM and a constant load. One notable outcome is the impact of adjusting the air-fuel ratio from 1.4 to 2.0, leading to a notable 20.8% reduction in output power and an increase in efficiency of 4.95% Conventionally, in ICE, the indicated efficiency reflects the processes within the cylinder, excluding mechanical losses. Conversely, brake efficiency is pivotal as it encompasses these mechanical losses, which can fluctuate based on engine operations. These insights suggest that a leaner mixture enhances the fuel's energy conversion into productive work. However, this doesn't fully account for what is emitted from the eccentric shaft of the HWRE, since mechanical losses aren't factored in. When considering these losses, the observations might differ and lead to alternate conclusions. Due to insufficient experimental data, brake efficiency wasn't explored in this study. It would be advisable to further investigate brake efficiency in future studies.

For one of the vehicles that resulted to be a viable solution, the HEV_B, the vehicle having a powertrain where the ICE must only work at a single operating point, whose role is to produce electricity via the generator instead of directly transmitting its power to the wheels. This power diminution, due to the seek for a

better performance, could be acceptable, always in the case that it matches the power required by the generator. When evaluating such a vehicle under the same conditions as the performance analysis, that is operating at 3000 RPM with same constant load, an increase in the air-fuel ratio resulted in a decrease in power from 39.8 kW to 31.9 kW. It's worth noting that these power figures are on par with smaller hybrid vehicles such as the BMW i3 Rex, which has a 25kW ICE, and the Mazda MX30 REV with its 55kW ICE. Given that this reduction in power is tolerable, elevating the lambda value from 1.4 to 2.0 can improve efficiency by 4.95%. This boost in efficiency can lead to longer driving ranges and reduced fuel consumption, due to the enhanced fuel-to-electricity conversion efficiency in ICE.

However, if the observation pointed out from the performance study is considered for the other HWRE powered vehicle that resulted to be viable in the LCA, the ICEV, the outcome of the discussion is different. Indeed, since in this vehicle the role of the engine is to deliver its power directly to the wheels, a decrement of 20.8% of the engine's output power would be of substantial concern. It should be emphasized that is crucial to contextualize these findings for broader operating conditions. Engines exhibit nuanced power and efficiency traits across varying RPMs and loads. Therefore, while the data gleaned at 3000 RPM and a constant load offers vital insights into ICE dynamics in hybrid configurations, it's essential to consider a comprehensive approach. Operating at different RPMs and loads could yield divergent dynamics between power and efficiency, necessitating a more encompassing analysis.

In summary, this study's data, derived from the 3000 RPM and constant load paradigm, delivers crucial insights into ICE operations within hybrid vehicles. However, a more comprehensive analysis, embracing a wider spectrum of operating points, is imperative to truly ascertain the efficacy and viability of ICEs in series hybrid powertrains across real-world scenarios.

Conclusion

With a globally increasing energy demand and the urgent need to deal with environmental issues, finding sustainable energy solutions is now really important. By considering hydrogen as a potential sustainable energy carrier, going through this fuel attributes and its integration into an ICE, and realizing the good match that this fuel makes with the HWRE. Considering the operational unique characteristics of this engine, this study has undertaken a comprehensive exploration into the feasibility and potential impacts of the HWRE within a green automotive sector.

Firstly, a comprehensive review of existing literature was carried out, analyzing the larger context of sustainable transportation, emphasizing the critical role of hydrogen as a cleaner energy alternative. By carrying out this review, a knowledge base leading to the HWRE potential was established. It identified the challenges of hydrogen due to its tendency to cause abnormal combustion and heightened heat flux. This necessitates lean operations, which can reduce power output. These challenges become even more pronounced when hydrogen is utilized within the WRE. The unique design of the WRE, characterized by its higher surface-to-volume ratio and longer strokes, inherently leads to greater heat loss and diminished efficiency.

A significant contribution of this thesis is in the methodological frameworks developed to evaluate both the viability of vehicles powered by HWRE and the detailed performance aspects. The methodology is divided into a big-picture perspective, focusing on vehicle viability and covering all stages of an LCA, and a small-picture perspective which focuses on the performance of the HWRE. The latter involves an assessment of the engine behavior through in-cylinder pressure measurements, detailing procedures from pre-processing to post-processing. The analysis culminates in a deeper understanding of the role of the air-fuel ratio in the combustion process and its effects on power, heat loss, and efficiency.

Key findings have underscored the complexity of evaluating environmental impacts, emphasizing the importance of considering diverse impact categories beyond CO_2 emissions. As a significant outcome, it can be highlighted that ICEVs, followed

by FCVs and HEV_Bs, using grey or blue hydrogen came out as the most viable vehicles, with their impact scores being lower than those of the BEVs or HEV_As, even when the battery replacement is not considered. Furthermore, the analysis of HWRE performance revealed the delicate trade-off between efficiency and power output, showing how leaning out the mixture from $\lambda = 1.4$ to $\lambda = 2.0$ can slower combustion, decrease heat loss ratio by 15%, enhance fuel conversion efficiency by 4.95%, but also reduce power by 20.8%.

Bibliography

[1] Andrew Simons and Christian Bauer. Life cycle assessment of hydrogen production. *Transition to Hydrogen: Pathways toward Clean Transportation; Wokaun, A., Wilhelm, E., Eds*, pages 13–57, 2011.

[2] United Nations Industrial Development Organization. Technology database - unido, 2023.

[3] Diogo MF Santos, César AC Sequeira, and José L Figueiredo. Hydrogen production by alkaline water electrolysis. *Química Nova*, 36:1176–1193, 2013.

[4] Pyoungho Choi, Dmitri G Bessarabov, and Ravindra Datta. A simple model for solid polymer electrolyte (spe) water electrolysis. *Solid State Ionics*, 175(1-4):535–539, 2004.

[5] K. Yamamoto. *Rotary Engine*. Toyo Kogyo Co., Ltd, 1981.

[6] Ömer Cihan, Hüseyin Emre Doğan, Osman Akın Kutlar, Abdurrahman Demirci, and Majid Javadzadehkalkhoran. Evaluation of heat release and combustion analysis in spark ignition wankel and reciprocating engine. *Fuel*, 261:116479, 2020.

[7] Ecochain. Ecochain. https://ecochain.com/knowledge/cradle-to-grave-in-lca/. Accessed: 19/08/2023.

[8] Anders Nordelöf, Maarten Messagie, Anne-Marie Tillman, Maria Ljunggren Söderman, and Joeri Van Mierlo. Environmental impacts of hybrid, plug-in hybrid, and battery electric vehicles—what can we learn from life cycle assessment? *The International Journal of Life Cycle Assessment*, 19:1866–1890, 2014.

[9] Andrew Simons. The ecoinvent database v3: Road transport: new life cycle inventories for fossil-fuelled passenger cars and non-exhaust emissions in ecoinvent v3. *International Journal of Life Cycle Assessment*, 2013.

[10] Gonzalo Puig-Samper Naranjo, David Bolonio, Marcelo F Ortega, and María-Jesús García-Martínez. Comparative life cycle assessment of conventional, electric and hybrid passenger vehicles in spain. *Journal of Cleaner Production*, 291:125883, 2021.

[11] M. Hoornaert. Design of a test setup for a mazda wankel engine, 2015.

[12] EngineLand. Jdm mazda rx7 fc turbo 1.3l rotary engine with auto transmission jdm 13b.

[13] John Haynes Mike Stubblefield. *Haynes Repair Manual Mazda RX7 1986 - 1991 all models*. Haynes Publishing Group, Newbury Park, California USA, 1991.

[14] Verhelst. Hydrogen-fueled internal combustion engines. *Progress in Energy and Combustion Science*, 35(6):490–527, 2009.

[15] Ghazi A. Karim. Hydrogen as a spark ignition engine fuel. *International Journal of Hydrogen Energy*, 28(5):569–577, 2003.

[16] Gonzalo Puig-Samper Naranjo, David Bolonio, Marcelo F. Ortega, and María-Jesús García-Martínez. Comparative life cycle assessment of conventional, electric and hybrid passenger vehicles in spain. *Department of Energy and Fuels - Escuela Técnica Superior de Ingenieros de Minas y Energía, Universidad Politécnica de Madrid, Calle Ríos Rosas 8 28003, Madrid, Spain*, 2023.

[17] Scott McWhorter and Grace Ordaz. Onboard type iv compressed hydrogen storage systems – current performance and cost. Technical Report DOE Record 13010, DOE Fuel Cell Technologies Office, June 11 2013.

[18] Amjad Al-Qahtani, Brett Parkinson, Klaus Hellgardt, Nilay Shah, and Gonzalo Guillen-Gosalbez. Uncovering the true cost of hydrogen production routes using life cycle monetisation. *Applied Energy*, 281:115958, 2021.

[19] Huaiyu Wang, Changwei Ji, Cheng Shi, Yunshan Ge, Hao Meng, Jinxin Yang, Ke Chang, Zhenyu Yang, Shuofeng Wang, and Xin Wang. Modeling and parametric study of the performance-emissions trade-off of a hydrogen wankel rotary engine. *Fuel*, 318:123662, 2022.

[20] Hao Meng, Changwei Ji, Jinxin Yang, Ke Chang, Gu Xin, and Shuofeng Wang. A knock study of hydrogen-fueled wankel rotary engine. *Fuel*, 321:124121, 2022.

[21] Manish Kumar Singla, Parag Nijhawan, and Amandeep Singh Oberoi. Hydrogen fuel and fuel cell technology for cleaner future: a review. *Environmental Science and Pollution Research*, 28:15607–15626, 2021.

[22] Mustafa Ozcanli, Oguz Bas, Mustafa Atakan Akar, Safak Yildizhan, and Hasan Serin. Recent studies on hydrogen usage in wankel si engine. *International Journal of Hydrogen Energy*, 43(38):18037–18045, 2018. The 2nd International Mediterranean Science and Engineering Congress (IMSEC 2017), 25-27 October 2017, Adana, Turkey.

[23] Jinxin Yang, Changwei Ji, Shuofeng Wang, and Hao Meng. An experimental study on ignition timing of hydrogen wankel rotary engine. *International Journal of Hydrogen Energy*, 47(39):17468–17478, 2022.

[24] Joachim Demuynck, Michel De Paepe, Ivan Verhaert, and Sebastian Verhelst. Heat loss comparison between hydrogen, methane, gasoline and methanol in a spark-ignition internal combustion engine. *Energy Procedia*, 29:138–146, 2012. WHEC 2012 Conference Proceedings – 19th World Hydrogen Energy Conference.

[25] Dinçer Akal, Semiha Öztuna, and Mustafa Kemalettin Büyükakın. A review of hydrogen usage in internal combustion engines (gasoline-lpg-diesel) from combustion performance aspect. *International Journal of Hydrogen Energy*, 45(60):35257–35268, 2020. 4th International HYDROGEN TECHNOLOGIES Congress.

[26] Alexandru CERNAT Niculae NEGURESCU, Constantin PANA. Aspects of using hydrogen in si engine. 2012.

[27] Mustafa Balat. Potential importance of hydrogen as a future solution to environmental and transportation problems. *International Journal of Hydrogen Energy*, 33(15):4013–4029, 2008.

[28] V. Rapp, N. Killingsworth, P. Therkelsen, and R. Evans. 4 - lean-burn internal combustion engines. In Derek Dunn-Rankin and Peter Therkelsen, editors, *Lean Combustion (Second Edition)*, pages 111–146. Academic Press, Boston, second edition edition, 2016.

[29] Gregory K. Lilik, Hedan Zhang, José Martin Herreros, Daniel C. Haworth, and André L. Boehman. Hydrogen assisted diesel combustion. *International Journal of Hydrogen Energy*, 35(9):4382–4398, 2010.

[30] Farzad Poursadegh, Michael Brear, Barnaby Hayward, and Yi Yang. Autoignition, knock, detonation and the octane rating of hydrogen. *Fuel*, 332:126201, 2023.

[31] Mara Hauck, Miralda van Schot, and Joris Koornneef. Carbon footprint of grey, blue and green hydrogen. Technical report, TNO, Year of Publication. TNO: Madelaine Halter NSE coordinator et al. The project is uitgevoerd met subsidie van het Ministerie van Economische Zaken, Nationale regelingen EZ-subsidies, Topsector Energie uitgevoerd door Rijksdienst voor Ondernemend Nederland.

[32] ecoinvent. The ecoinvent Association, 2023. Accessed 19/08/2023.

[33] NyOrka Page 1 12/18/2008. NEEDS: New Energy Externalities Developments for Sustainability. Deliverable n° 8-5 RS1a, June 2008. Project no: 502687, INTEGRATED PROJECT, Priority 6.1: Sustainable Energy Systems and, more specifically, Sub-priority 6.1.3.2.5: Socio-economic tools and concepts for energy strategy. Corresponding author: maria.maack@newenergy.is. Due date of deliverable: June 2008. Start date of project: 1 September 2004. Duration: 48 months. Organisation name for this deliverable: Icelandic New Energy. Project co-funded by the European Commission within the Sixth Framework Programme (2002-2006). Dissemination Level: PU Public X.

[34] JRC/IES. Well-to-Wheels Analysis of Future Automotive Fuels and Powertrains in the European Context. Well-to-Tank Report Version 2b, Joint Research Centre, Institute for Energy and Transport, May 2006.

[35] Yaser Khojasteh Salkuyeh, Bradley A Saville, and Heather L MacLean. Techno-economic analysis and life cycle assessment of hydrogen production from natural gas using current and emerging technologies. *International Journal of hydrogen energy*, 42(30):18894–18909, 2017.

[36] Christos M Kalamaras and Angelos M Efstathiou. Hydrogen production technologies: current state and future developments. In *Conference papers in science*, volume 2013. Hindawi, 2013.

[37] Autothermal reforming (atr) for low-carbon hydrogen production. https://engineering.airliquide.com/technologies/low-carbon-hydrogen. Accessed on 19/08/2023.

[38] V Utgikar and Todd Thiesen. Life cycle assessment of high temperature electrolysis for hydrogen production via nuclear energy. *International Journal of Hydrogen Energy*, 31(7):939–944, 2006.

[39] Ramchandra Bhandari, Clemens A Trudewind, and Petra Zapp. Life cycle assessment of hydrogen production via electrolysis–a review. *Journal of cleaner production*, 85:151–163, 2014.

[40] J. B. Heywood. *Internal combustion engine fundamentals*. Mc Graw Hill Eduction, 2018.

[41] Mustafa Ozcanli, Oguz Bas, Mustafa Atakan Akar, Safak Yildizhan, and Hasan Serin. Recent studies on hydrogen usage in wankel si engine. *International Journal of Hydrogen Energy*, 43(38):18037–18045, 2018. The 2nd International Mediterranean Science and Engineering Congress (IMSEC 2017), 25-27 October 2017, Adana, Turkey.

[42] F. V. BRACCO and W. A. SIRIGNANO. Theoretical analysis of wankel engine combustion. *Combustion Science and Technology*, 7(3):109–123, 1973.

[43] Roger Sierens, Rik S. G. Baert, Desmond E. Winterbone, and P. C. Baruah. A comprehensive study of wankel engine performance. 1983.

[44] F. Amrouche, P.A. Erickson, S. Varnhagen, and J.W. Park. An experimental analysis of hydrogen enrichment on combustion characteristics of a gasoline wankel engine at full load and lean burn regime. *International Journal of Hydrogen Energy*, 43(41):19250–19259, 2018.

[45] Hao Meng, Changwei Ji, Jinxin Yang, Ke Chang, Gu Xin, and Shuofeng Wang. A knock study of hydrogen-fueled wankel rotary engine. *Fuel*, 321:124121, 2022.

[46] Boestfleisch V Basshuysen R van Stutzenberger, H and F Pischinger. Suitability of rotary engines for hydrogen operation.

[47] Toshio Shudo and Shigeki Nabetani. Analysis of degree of constant volume and cooling loss in a hydrogen fuelled si engine. *SAE Technical Papers*, 09 2001.

[48] Mazda Newsroom. Mazda's new technology enables both improved environmental and driving performance - mazda to premiere i-stop idling stop system at the 2009 tokyo motor show, 2010.

[49] Dominic A Notter, Katerina Kouravelou, Theodoros Karachalios, Maria K Daletou, and Nara Tudela Haberland. Life cycle assessment of pem fc applications: electric mobility and μ-chp. *Energy & Environmental Science*, 8(7):1969–1985, 2015.

[50] P Masoni, A Zamagni, M Bode, M Finkbeiner, and K Chomkhamsri. Guidance document for performing lcas on fuel cells and h_2 technologies. *Rapport, nD3*, 3:109, 2011.

[51] Andrew Simons and Christian Bauer. A life-cycle perspective on automotive fuel cells. *Applied Energy*, 157:884–896, 2015.

[52] Marco Miotti, Johannes Hofer, and Christian Bauer. Integrated environmental and economic assessment of current and future fuel cell vehicles. *The International Journal of Life Cycle Assessment*, 22:94–110, 2017.

[53] Elsa Weiszflog and Manan Abbas. Life cycle assessment of hydrogen storage systems for trucks. Master's thesis, Chalmers University of Technology, Gothenburg, Sweden, 2022. Report No. E2022:089.

[54] Sara Evangelisti, Carla Tagliaferri, Dan JL Brett, and Paola Lettieri. Life cycle assessment of a polymer electrolyte membrane fuel cell system for passenger vehicles. *Journal of cleaner production*, 142:4339–4355, 2017.

[55] LCA-ActivityBrowser. https://github.com/LCA-ActivityBrowser/activity-browser/blob/master/README.md. Accessed 19/08/2023.

[56] Mary Ann Curran. *Overview of goal and scope definition in life cycle assessment*. Springer, 2017.

[57] Kun-Mo Lee and Atsushi Inaba. Life cycle assessment best practices of iso 14040 series. *Committee on Trade and Investment*, February 2004.

[58] International Organization for Standardization. ISO 14040:2006(en): Environmental management — Life cycle assessment — Principles and framework. International Organization for Standardization, 2006. ISO.

[59] Hans-Jörg Althaus and Marcel Gauch. Vergleichende ökobilanz individueller mobilität. *Elektromobilität versus konventionelle Mobilität mit Bio-und fossilen Treibstoffen, Empa, Dübendorf, Switzerland*, 2010.

[60] rx7club.com. Engine Bay Weights, 2023. Accessed 19/08/2023.

[61] auto-data.net. Mazda MX-30 0.8 e-SkyActiv R EV (170 Hp) Plug-in Hybrid, 2023. Accessed 19/08/2023.

[62] The ecoinvent database - electricity sector. https://ecoinvent.org/the-ecoinvent-database/sectors/electricity/. Accessed [Insert Date].

[63] Qiang Dai and Christian M Lastoskie. Life cycle assessment of natural gas-powered personal mobility options. *Energy & fuels*, 28(9):5988–5997, 2014.

[64] Hao Meng, Changwei Ji, Gu Xin, Jinxin Yang, Ke Chang, and Shuofeng Wang. Comparison of combustion, emission and abnormal combustion of hydrogen-fueled wankel rotary engine and reciprocating piston engine. *Fuel*, 318:123675, 2022.

[65] Andrea Del Duce, Marcel Gauch, and Hans-Jörg Althaus. Electric passenger car transport and passenger car life cycle inventories in ecoinvent version 3. *The International Journal of Life Cycle Assessment*, 21:1314–1326, 2016.

[66] ReCiPe. Recipe, 2016. Accessed on 19/08/2023.

[67] Timothy John Norman. A performance model of a spark ignition wankel engine: including the effects of crevices volumes, gas leakage, and heat transfer. *B.S.M.E University of Massachusetts, Amherst*, 1981.

[68] Guido A. Danieli, Colin R. Ferguson, John B. Heywood, and James C. Keck. Predicting the emissions and performance characteristics of a wankel engine. *SAE Transactions*, 83:805–820, 1974.

[69] J. A. Gatowski, E. N. Balles, K. M. Chun, F. E. Nelson, J. A. Ekchian, and J. B. Heywood. Heat release analysis of engine pressure data. *SAE Transactions*, 93:961–977, 1984.

[70] Bonnie J. Mcbride, Sanford D. Gordon, and Martin A. Reno. Coefficients for calculating thermodynamic and transport properties of individual species. 1993.

[71] H. Jeanmart F. Contino. Lmeca2220 - internal combustion engines. Handouts, Thermodynamics of the fuel-air cycle, 2004. UCLouvian.

[72] Simon Guen, Alain Maiboom, Sabre Bougrine, and Xavier Tauzia. Analysis of systematic calibration of heat transfer models on a turbocharged gdi engine operating map. 04 2018.

[73] H. Jeanmart F. Contino. Lmeca2220 - internal combustion engines. Handouts, Energy flows and in-cylinder heat transfer, 2004. UCLouvian.

[74] H. Jeanmart F. Contino. Lmeca2220 - internal combustion engines. Course syllabus - chapitre 2, ASPECTS THERMIQUES ET PRESSION MOYENNE INDIQUEE, 2004. UCLouvian.

[75] Denys STEPANENKO and Zbigniew KNEBA. Thermodynamic modeling of combustion process of the internal combustion engines – an overview. *Combustion Engines*, 178(3):27–37, 2019.

[76] Zhenyu Yang, Changwei Ji, Jinxin Yang, Huaiyu Wang, Xionghui Huang, and Shuofeng Wang. The optimization of leading spark plug location and its influences on combustion and leakage in a hydrogen-fueled wankel rotary engine. *International Journal of Hydrogen Energy*, 48(53):20465–20482, 2023.

[77] Toshio Shudo and Hiroyuki Suzuki. Applicability of heat transfer equations to hydrogen combustion. *JSAE Review*, 23(3):303–308, 2002.

[78] Toshio Shudo and Hiroyuki Suzuki. Applicability of heat transfer equations to hydrogen combustion. *JSAE Review*, 23(3):303–308, 2002.

[79] K-W Cho, Dennis Assanis, Z Filipi, G Szekely, P Najt, and R Rask. Experimental investigation of combustion and heat transfer in a direct-injection spark ignition engine via instantaneous combustion chamber surface temperature measurements. *Proceedings of The Institution of Mechanical Engineers Part D-journal of Automobile Engineering - PROC INST MECH ENG D-J AUTO*, 222:2219–2233, 11 2008.

[80] Jeongwoo Lee, Cheolwoong Park, Jongwon Bae, Yongrae Kim, Young Choi, and Byeungjun Lim. Effect of different excess air ratio values and spark advance timing on combustion and emission characteristics of hydrogen-fueled spark ignition engine. *International Journal of Hydrogen Energy*, 44(45):25021–25030, 2019.

[81] Hao Meng, Changwei Ji, Jinxin Yang, Shuofeng Wang, Ke Chang, and Gu Xin. Experimental study of the effects of excess air ratio on combustion and emission characteristics of the hydrogen-fueled rotary engine. *International Journal of Hydrogen Energy*, 46(63):32261–32272, 2021.

[82] *Investigation of the Performance of Hydrogen-Fueled Wankel Rotary Engine Using 0-D Model*, volume Volume 1: Aircraft Engine; Ceramics and Ceramic Composites of *Turbo Expo: Power for Land, Sea, and Air*, 06 2022.

[83] Stijn Broekaert, Thomas De Cuyper, Michel De Paepe, and Sebastian Verhelst. Evaluation of empirical heat transfer models for hcci combustion in a cfr engine. *Applied Energy*, 205:1141–1150, 2017.

[84] Leonid Tartakovsky, Vladimir Baibikov, Marcel Gutman, Veinblat Mark, and Jonathan Reif. Simulation of wankel engine performance using commercial software for piston engines. *SAE Technical Papers*, 4, 10 2012.

[85] A.-C. MUNTEANU, N. BUZBUCHI, and L.-C. STAN. Rotary internal combustion engines. *Constanta Maritime University Annals*, 15:93–99, 2014.

[86] Hailin Li and Ghazi A. Karim. Hydrogen Fueled Spark-Ignition Engines Predictive and Experimental Performance. *Journal of Engineering for Gas Turbines and Power*, 128(1):230–236, 07 2004.

[87] Hao Meng, Changwei Ji, Du Wang, Gu Xin, Ke Chang, Jinxin Yang, and Shuofeng Wang. Research on the load control of hydrogen-fueled wankel rotary engine. *International Journal of Hydrogen Energy*, 47(37):16665–16675, 2022.

[88] Gerhard Woschni. A universally applicable equation for the instantaneous heat transfer coefficient in the internal combustion engine. *SAE transactions*, 76, 1967.

[89] Racext. A quel régime tourne un démarreur ?

[90] Racing Beat. How to perform a rotary engine compression check.

Appendix A

Experimental Part

This portion of the appendix documents the activities undertaken in the laboratory during the academic year. While this report is not exhaustive, it is crafted with the intention of serving as a technical reference for future work related to the Wankel engine within the lab.

A.1 Engine Identification

The engine present in the laboratory is a water-cooled, twin-scroll turbocharged 13B-DEI WRE, from a Mazda RX7 FC3S S5 Turbo II (1989-1991) with a power output of 147 kW at 6500 RPM. Detailed specifications can be found in Table A.1.

The initial action taken was to disassemble the engine (excluding the engine block) to thoroughly recognize its components and assess their conditions. Through this process, both missing and modified parts were identified.

Engine name				13B-DEI S5 Turbo II
Engine type				Rotary engine
Displacement cc (cu in)				654 x 2 (40.0 x 2)
Number of rotors and arrangement				2 rotors, longitudinal
Combustion chamber type				Bathtub
Compression ratio				9.0:1
Air induction				4 port induction
Maximum power hp (kW)				200 (149) @ 6500 RPM
Maximum torque Nm (lb·ft)				266 (196) @ 3500 RPM
Port timing	Intake	Open	Primary	45° ATDC
			Secondary	32° ATDC
		Close	Primary	50° ABDC
			Secondary	50° ABDC
	Exhaust	Open		75° BBDC
		Close		48° ATDC
Fuel supply system				EGI
Ignition timing			Trailing	20° ± 2° ATDC
			Leading	5° ± 1° ATDC
Idle speed RPM				750 ± 25

Figure A.1: Wankel 13B-DEI detailed specifications [11]

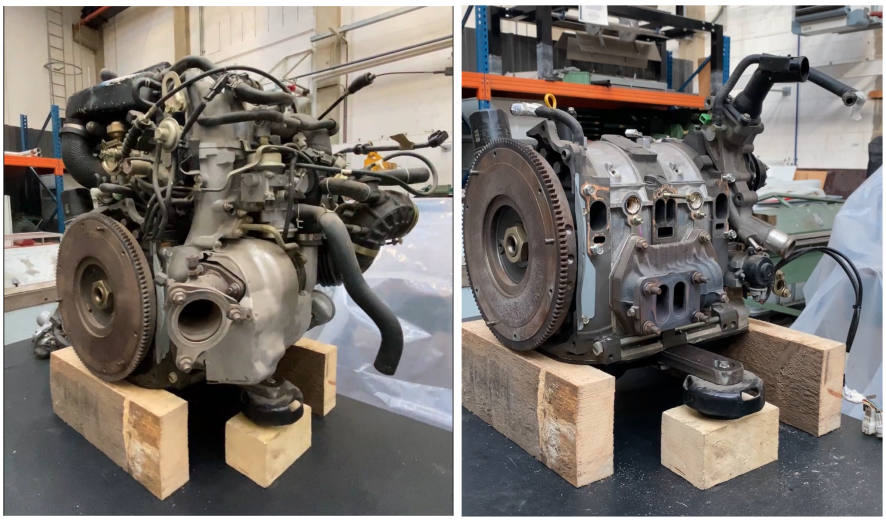


Figure A.2: Engine pre and post-disassembly

A.1.1 Modified Parts

The intercooler was observed to have modifications. While the original design used an air-to-air system, the present engine is equipped with an air-water intercooler. The exact reason behind this change remains unclear. For initial testing and simplicity, the decision was made to replace this modified intercooler with an available air-to-air version, paired with a cooling fan from the laboratory.



Figure A.3: Intercooler comparison [11, 12]

A.1.2 Missing Parts

As determined by Hoornaert in [11], the engine lacks multiple components. The main missing parts are listed here below :

1. Water Cooling system
2. Fresh air duct and air cleaner
3. Fuel tank, fuel filter and fuel pump
4. Exhaust system
5. Battery, Coil and igniter
6. Engine Control Unit

A.1.3 Oil Nozzles

While disassembling, the oil nozzles located at the top of the engine block were extracted and examined as per the methodology outlined in figure A.4, but with pressurized air. Good conditions were reported.

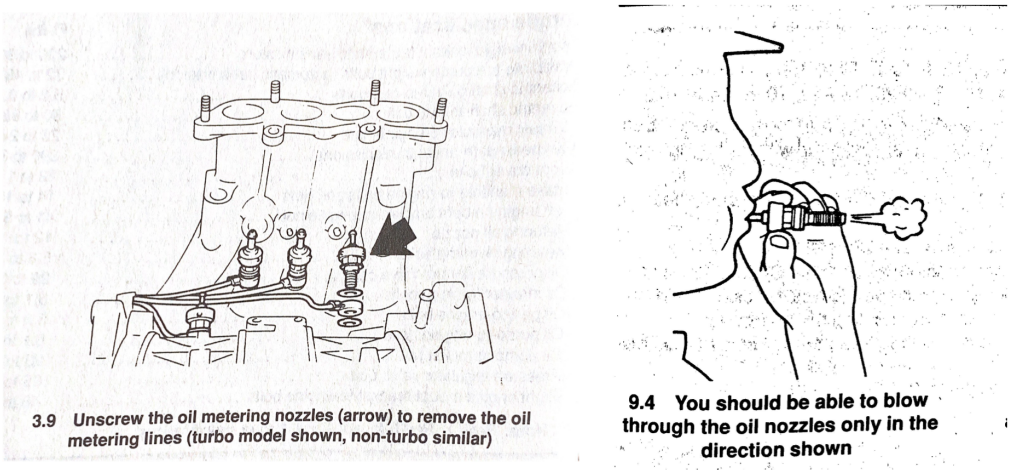


Figure A.4: Oil Nozzle test [13]

A.1.4 Injectors

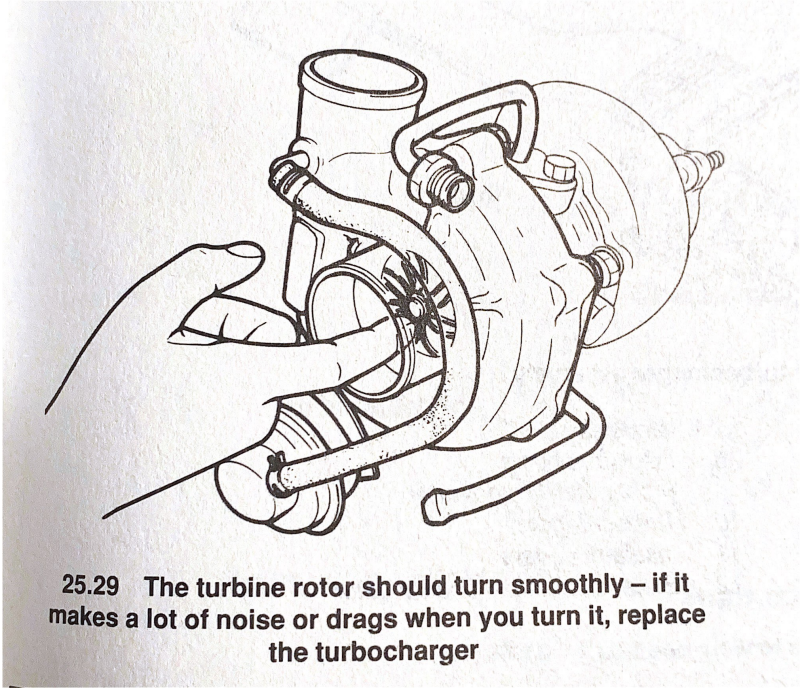
During disassembly, the fuel injectors were extracted and evaluated. They were connected to a power supply and tested using compressed air. Good conditions were reported.

A.1.5 Turbocharger

During the disassembly process, the turbocharger underwent manual testing, as illustrated in figure A.5, reporting good condition. Furthermore, its control system was investigated. The turbocharger operates through a mechanical wastegate, which activates once the pressure reaches a specified boost threshold. Additionally, a two-port solenoid valve adjusts the pressure exerted on the wastegate actuator, altering its function. Initially, to achieve purely mechanical control of the turbocharger, the wastegate can be disconnected from its boost pressure control system.

A.1.6 Metering Oil Pump

The metering oil pump is responsible for injecting small amounts of oil into the cylinder via the oil injectors. Its functioning was scrutinized. Originally, this pump was managed by the factory ECU. However, given the absence of the original ECU and the incapability of the Motec M84 ECU to oversee its operation, an Arduino has been employed to regulate the stepper motor within the pump. The Arduino



25.29 The turbine rotor should turn smoothly – if it makes a lot of noise or drags when you turn it, replace the turbocharger

Figure A.5: Turbocharger test [13]

program processes inputs from the intake manifold pressure via the MAP sensor and the RPM through the crank angle sensor. Based on the data from Table A.1, the program outputs a specific position in %age. This position determines the alignment of a screw within the pump, adjusting the volume of oil supplied to the cylinders.

RPM/kPa	500	1000	1500	2000	2500	3000	3500	4000	4500	5000	5500	6000	6500	7000	8000
-98.2	8.00	8.00	8.00	8.00	8.00	8.00	8.00	8.00	8.00	8.00	8.00	8.00	8.00	8.00	8.00
-81.3	8.00	8.66	9.08	9.50	9.92	10.32	10.32	10.32	10.32	10.32	10.32	10.32	10.32	10.32	10.32
-60.9	8.00	9.32	10.16	11.00	11.82	12.66	12.66	12.66	12.66	12.66	12.66	12.66	12.66	12.66	12.66
-40.6	8.00	10.00	11.24	12.50	13.74	15.00	15.00	15.00	15.00	15.00	15.00	15.00	15.00	15.00	15.00
-20.3	8.00	12.66	14.50	16.32	10.16	20.00	20.02	21.66	22.50	23.32	23.32	23.32	23.32	23.32	23.32
0	8.00	15.32	17.74	20.16	22.58	25.00	26.66	28.32	30.00	31.66	31.66	31.66	31.66	31.66	31.66
20.7	8.00	18.00	21.00	24.00	27.00	30.00	32.50	35.00	37.50	40.00	40.00	40.00	40.00	40.00	40.00
41.4	8.00	28.66	31.50	34.32	37.16	40.00	43.32	46.66	50.00	53.32	53.32	53.32	53.32	53.32	53.32
62	39.32	39.32	42.00	44.66	47.32	50.00	54.16	58.32	62.50	66.66	6.6 .66	66.66	66.66	6.6 .66	66.66

Table A.1: Metering oil pump inputs and outputs table: Vertical axis: pressure (kPa) ; Horizontal axis: Speed (RPM) ; Table values: Position of stepper (%)

A.2 Engine Block condition assessment

The initial step involves assessing the engine health. Given the uncertainty regarding the last time the engine operated, evaluating its current condition is crucial to pinpoint potential failures or required repairs.

To avoid replacing internal seals, dismantling the engine block was deemed unnecessary at this stage. Instead, two preliminary tests were chosen: a visual inspection utilizing a camera for assessing the engine's state and a compression test conducted in both chambers using a compression gauge. Should the visual assessment reveal no significant concerns and the compression test produces anticipated outcomes, there will be no immediate imperative to open the engine block.

A.2.1 Visual Inspection

Initially, an attempt was made to assess the engine's condition through a visual inspection of its in-cylinder state. This examination was performed using a professional in-cylinder stethoscope, with a representative screenshot provided in figure A.6.

During the visual assessment, carbon deposits (often referred to as calamine) resulting from accumulated unburned hydrocarbons were noticed on the rotor. To address these deposits, chemical cleaners may be introduced to the fuel while the engine operates.

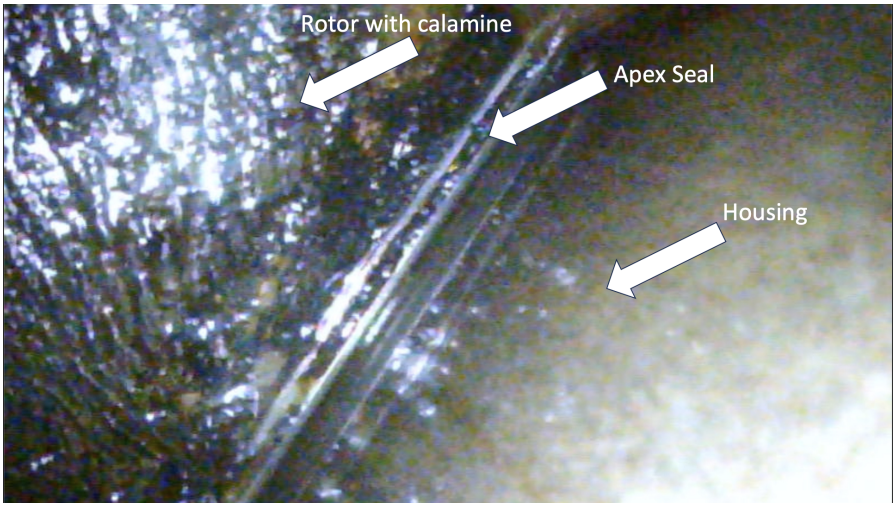


Figure A.6: In-cylinder Inspection

A.2.2 Compression and Starter Test

An experimental compression and starter test was conducted with two primary objectives :

1. To assess the condition of the starter: The starter functionality was evaluated by measuring its rotational speed, indicating its ability to efficiently initiate engine operation.

2. To evaluate the health of the engine: The test sought to determine if any gas leakage occurred at the apex, side, or corner seals of the engine. By meticulously observing these areas, the intention was to pinpoint potential issues that might undermine the engine's performance and overall health.

Through this comprehensive compression and starter test, the aim was to ensure the optimal functioning of both the starter and the engine, providing valuable insights into their respective conditions.

The cranking compression reading during the test provides valuable insights into the condition of the seals within the rotor. By observing the pattern of compression increments, Potential faults can be identified, and the overall health of the engine assessed:

- If the pressure peaks in the compression reading have similar magnitudes and remain consistent, it indicates even compression across all rotor sides. Additionally, if the compression peaks exhibit a sufficiently high magnitude, it suggests that the side, corner and apex seals are in proper functioning condition, maintaining effective compression.

- If the pressure graph shows a high-pressure peak followed by two lower compression peaks, repeating in this pattern, it strongly suggests the failure of one apex, corner, or side seal. This occurrence happens because a damaged seal can lead to gas leakage in two combustion chambers, resulting in two subsequent lower-pressure peaks.

- Alternatively, if the pressure graph displays three consecutive low-pressure peaks, it indicates the failure of one apex, corner, or side seal. This scenario arises when two seals are damaged, causing gas leakage in all three combustion chambers and resulting in the three observed low-pressure peaks.

To ensure proper engine and starter performances, a few conditions should be respected [89, 90]:

1. Normal compression should fall within the range of 7.6 to 10.3 bar.
2. The minimum compression should exceed 5.2 bar to ensure adequate engine functionality.
3. The maximum pressure difference between pressure peaks should not exceed 1.4 bar, indicating consistent compression levels across the rotor.
4. The desired rotational speed range for the starter should fall within 200 and 300 RPM.

Setup

The experimental setup for the compression and starter test involves the following setup:

- Engine Mounting (figure A.9): The engine is securely mounted on four wooden blocks, which are tightly strapped to the table. Additionally, for safety purposes, the engine is attached to a supporting structure known as a Girafe.
- Front Setup (figure A.7): The front setup consists of a power source that supplies the 24V pressure sensors. These sensors are carefully adjusted and screwed into the trailing spark plug holes of the engine. The pressure sensors are then connected to an oscilloscope, which allows for the real-time display and recording of the pressure trace during the test.
- Back Setup (figure A.8): The back setup comprises a 12V car battery, which serves as the power supply for the starter. The starter is mounted on the engine and positioned to engage with the flywheel gear. To ensure safety, a switch is incorporated into the setup. Once the switch is turned on, the starter gear meshes with the flywheel gear, initiating the rotation of the engine's crankshaft. Prior to starting the engine, oil is added to the working chambers to facilitate smooth operation and reduce friction.

By implementing this experimental setup, it becomes possible to measure and analyze the pressure variations within the engine during the compression and starter test. The oscilloscope provides a visual representation of the pressure trace, while the starter enables the engine to rotate, allowing for the assessment of its mechanical performance.

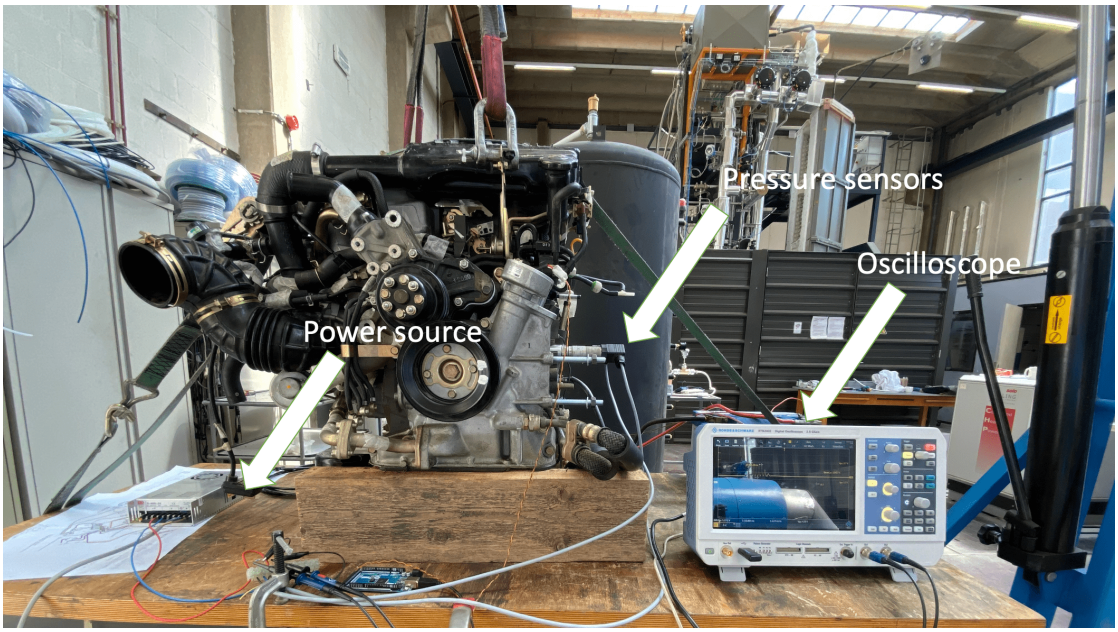


Figure A.7: Front Setup

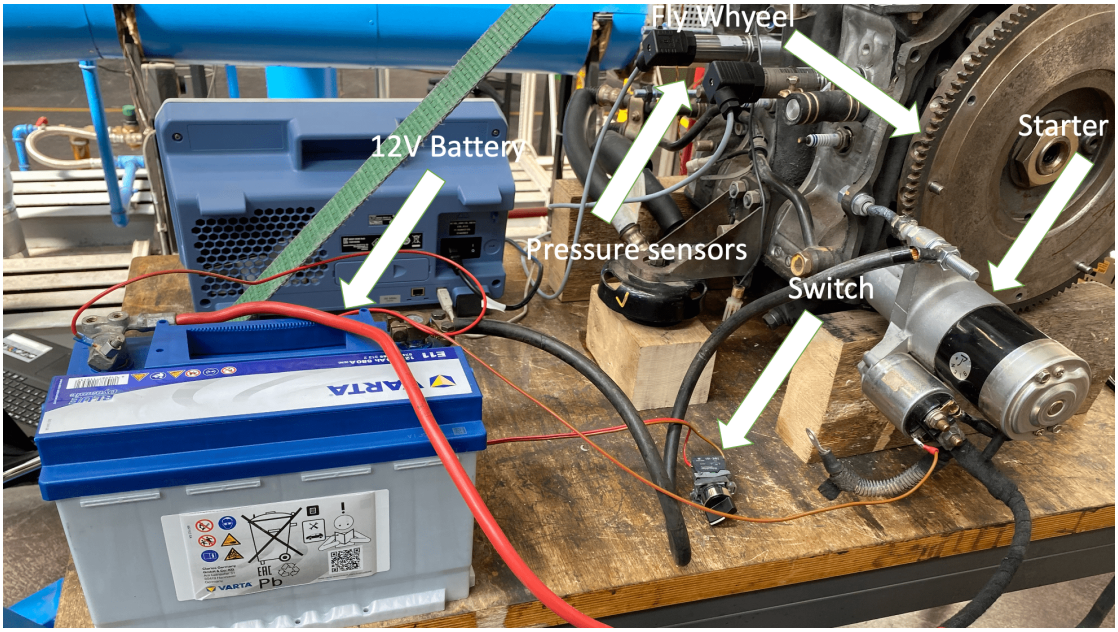


Figure A.8: Back Setup (1/2)

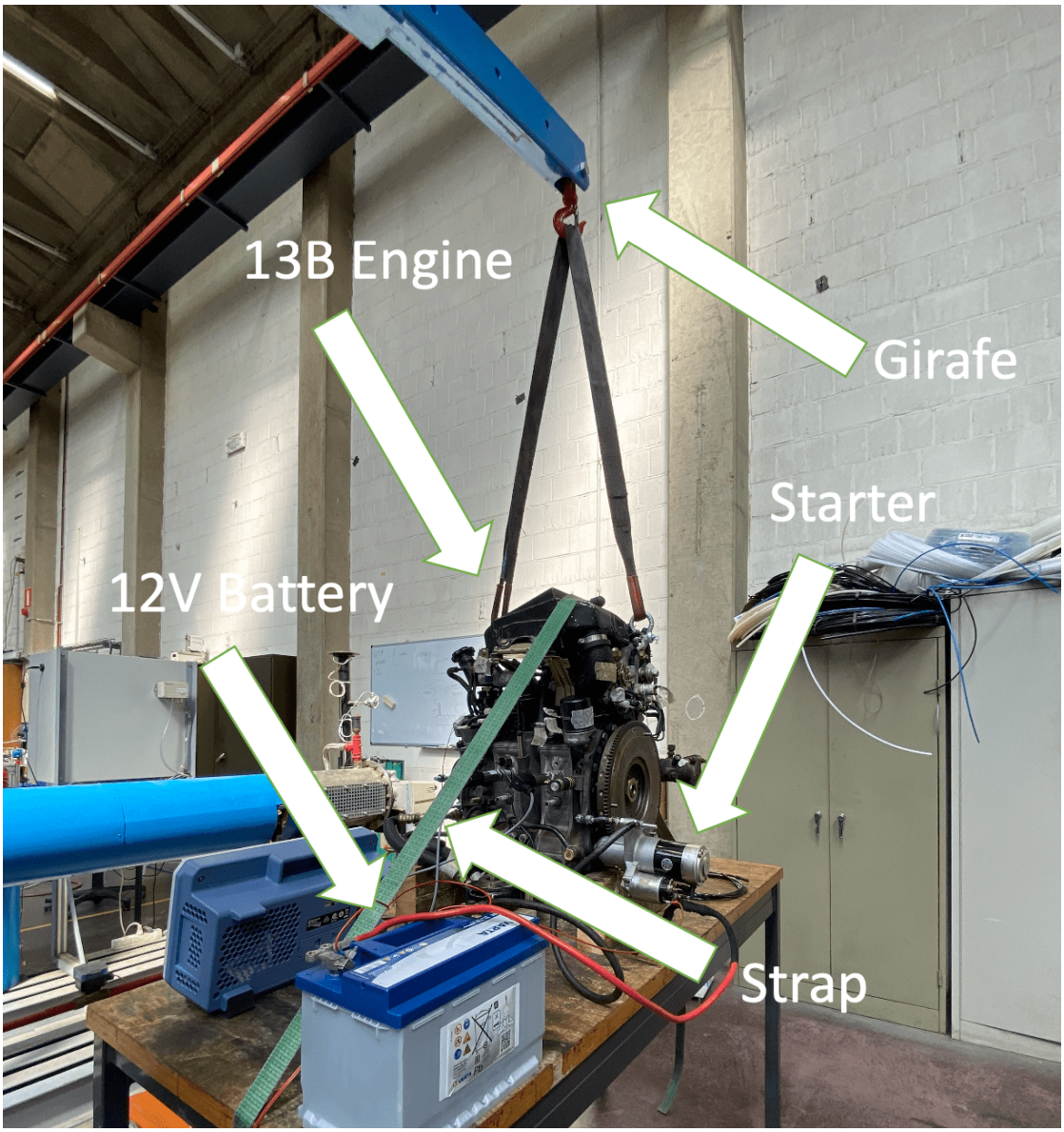


Figure A.9: Back Setup (2/2)

Results

Upon retrieving the data from the oscilloscope, a post-processing step was conducted to enhance the accuracy and reliability of the results. A low-pass filter was applied to isolate and retain the low-frequency components while effectively removing any noise or unwanted interference from the data. This filtering process ensured that the subsequent analysis was based on the essential information necessary for evaluating the engine and starter performances.

The analysis of the experiment results provides valuable insights into the performance and health of the engine. Here is an explanation of the findings:

1. Starter Assessment: The extracted frequency from the data is determined to be 4.41 Hz, which is equivalent to a rotational speed of 265 RPM. This falls within the correct range of rotational speed, indicating that the starter is in good working condition and suitable for use.

2. First Rotor Evaluation (figure A.10): The first rotor exhibits a minimum pressure value of 7.27 bar and a maximum value of 10.8 bar. The maximum difference observed between two consecutive pressure peaks is 2.4 bar, occurring between the 16th and 17th peaks. These values indicate a moderate level of health for this rotor. On the pressure graph, there is a consistent pattern of one higher peak pressure followed by two lower peaks, repeating. This pattern suggests that one seal set may not be in optimal condition. However, despite this observation, the minimum pressure remains sufficiently high for the engine to be usable.

3. Second Rotor Assessment (figure A.11): The second rotor showcases a minimum pressure value of 9.7 bar and a maximum value of 11 bar. The maximum difference between two consecutive pressure peaks is 1.2 bar, which occurs between the first and second peaks. These values signify a very good health status for this rotor. It adheres to all the specified conditions and delivers excellent results.

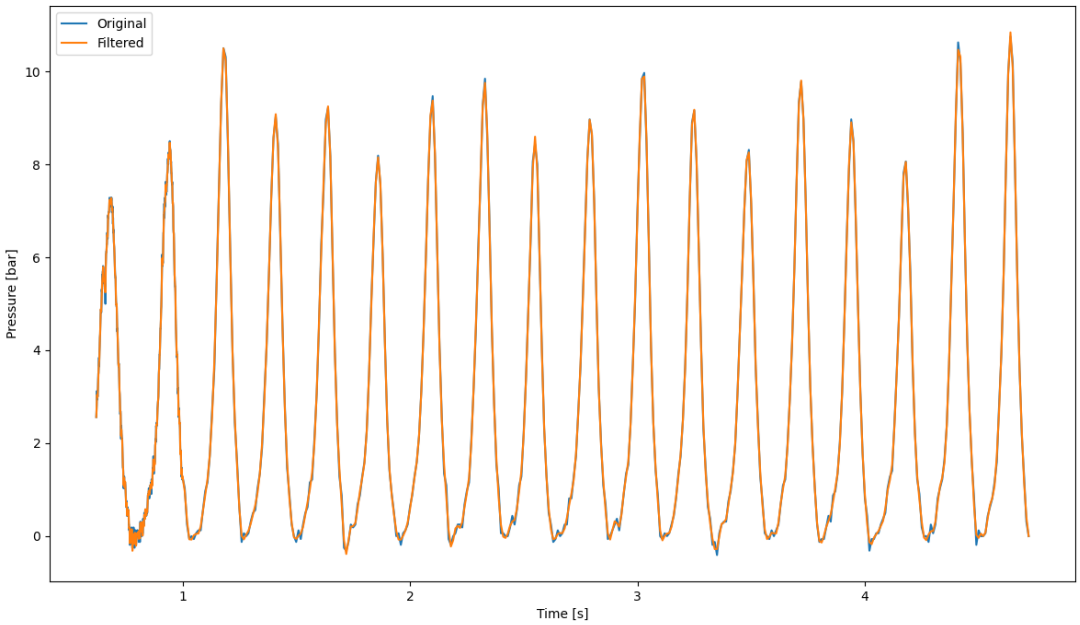


Figure A.10: First rotor

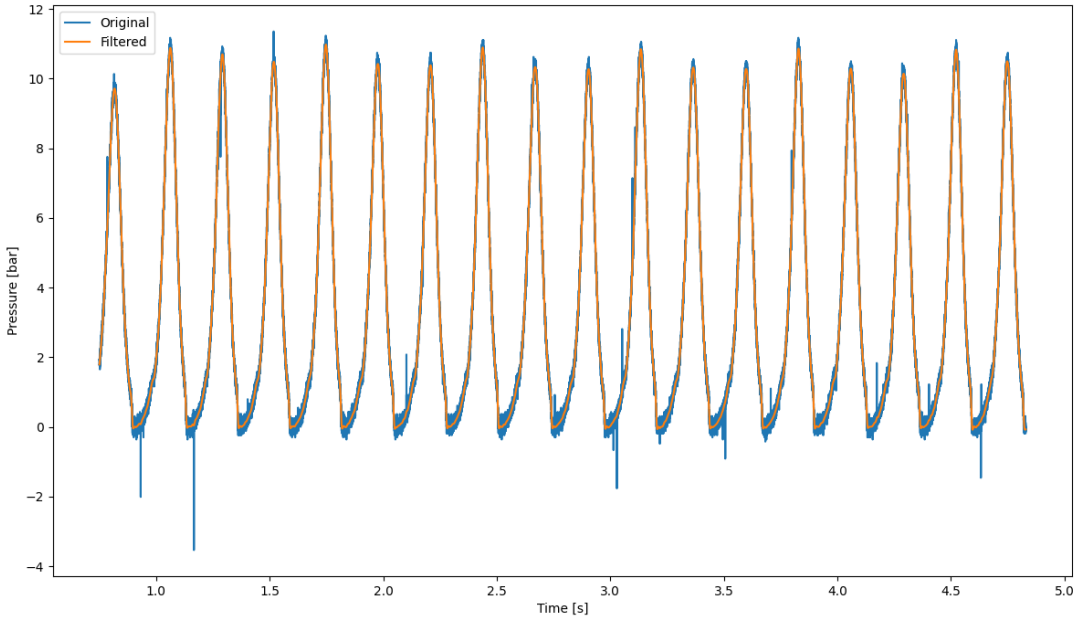


Figure A.11: Second rotor

A.2.3 Engine Block Condition Conclusion

From the observations, it's evident that the starter is in prime condition, well-suited for initiating engine startup. The first rotor's health is average, with a potential concern spotted in one of its seal sets. However, due to the minimum pressure value remaining within an acceptable range, the engine is still operational. In contrast, the second rotor is in outstanding condition, fulfilling all criteria and showcasing commendable results. This information paints a clear picture of the engine's operational status, offering insights for forthcoming maintenance or enhancements.

There's notable carbon buildup on the engine rotors, but this can be addressed by incorporating a chemical additive to the fuel during its initial run.

Additionally, collaboration with Mr. Saey from Automobile Saey Beauvechain, an expert in rotary engines, resulted in a secondary compression test at his facility. Given his expertise combined with the data collected, there's no immediate requirement to disassemble the engine block, which meets the minimum requirements for proper operation.

A.3 Sensors

A.3.1 MAP Sensor

A new MAP sensor was bought, since the original one was not compatible with the Motec M84 ECU. It is a 2 bar (absolute) sensor.

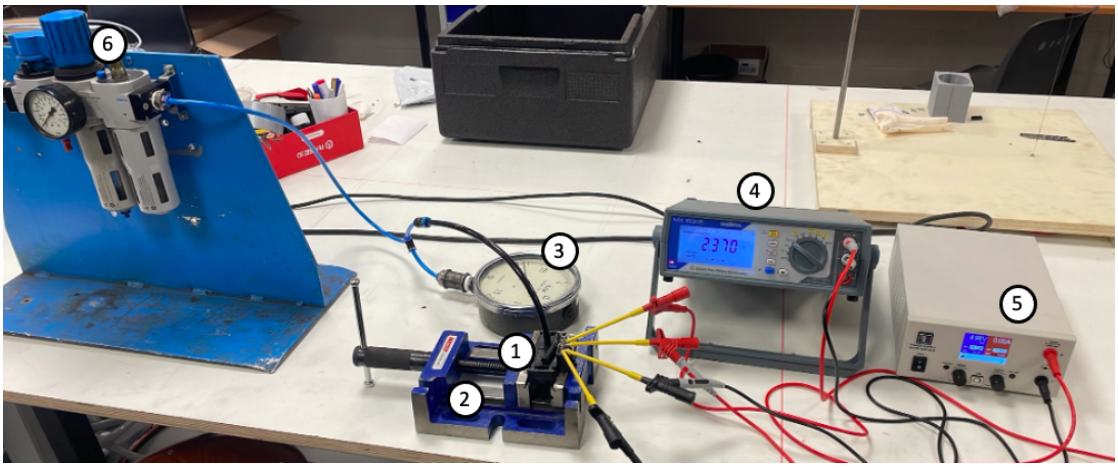


Figure A.12: MAP sensor calibration setup

The setup for calibrating the Map sensor is composed of several elements that are shown in fig.A.12:

1. MAP sensor
2. Clamping tool
3. Diaphragm pressure sensor
4. Multimeter
5. Power supply
6. Pneumatic circuit

By taking several measurements among the measurement range of the sensor, a linear interpolation was done in order to calibrate it. The results are shown in fig.A.13.

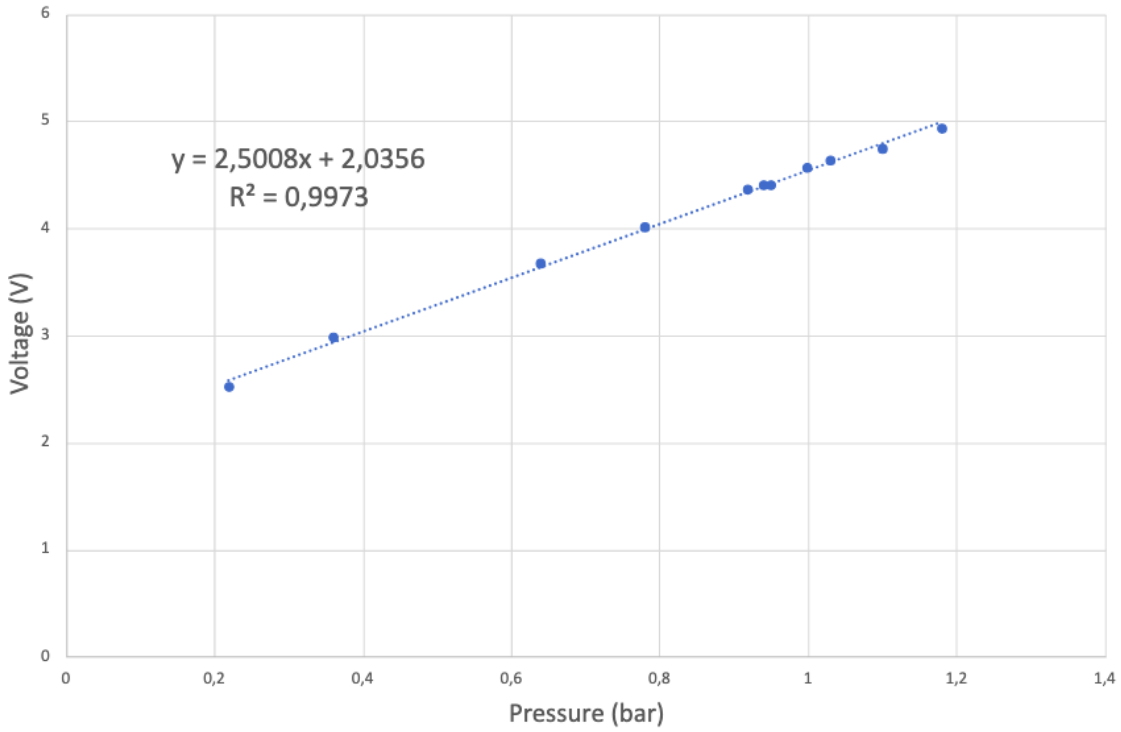


Figure A.13: Map sensor calibration (relative pressure)

A.3.2 Temperature Sensors

The setup for calibrating all of the temperature sensors is composed of several elements that are shown in fig.A.14:

1. Calibrated temperature sensor
2. Circulator's bath vessel
3. Circulator's control unit
4. Circulator's reservoir where sensors are submerged
5. Ohmmeter
6. Thermometer
7. Other temperature sensors

The calibration of three temperature sensors has been done. These sensors measure the temperature of the intake air, of the water, and of the water after heat exchange. The results are shown in figs. A.15, A.16, and A.17.

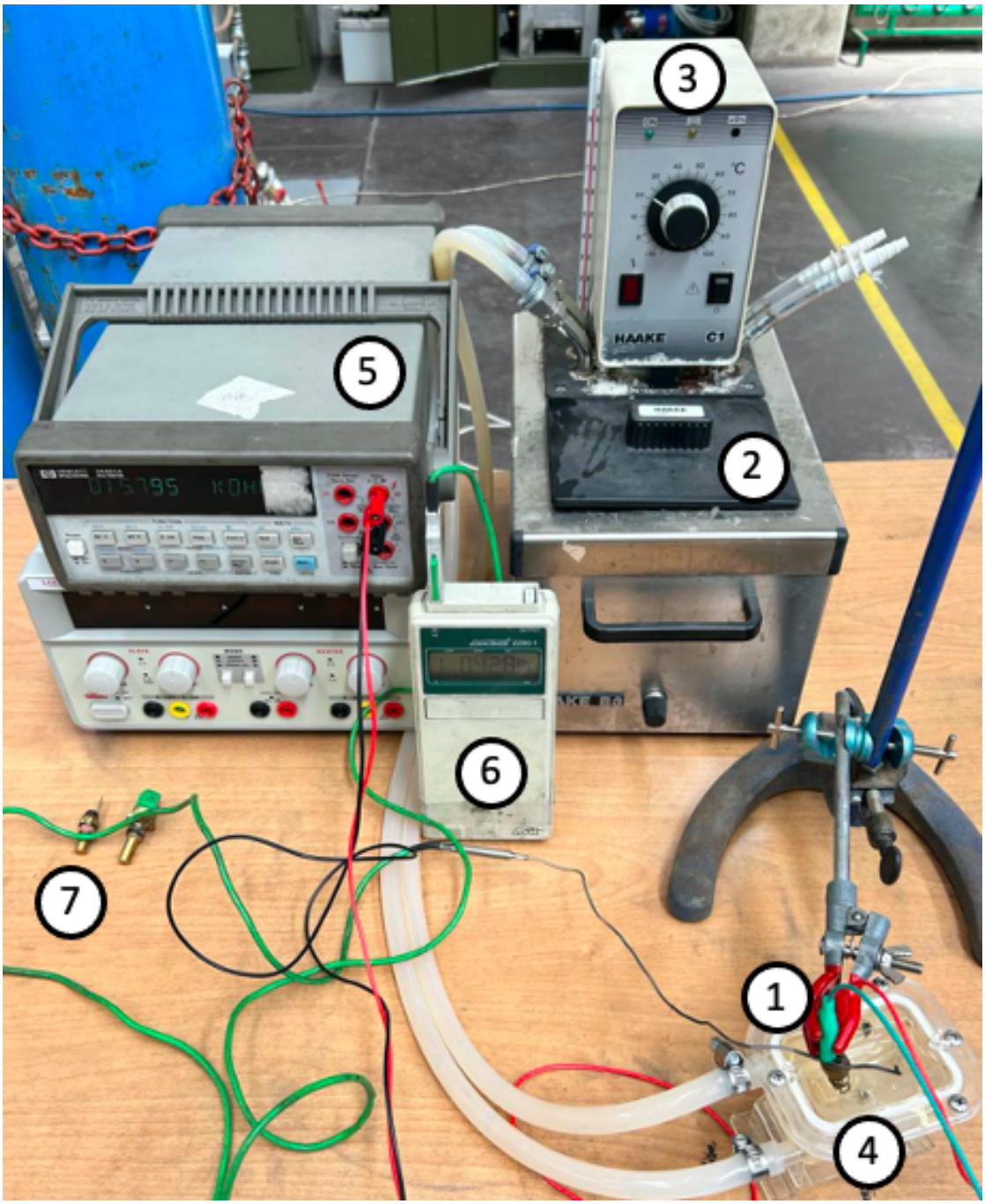


Figure A.14: Temperature sensors calibration setup

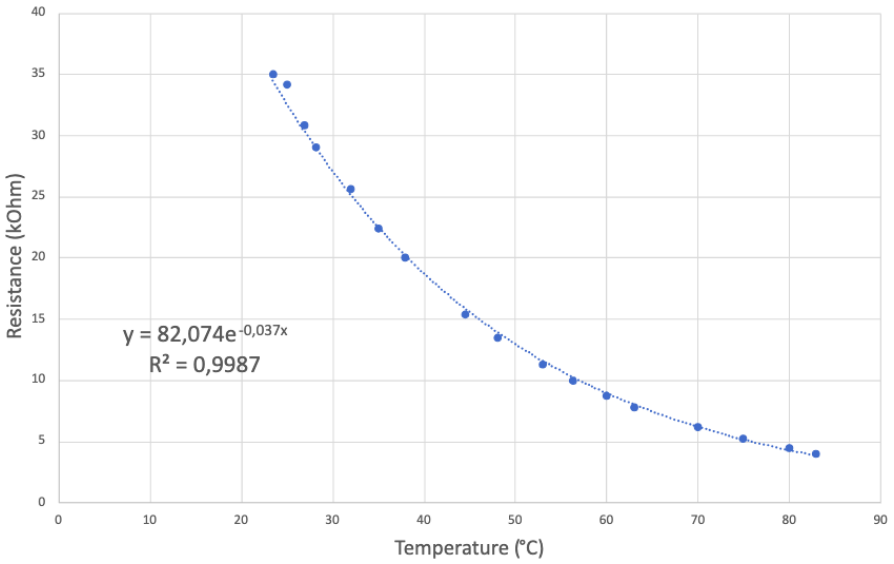


Figure A.15: Intake air temperature sensor calibration

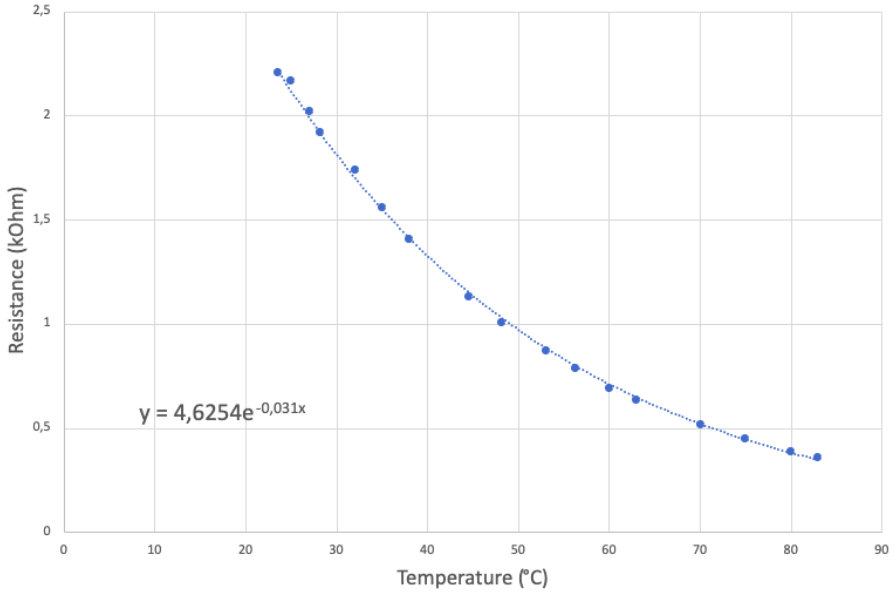


Figure A.16: Water temperature sensor calibration

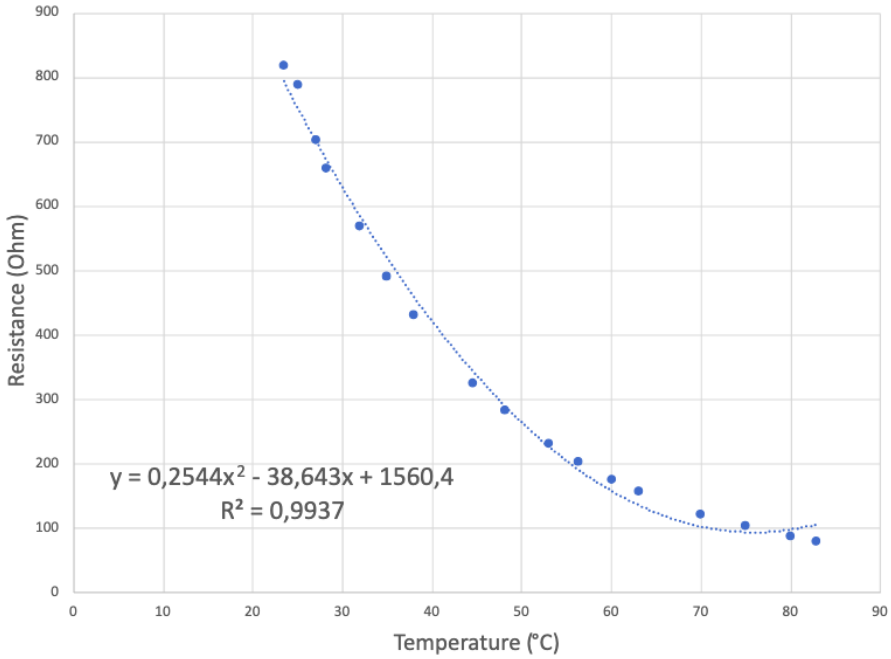


Figure A.17: Water (after exchange) temperature sensor calibration

A.3.3 Oil Pressure Sensor

The oil pressure sensor is a resistive sensor that has only two values as output. The normal output has a value around 113Ω. When the oil's pressure (relative) is above 0.5 bar, the resistance of the sensor drops to a value around 42Ω.

A.3.4 Crank Angle Sensor

The crank angle sensor is a magnetic sensor. It is composed of two single sensors: the NE and the G, which correspond to the Ref and to the Sync sensors respectively. The NE sensor is composed of a 24-teeth gear, whereas the G sensor is composed of a 2-teeth gear. There is a rotation ratio of 2 between the engine's rotor and these two sensors, therefore, for one rotation of the rotor, these two gears make a half of a rotation. These parameters have been introduced in the ECU's software, and by rotating the crank angle sensor with a screwdriver, the correct speed is displayed.

A.4 Ignition circuit

The ignition circuit is shown in details in fig.A.25. It is composed of an ignitor, three ignition coils, and four spark plugs. The ignitor, commanded by the ECU, provides voltage to the indicated coil. The coil's job is to amplify this voltage, in order for the spark plug connected to it to produce a spark.

There are three coils for four spark plugs. Both trailing spark plugs are connected to an independent coil, and both leading spark plugs are connected to the same one. Since both rotors are dephased of 180ř, sparks coming from the two leading spark plugs should be dephased by this value as well. The same stands for the two leading spark plugs, they should both produce a spark dephased by 180ř. However, since both spark plugs are connected to the same coil, they will always produce sparks at the same time. The reason for this is that it works with a "lost spark". Indeed, the coil where both leading spark plugs are connected will deliver a signal with a frequency that is twice the one of both coils where trailing spark plugs are connected.
In fig.A.18 the following elements can be found:

1. Crank angle mechanism, rotation provided by a screwdriver
2. Motec M84 calculator
3. Motec software
4. Power supply
5. 2 oscilloscopes used in order to have enough channels available
6. Coils
7. Spark plugs
8. Circuit: Motec safety circuit + ignition circuit

To illustrate this, fist the signals from each coil is individually shown, accompanied by the Sync signal, in order to clearly see at what moment of the engine's rotation the spark plugs are going to fire. This is shown in figs A.20, A.21 and A.22, where the yellow signal is the Sync signal, and the green signal is the signal from the respective coil. A full rotation of the rotor happens between two triggers of the yellow signal.

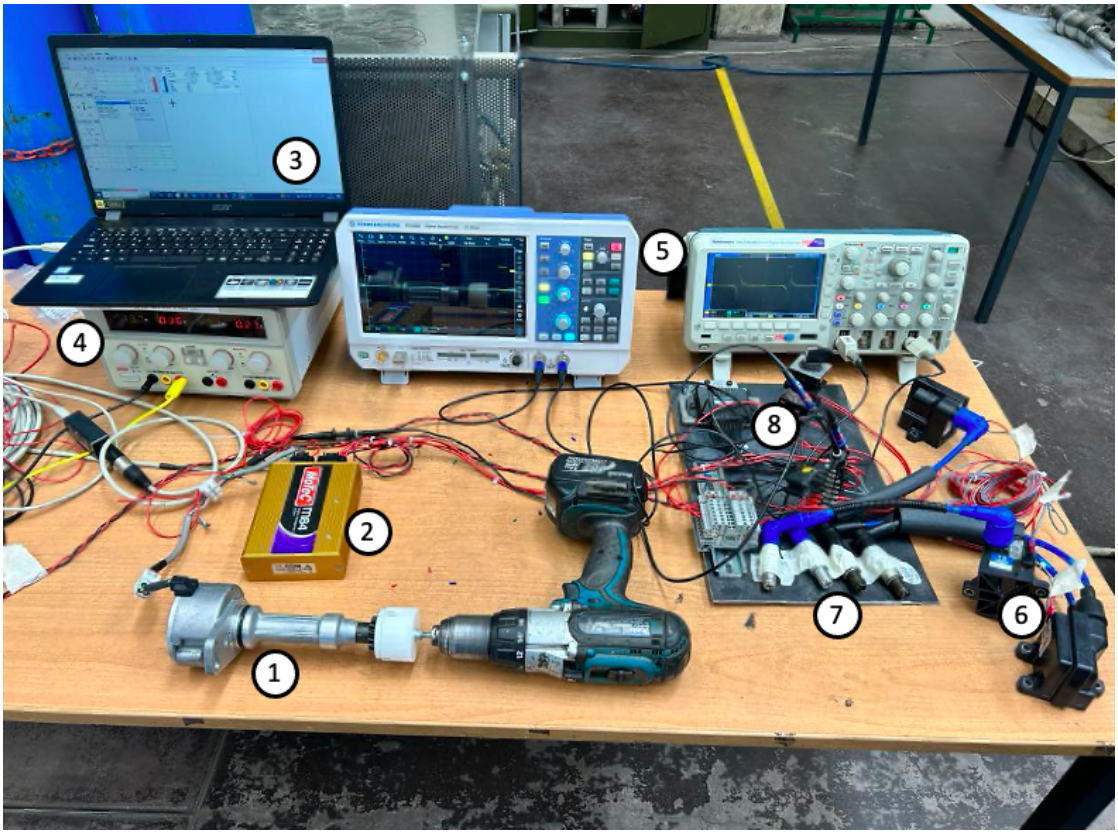


Figure A.18: Ignition circuit setup

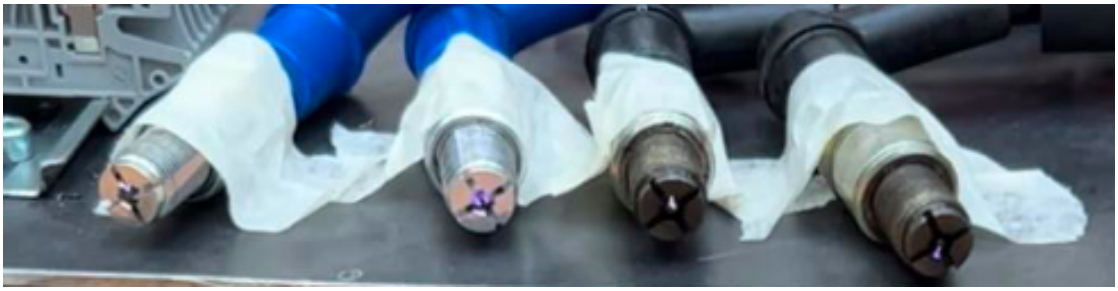


Figure A.19: Visible sparks on spark plugs

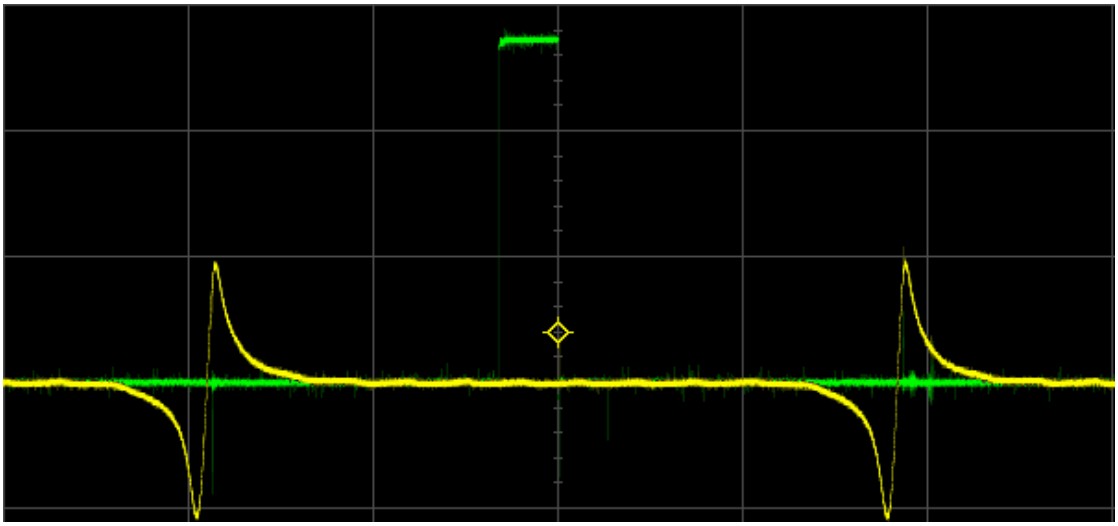


Figure A.20: Trailing coil 1 - ignition timing

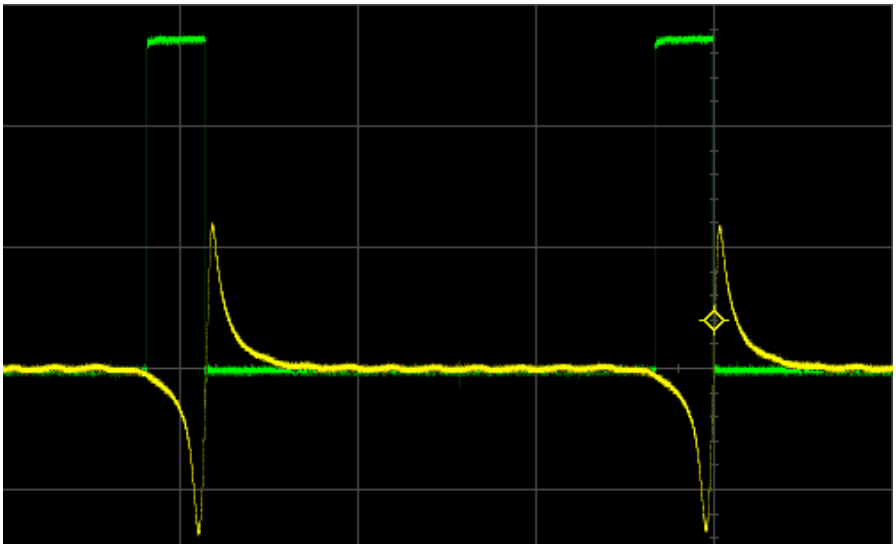


Figure A.21: Trailing coil 2 - ignition timing

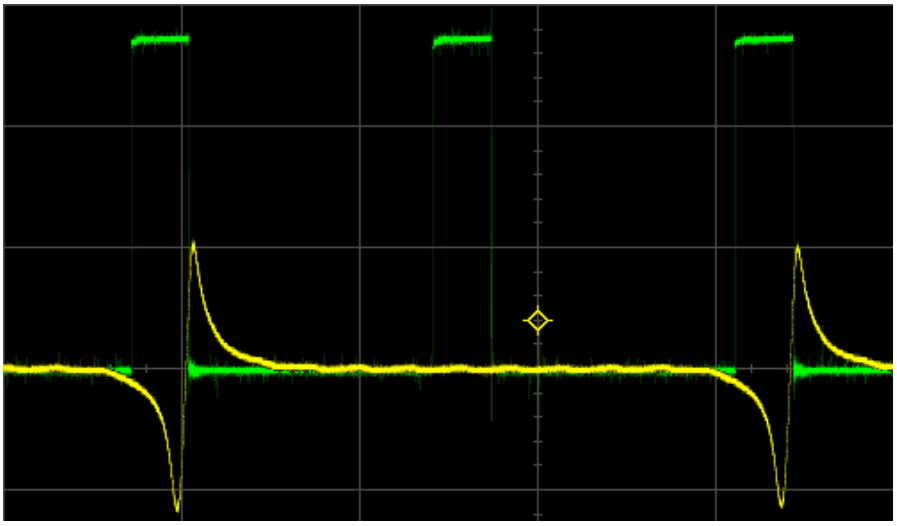


Figure A.22: Double leading coil - ignition timing

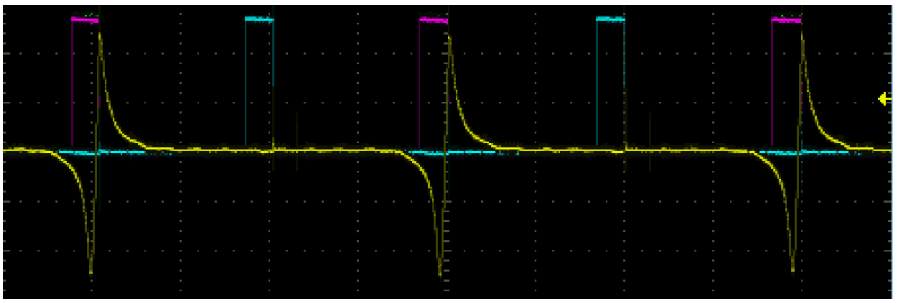


Figure A.23: Signals from the three coils - ignition timing

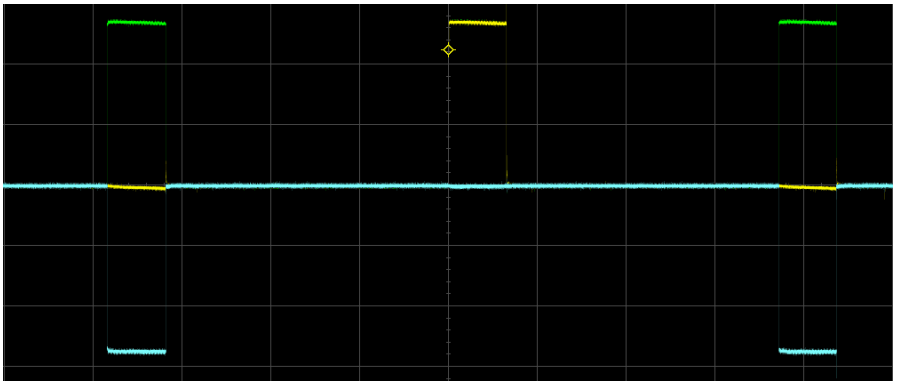


Figure A.24: Leading coil signal subtracted from trailing coil signal

In figs. A.20 and A.21, it is clear that in one rotation of the rotor, both trailing spark plugs fire with a certain phase shift.

In fig.A.22, it is clear that both leading spark plugs fire twice during the rotation of one rotor. As it has been explained, this is due to the fact that they are connected to the same coil and that there is one "lost spark" for each rotor.

After having tested each coil's signal individually, all of them have been tested together, in order to see the phase shift between leading and trailing signals. This is shown in fig.A.23. In this figure, the signal of the leading coil seems to overlap the signals from both trailing coils. Indeed, it is barely possible to see that the signal from three different coils are tested only by seeing the signals displayed in the oscilloscope without knowing the setup. In order to check if there is a certain phase shift between leading and trailing spark plugs, in fig.A.24 the subtraction of both signals is shown. The yellow signal comes from one of the trailing coils, the green signal comes from the leading coil, and the blue signal is the subtraction of these signals. It can be noted that there is indeed no phase shift between the leading and the trailing signals, since when the trailing signal is not equal to zero, the subtraction of both signals is zero.

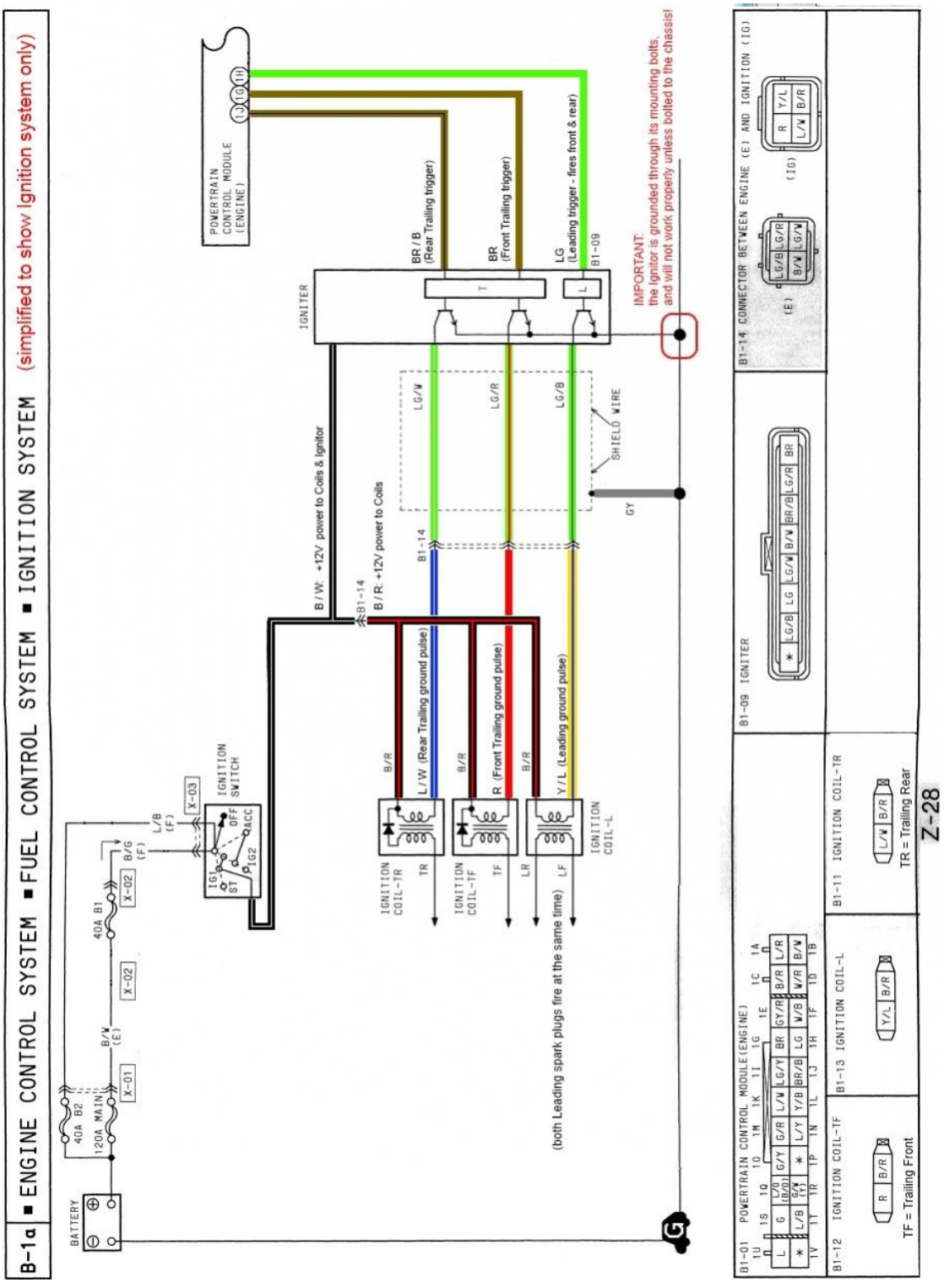


Figure A.25: Ignition circuit

A.5 Bench

A.5.1 P&ID

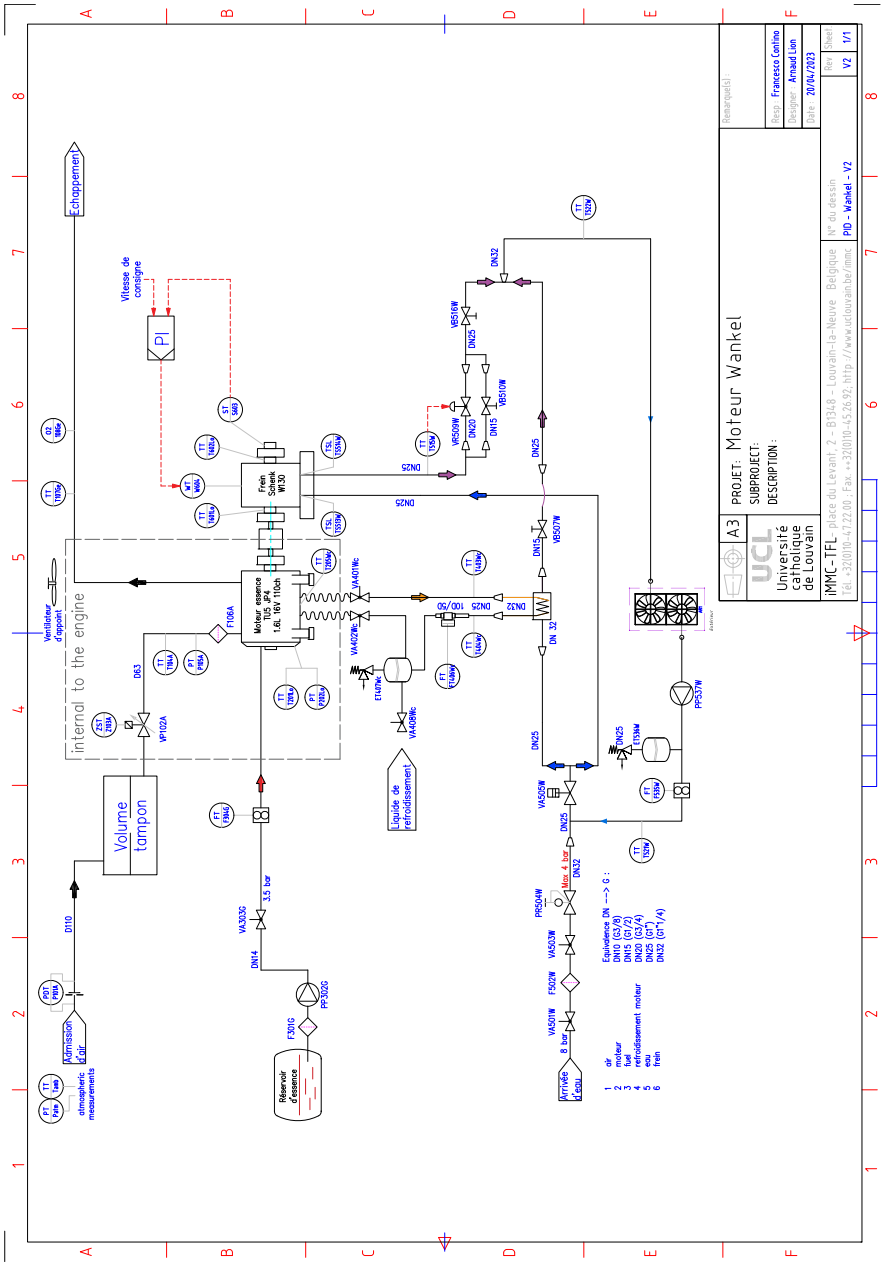


Figure A.26: P&ID

A.5.2 Engine mounts

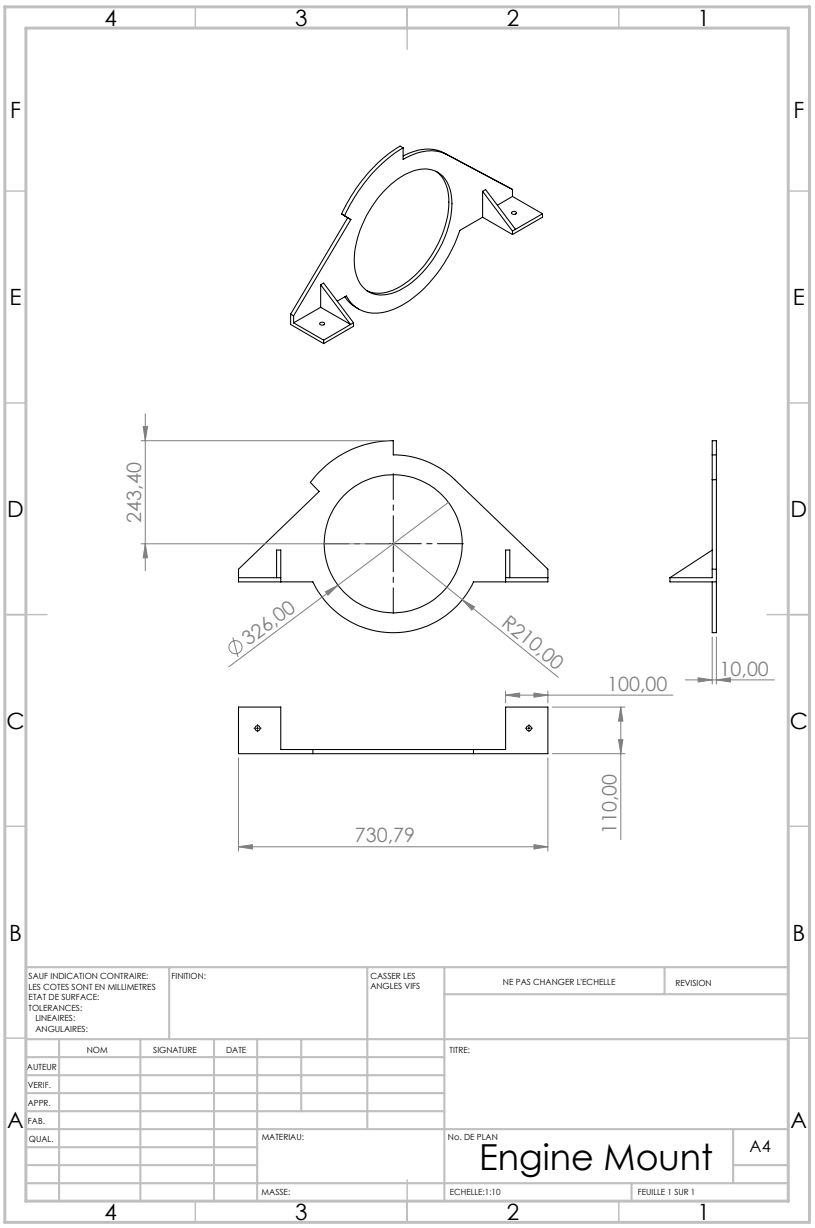


Figure A.27: Main engine mount

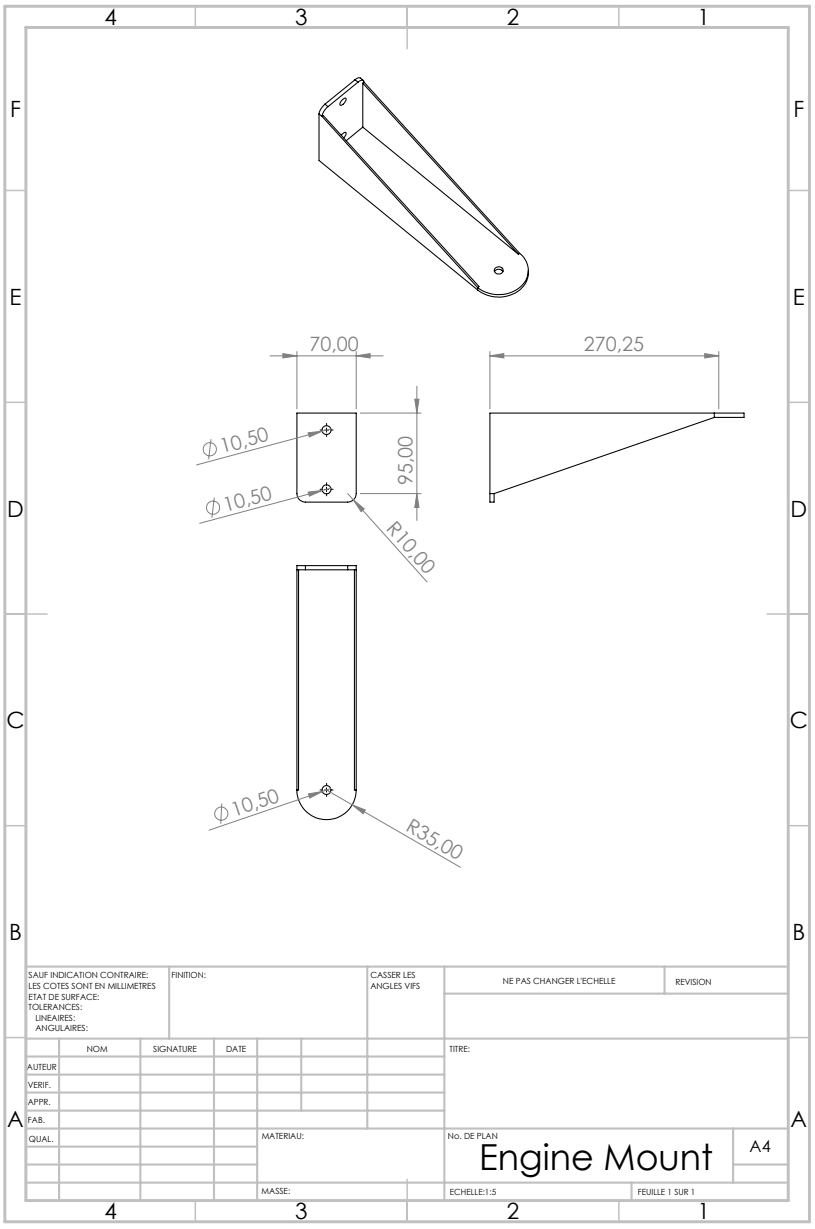


Figure A.28: Secondary engine mount

A.5.3 Pressure sensor adaptor

For subsequent research, a component has been developed to integrate a glow plug with a pressure sensor into the combustion chamber, replacing one spark plug.

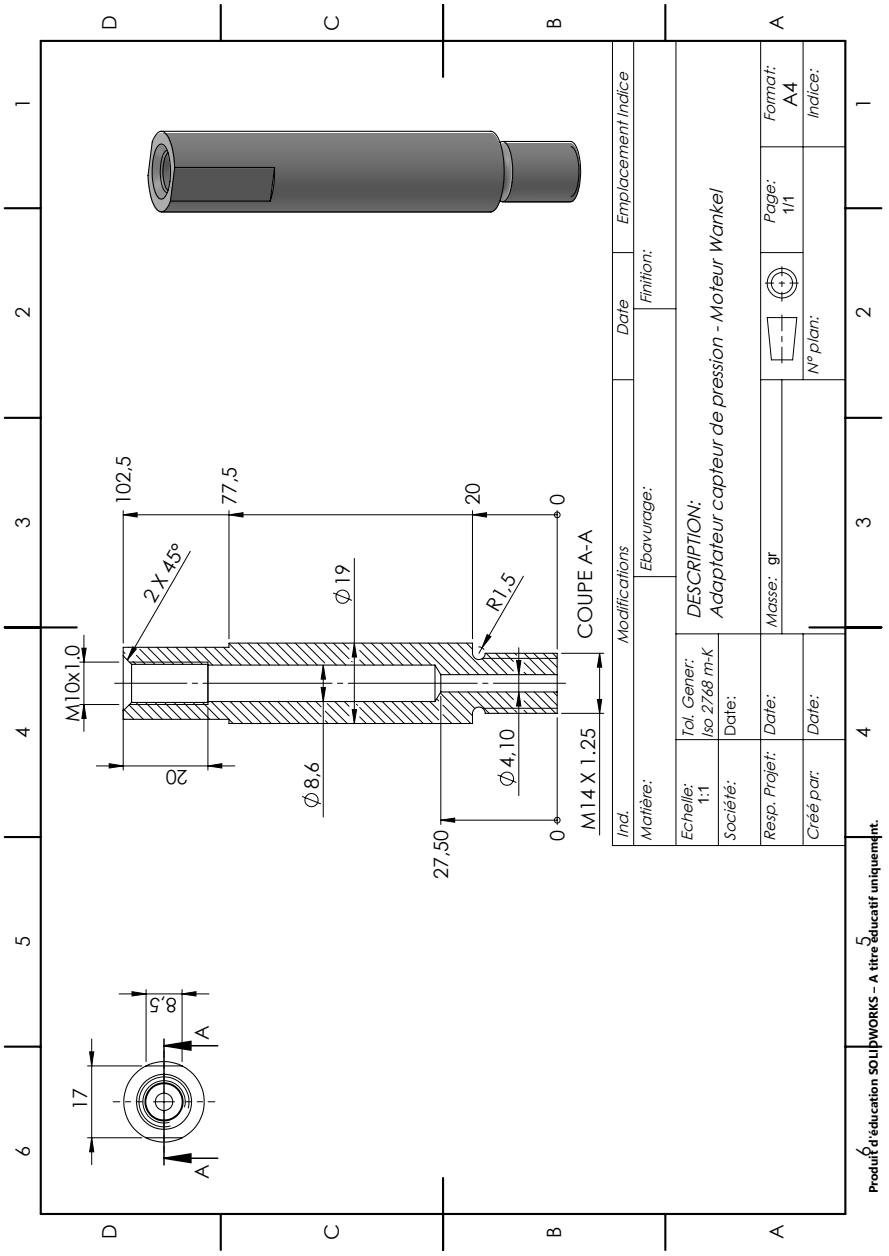


Figure A.29: Pressure sensor adaptor

UNIVERSITÉ CATHOLIQUE DE LOUVAIN
École polytechnique de Louvain
Rue Archimède, 1 bte L6.11.01, 1348 Louvain-la-Neuve, Belgique | **www.uclouvain.be/epl**